NATIONAL AERONAUTICS AND SPACE ADMINISTRATION

*Technical Memorandum 33-497*

# *Supporting Data Package for TR 32-1541, Effects of Storage Temperatures on Silicon Solar Cell Contacts*

*Paul A. Berman*

*Robert K. Yasui*



JET PROPULSION LABORATORY

CALIFORNIA INSTITUTE OF TECHNOLOGY

PASADENA, CALIFORNIA

October 15, 1971

NATIONAL AERONAUTICS AND SPACE ADMINISTRATION

*Technical Memorandum 33-497*

# *Supporting Data Package for TR 32-1541, Effects of Storage Temperatures on Silicon Solar Cell Contacts*

*Paul A. Berman*
*Robert K. Yasui*

JET PROPULSION LABORATORY
CALIFORNIA INSTITUTE OF TECHNOLOGY
PASADENA, CALIFORNIA

October 15, 1971

Prepared Under Contract No. NAS 7-100
National Aeronautics and Space Administration

Page intentionally left blank

# PREFACE

The work described in this report was performed by the Guidance and Control Division of the Jet Propulsion Laboratory.

## ACKNOWLEDGMENTS

The authors are indebted to Robert Mueller and Willard Wall for performing the large number of measurements discussed in this report.

CONTENTS

FIGURES (contd)

150°C Storage (contd)

FIGURES (contd)

150°C Storage (contd)



125°C Storage

FIGURES (contd)

FIGURES (contd)

-196°C (Liquid Nitrogen) Storage (contd)

## ABSTRACT

This data package is a companion document to JPL TR 32-1541 and contains a series of summary curves for cells having various contact systems, depicting the effects of temperature exposure as a function of time on the electrical and mechanical characteristics. Each curve represents the results obtained from a minimum of 32 and a maximum of 1104 individual data inputs and includes the 95% confidence limits associated with each time-temperature combination for which measurements were obtained. The curves are useful for detailed analysis and comparison of the behavior of the contact systems as a function of the environmental conditions studied.

# I. INTRODUCTION

This data package summarizes an extremely large body of data obtained as a result of investigations of the effects of storage temperatures on silicon solar cell contacts. A companion document has been published as JPL Technical Report 32-1541 (Ref. 1), but because of the almost overwhelming quantity of data and the limited time available to analyze it, only comparisons of average values were considered. Significant information exists, however, in the form of the 95% confidence limits associated with measurements of each contact system at each of the test conditions (time-temperature) and it was therefore decided to make the information available by means of this technical memorandum so that investigators closely associated with the field of photovoltaics might construct comparisons better suited to their particular needs. Within the scope of a single report (Ref. 1), the authors were able to deal with only one aspect of what they believe to be many possible interpretations and analyses of the data.

Each point on each figure included in this data package represents the results obtained from 16 to 69 individual measurements, and each figure contains from 2 to 16 such points. Thus, each figure represents a minimum of 32 and a maximum of 1104 data inputs and includes the 95% confidence limits associated with each time-temperature combination for which measurements were obtained.

## II. BACKGROUND

The silicon solar cell is potentially an extremely reliable and long-lived device for conversion of solar energy into electrical energy. Because the cell has no moving parts and operates at relatively low temperatures as compared with thermoelectric and thermionic devices, a system making use of such energy converters could conceivably have an infinite lifetime. At present, there appear to be two major factors which inhibit such an indefinite lifetime: (1) the sensitivity of the device to exposure to radiation and (2) the degradation of the device as a function of the environmental conditions to which it has been exposed. With respect to the latter source of degradation, the stability of the metal-to-semiconductor contacts appears to be the major concern. The effects of high-temperature, high-humidity environments on contact stability from both a mechanical and electrical viewpoint have been treated extensively in a previous JPL technical report (Ref. 2).

In this present memorandum, the same extensive analysis has been performed as a function of storage at various temperatures without the addition of the high-humidity requirement.

## III. DISCUSSION OF EXPERIMENTS

The types of solar cells investigated and the ultimate test levels are shown in Table 1. Only cells fabricated by the two cell manufacturers presently supplying cells for flight programs were investigated. Both p diffused into n (p/n) and n diffused into p (n/p) cell configurations were investigated, as well as some preliminary lithium-containing p/n cells (for increased radiation resistance). Also included in this study were submodules fabricated from n/p and p/n cells similar to those used on the Mariner Mars 1969 program and the Mariner Venus 67/Surveyor programs, respectively. The n/p submodule utilized 0.51-mm (20-mil) fused silica coverglasses and the p/n submodules used 0.15-mm (6-mil) microsheet coverglasses.

The majority of the cells had a nominal base resistivity of 2 ohm-cm with the exception of cell designs H-11 and H-13, n/p cells using 10 ohm-cm base material, and the lithium-doped cells, which had a resistivity of 20 ohm-cm before lithium diffusion. All n/p cells had dimensions of 2 × 2 cm and all p/n cells had dimensions of 1 × 2 cm except for H-17, which was 2 × 2 cm. All cells had a nominal thickness of 0.46 mm (18 mils).

The four contact systems investigated here were (1) silver over titanium without solder coating, (2) silver over palladium over titanium without solder coating, (3) silver over titanium with solder coating, and (4) electroless nickel with solder coating. Two basic top-surface contact configurations were investigated: (1) a configuration using a "bar" contact extending along one edge of the cell and (2) a "corner dart" contact configuration utilizing two triangular pads, one at each of two corners of the cell, with a very narrow strip connecting the two triangles. All the contact configurations and systems have been used on flight programs with the exception of the palladium-containing systems. In all cases, except for the submodules, the sample size was nine or ten for each test condition. Control samples which remained unexposed to the various environments ranged from a sample size of two to a sample size of six, as shown in Table 1. As can be seen from the table, not all cell types were exposed to each of the environmental conditions, but rather emphasis was placed on the 1000-h storage at 150°C exposure, since this was expected to be the most severe environment of those studied here. While all the contact systems and configurations are of interest, those of prime interest are the palladium-containing and non-palladium-containing silver-titanium contacts without solder and the silver-titanium contacts with solder coating.

At each exposure time and temperature (indicated as data points on the curves) the quantities of cells indicated in column 12 ("Number of Test Samples at Each Exposure Time") of Table 1 were removed from the test chamber, electrically measured, and pull tested. The cells for each exposure time and temperature were systematically selected to initially represent the electrical characteristics of the unexposed groups. Electrical data were tabulated with respect to short-circuit current, open-circuit voltage, maximum-power current, maximum-power voltage, and maximum power for each of the exposure times and for the unexposed condition. The ratios of these values to the unexposed values were also tabulated. The average value, the standard deviation, and the 95% confidence limits were determined for each of the parameters. Similarly, the contact pull strengths at each of the exposure times for each of the contact system designs were determined, as were the average pull strength, the standard deviation, and the 95% confidence limits.

Table 1. Solar cell high- and low-temperature storage

| Designation | Cell vendor[a] | Cell type | Base resistivity, ohm-cm | Size, cm | Thickness, cm | Material | Contact metals | Contact type | Coverglass | Miscellaneous | Number of test samples at each exposure time | Number of control samples |
|---|---|---|---|---|---|---|---|---|---|---|---|---|
| 1000 h storage at 150°C | | | | | | | | | | | | |
| HL | HEK | p/n | 20[d] | 1 × 2 | 0.046 | Si | Ag-Ti, solderless | Corner dart | None | Lithium doped | 10 | 6 |
| CP | CRL | n/p | 2 | 2 × 2 | 0.046 | Si | Ag-Pd-Ti, solderless | Bar | None | | 10 | 6 |
| H | HEK | n/p | 2 | 2 × 2 | 0.046 | Si | Ag-Ti, solderless | Bar | None | | 10 | 6 |
| H-17 | HEK | p/n | 2 | 2 × 2 | 0.046 | Si | Ag-Ti, solder | Corner dart | None | | 9 | 6 |
| H-11 | HEK | n/p | 10 | 2 × 2 | 0.046 | Si | Ag-Ti, solder | Corner dart | None | | 10 | 6 |
| H-13 | HEK | n/p | 10 | 2 × 2 | 0.046 | Si | Ag-Ti, solderless | Corner dart | None | | 10 | 6 |
| -- | HEK | n/p | 2 | 2 × 2 | 0.046 | Si | Ag-Ti, solder | Bar | 0.51-mm[b] fused silica | M69[c] 4 cell submodules | 10 | 2 |
| H-3 | HEK | p/n | 2 | 1 × 2 | 0.046 | Si | Electroless Ni, solder | Bar | None | | 9 | 5 |
| M | HEK | n/p | 2 | 2 × 2 | 0.046 | Si | Ag-Ti, solder | Bar | None | | 10 | 5 |
| CL | CRL | p/n | 20[d] | 1 × 2 | 0.046 | Si | Ag-Ti, solderless | Bar | None | Lithium doped | 9 | 5 |
| 1000 h storage at 125°C | | | | | | | | | | | | |
| -- | HEK | n/p | 2 | 2 × 2 | 0.046 | Si | Ag-Ti, solder | Bar | 0.51-mm[b] fused silica | M69 4 cell submodules | 6 | 2 |
| -- | HEK | p/n | 2 | 1 × 2 | 0.046 | Si | Electroless Ni, solder | Bar | 0.15-mm[b]-microsheet | M67[e]/ Surveyor 7 cell submodules | 6 | 2 |
| 720 h storage at 80°C | | | | | | | | | | | | |
| M | HEK | n/p | 2 | 2 × 2 | 0.046 | Si | Ag-Ti, solder | Bar | None | | 10 | 5 |
| H | HEK | n/p | 2 | 2 × 2 | 0.046 | Si | Ag-Ti, solderless | Bar | None | | 10 | 5 |
| 1000 h storage at $LN_2$ (-196°C) | | | | | | | | | | | | |
| HP | HEK | n/p | 2 | 2 × 2 | 0.046 | Si | Ag-Pd-Ti, solderless | Bar | None | | 10 | 3 |
| H | HEK | n/p | 2 | 2 × 2 | 0.046 | Si | Ag-Ti, solderless | Bar | None | | 10 | 3 |
| M | HEK | n/p | 2 | 2 × 2 | 0.046 | Si | Ag-Ti, solder | Bar | None | | 10 | 3 |

[a]HEK = Heliotek, A Division of Textron, Inc., Sylmar, Calif.
CRL = Centralab, The Electronics Division of Globe-Union, Inc., Milwaukee, Wis.
[b]0.410 μm cutoff and antireflective coating.
[c]Mariner Mars 1969.
[d]Base resistivity prior to lithium diffusion process.
[e]Mariner Venus 67.

## IV. DATA REDUCTION AND ANALYSIS

To aid in the analysis of the effects of different environments on the performance characteristics of various types of photovoltaic devices, a computer program has been developed to show the behavior of five important solar cell parameters as a function of exposure to the environment. This behavior is depicted in three ways: (1) a plot of the actual parameter vs time of exposure, (2) a plot of the actual parameters "normalized" to unexposed values vs time of exposure, and (3) a printed output of actual raw data.

The five solar cell parameters considered for evaluation in the program are

Short-circuit current $I_{sc}$

Open-circuit voltage $V_{oc}$

Maximum-power current $I_{mp}$

Maximum-power voltage $V_{mp}$

Maximum power $P_{max}$

Values for the first four parameters are input values, and the fifth parameter is calculated from $P_{max} = I_{mp} \times V_{mp}$. For a particular test, a series of cells is exposed to an environment for a given length of time.

During the test, the temperature and light intensity remain constant. At the beginning of the test, the four input parameters are measured. Thus the test provides data as a function of exposure time. These exposed cells are referred to as "test cells." To obtain an estimate of measurement accuracy and repeatibility, a series of control cells of types similar to the test cells is also measured electrically and mechanically; these control cells are not exposed to the environmental test. At the same selected points as the test cells the four solar cell parameters of each control cell are measured. By monitoring changes in the control cell values as the test program progresses, one can correct the test cell values, thus reducing measurement-associated error due to instrumentation drift or similar causes. The printed output shows these values in detail.

To aid in determining statistical validity of the results of the tests, the 95% confidence limits are determined. Let $X_i$, $i = 1, 2, \cdots, n$, be the short-circuit current values for a series of n cells.

Define the following: Let

$$Y \equiv X_1 + X_2 +, \cdots, + X_n \tag{1}$$

$$Z \equiv X_1^2 + X_2^2 +, \cdots, + X_n^2 \tag{2}$$

The average, 95% confidence limits, and standard deviation are given by the formulas:

$$\text{Av.} = \frac{Y}{n} \tag{3}$$

$$SD = \sqrt{\frac{nZ - Y^2}{n(n-1)}} \tag{4}$$

$$\text{Conf.} = \frac{k \cdot SD}{\sqrt{n}} \tag{5}$$

where k is the multiplying factor that fixes the confidence limits at any desirable level. The values for Eqs. (3-5) appear on the printed output.

To present an overall view of the test results, a set of plots is also included as part of the output. Five plots show the change of the five solar cell parameters as a function of exposure time and five additional plots depict the normalized (to the unexposed) parameters as a function of the same variables. The plots consist of the average values, the 95% confidence limits and a least squares fit to the average using a polynomial of the second order ($Yc = a + bx + Cx^2$). If, however, data were taken at less than five points during the test program, no least squares fit is plotted by the computer. The contact strength test data are treated in a similar manner.

Representative computer printout plots of the data obtained (Figs. 1-112) are presented in this supporting data package as a detailed data supplement to JPL Technical Report 32-1541 (Ref. 1).

## V. CONCLUSIONS

Some extremely interesting conclusions can be drawn from the series of tests described in this report, especially when correlated to the high-humidity, high-temperature test previously reported (Ref. 2). The results of the 80°C soak clearly show that the severe degradations observed in contact strength for the silver-titanium solderless cells were directly a result of the combined humidity-temperature environment and not due to the temperature component alone. Exposure to an 80°C temperature for 720 h appears to be a very benign environment, resulting in no discernible degradation of either mechanical or electrical properties. When combined with a relative humidity of 95%, however, this environment can be extremely severe for contact systems without solder coating.

The M69 submodule design, including choice of cell type, contact system, and interconnections, was clearly shown to be superior to that of the M67 submodule design for exposure to 1000-h storage at 125°C.

Comparison between results of the 80°C and 150°C soaks indicates that the solder-coated silver-titanium M-type cell is adversely affected as the temperature is increased, probably due to the interaction of the tin component of the solder and the silver at the 150°C temperature. In this case, for temperatures of 150°C, the absence of solder seems desirable. At liquid nitrogen temperatures the solder coating also appears to adversely affect the mechanical stability of the back contact due to the thermal expansion coefficient mismatch between solder and silicon, although on an absolute pull strength basis, the solder-coated contact appeared to be no worse than the non-solder-coated contacts. The inherent solder-silicon thermal expansion coefficient mismatch might, however, be even more detrimental when the cells are interconnected and bonded to a substrate, and consideration should be given to this possibility. The addition of palladium to the solderless silver-titanium contact system appeared to present no advantages for the environments studied here.

The M69-type cell with solder-coated silver-titanium contacts appears to be as good as, if not better than, other cell types in all environments studied so far (including high-humidity, high-temperature) except for exposures at temperatures of +150°C and -196°C. For these cases, the M69 type cell is inferior to the solderless cell contact system.

For the +150°C exposure, although the solder-coated M-type cells exhibited mechanical and electrical degradation, the solder coated H-11 type cells did not. The only difference between the contacts of the two cell types was one of configuration, not composition (both cell types had silver-titanium solder-coated contacts), the former cell type utilizing a bar contact and the latter cell type utilizing a corner dart contact on the active cell face. The configuration difference would not be expected to influence the mechanical strength of the bottom contacts, which were similar for the two cell types. The fact that the H-11 type cells did not exhibit the degradation in bottom-contact strength that was observed in the M-type cells indicates that the presence of solder need not necessarily result in degradation at 150°C exposure, but that such degradation is a possibility. Thus for some missions there may be a tradeoff between protection against humidity degradation of contacts and protection against detrimental effects of extremely high or low temperature on the cell contacts.

In general, the lithium-containing cells exhibited electrical and mechanical contact stability as good as, it not better than, the other cells tested at the 150°C exposure temperature.

## REFERENCES


1. Berman, P. A., and Yasui, R. K., Effects of Storage Temperatures on Silicon Solar Cell Contacts, Technical Report 32-1541. Jet Propulsion Laboratory, Pasadena, Calif., Oct. 15, 1971.

2. Yasui, R. K., and Berman, P. A., Effects of High-Temperature, High Humidity Environment on Silicon Solar Cell Contacts, Technical Report 32-1520. Jet Propulsion Laboratory, Pasadena, Calif., Feb. 15, 1971.

Page intentionally left blank

150°C STORAGE

Page intentionally left blank

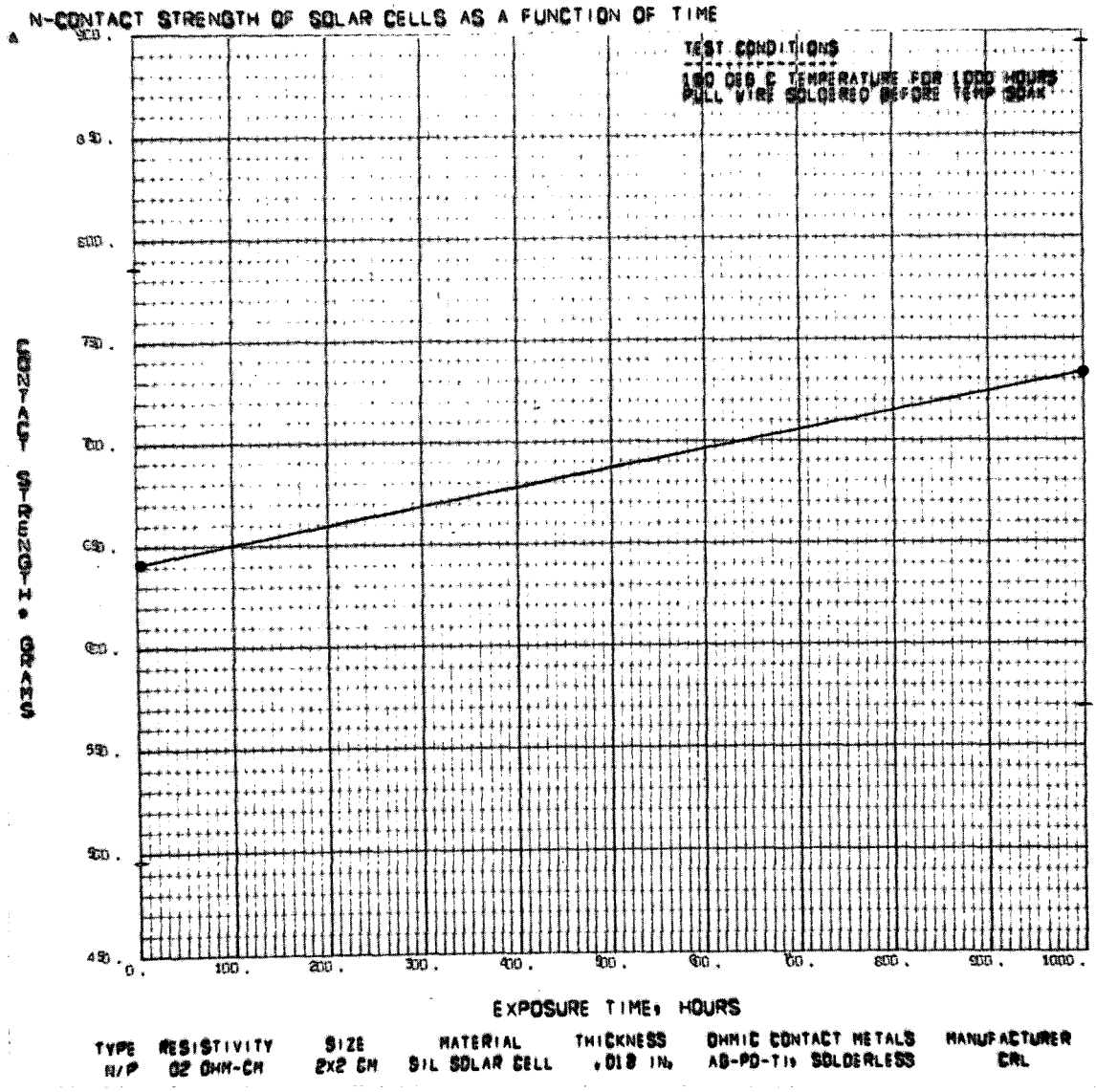


Fig. 1. Top-contact strength, cell type CP, as a function of time, 150 °C storage

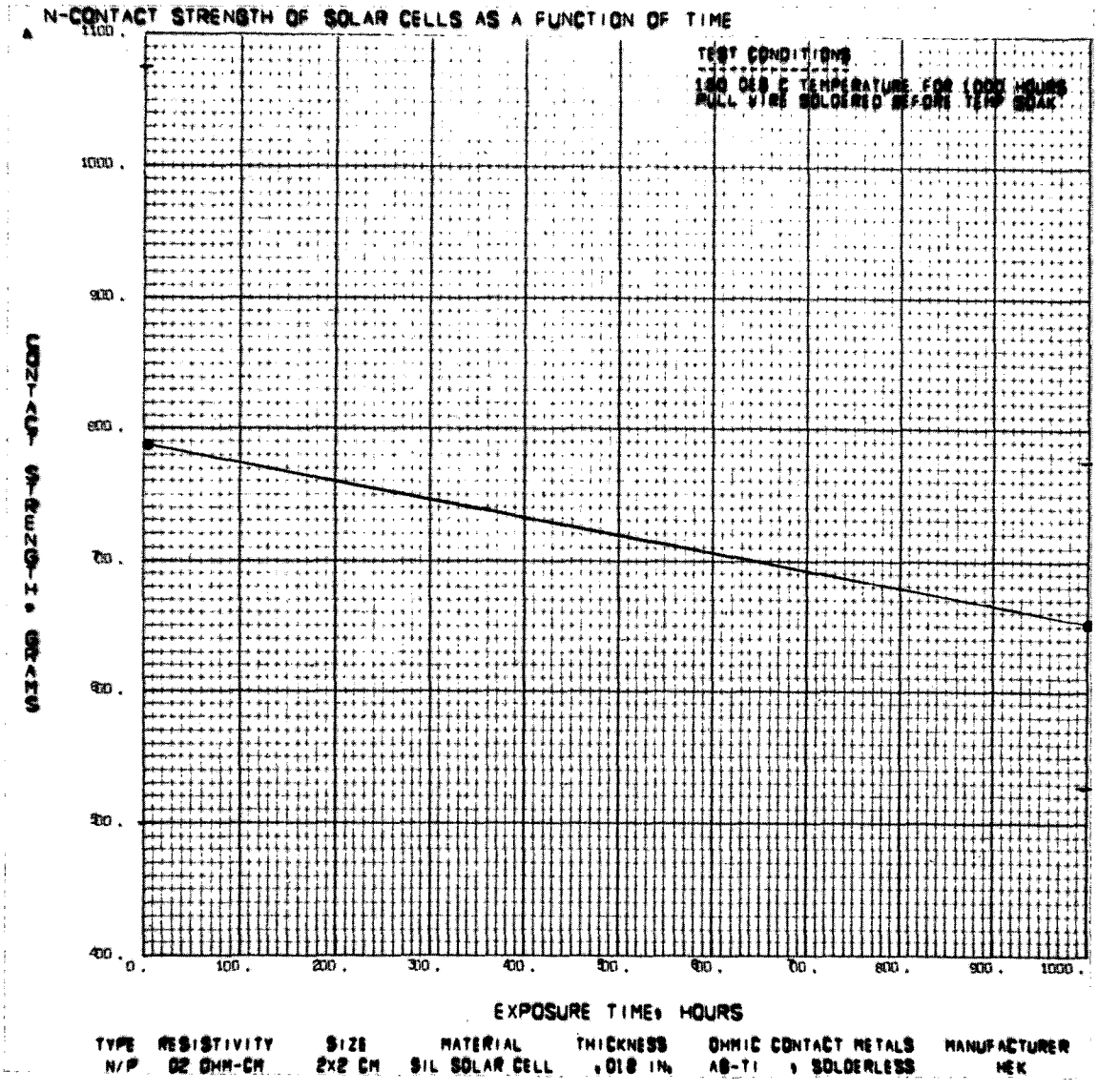


Fig. 2. Top-contact strength, cell type H, as a function of time, 150°C storage

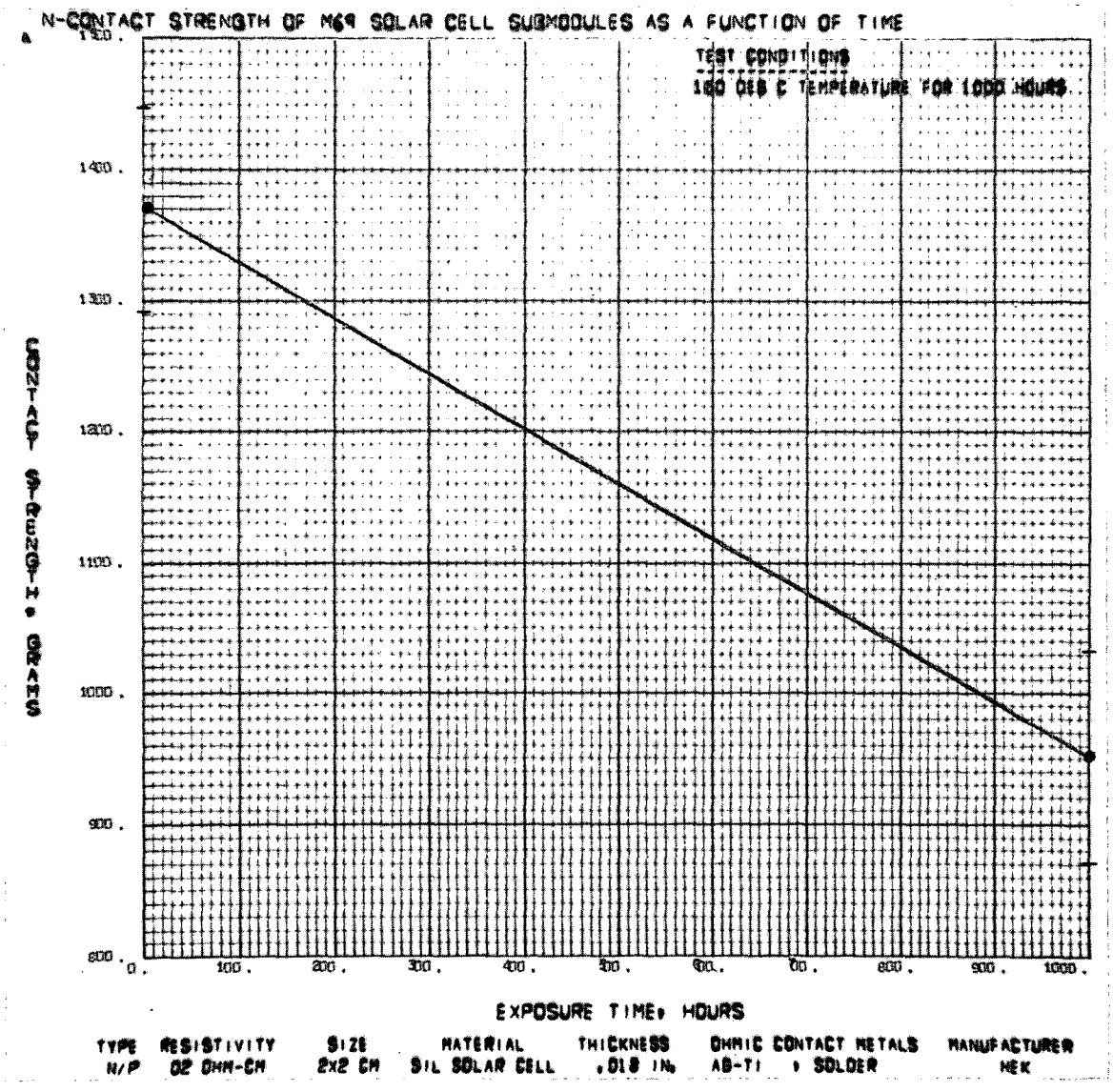


Fig. 3. Top-contact strength, cell type M69 module, as a function of time, 150 °C storage

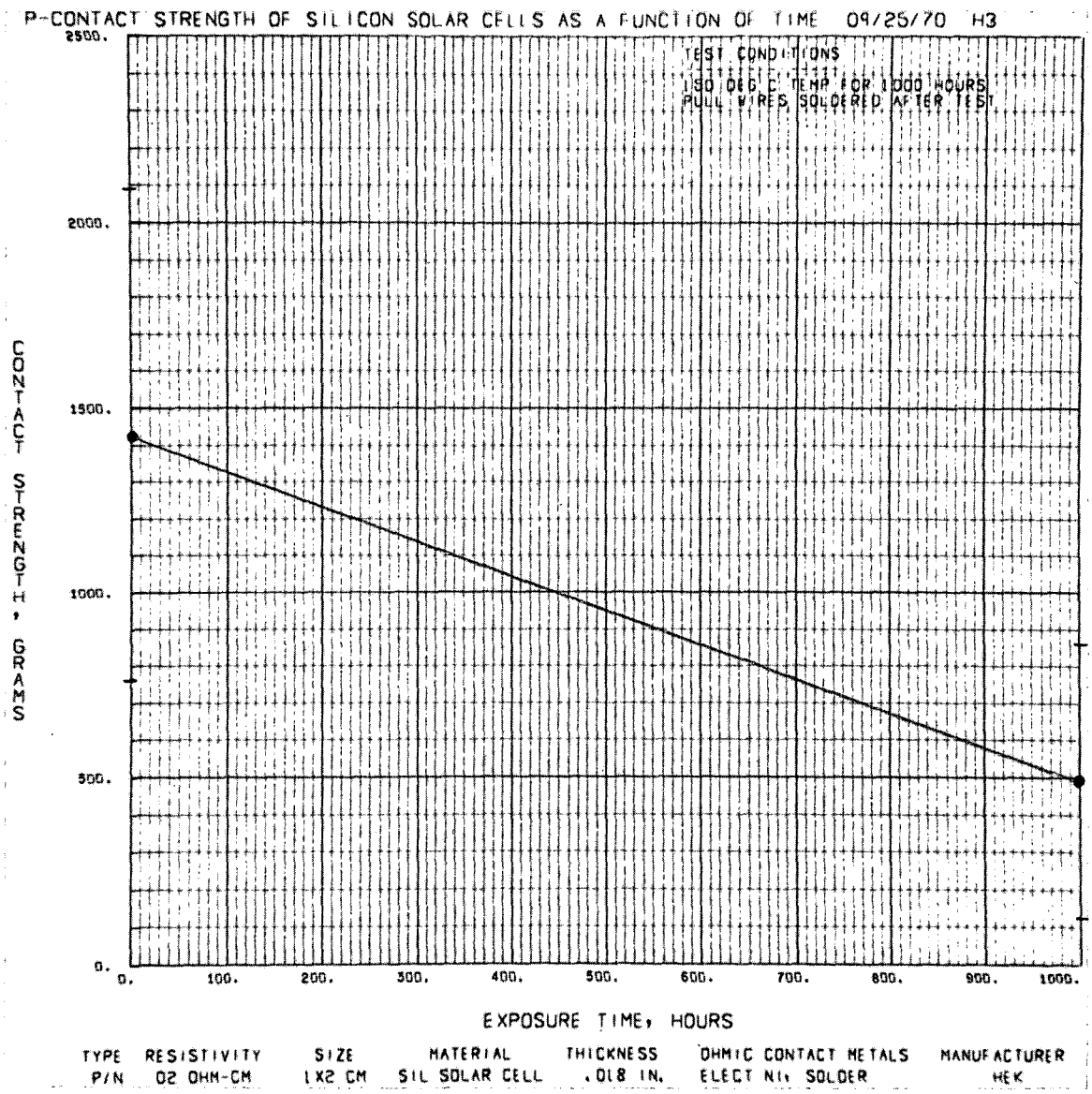


Fig. 4. Top-contact strength, cell type H-3, as a function of time, 150 °C storage

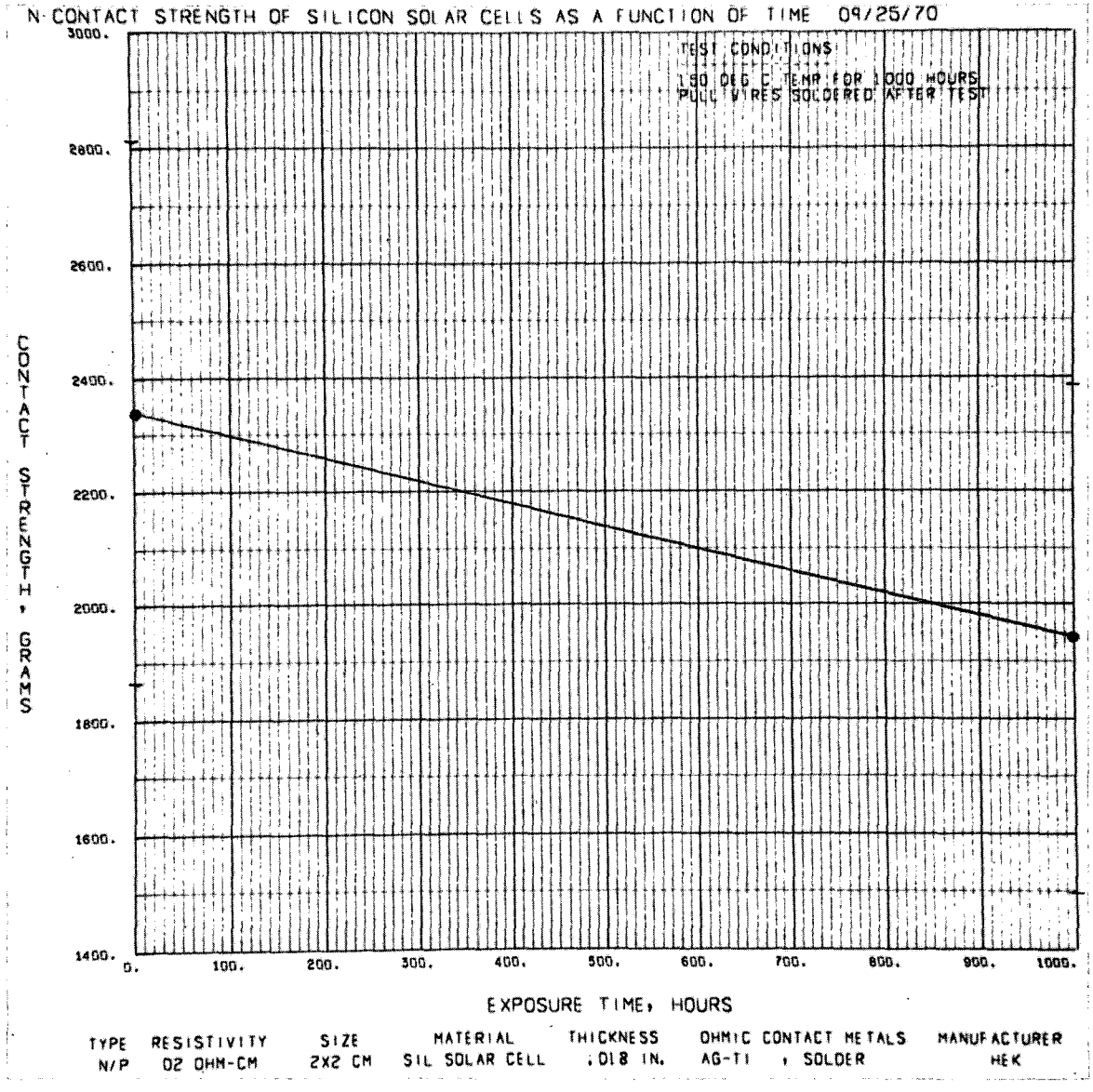


Fig. 5. Top-contact strength, cell type M, as a function of time, 150 °C storage

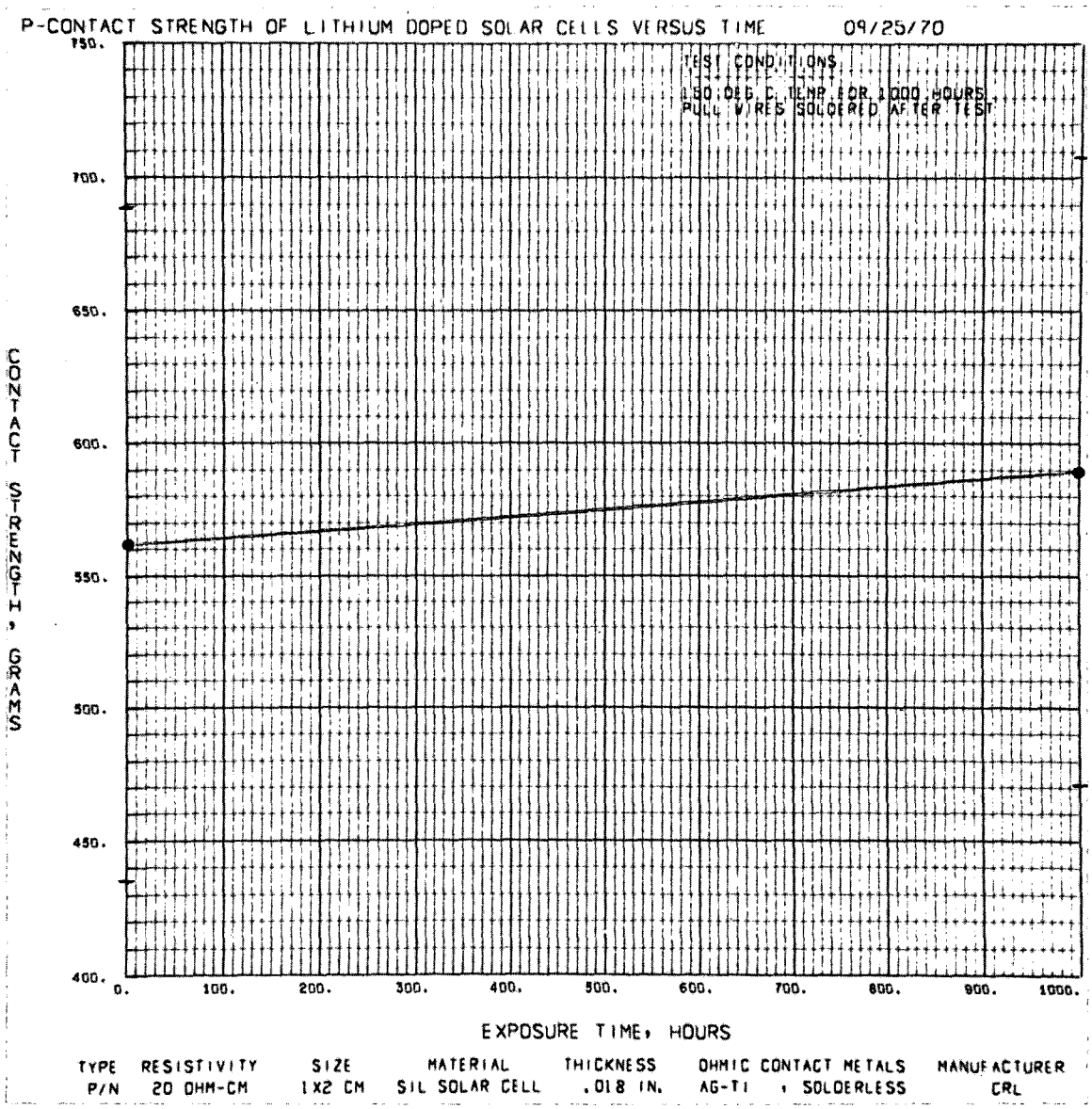


Fig. 6. Top-contact strength, cell type CL, as a function of time, 150 °C storage

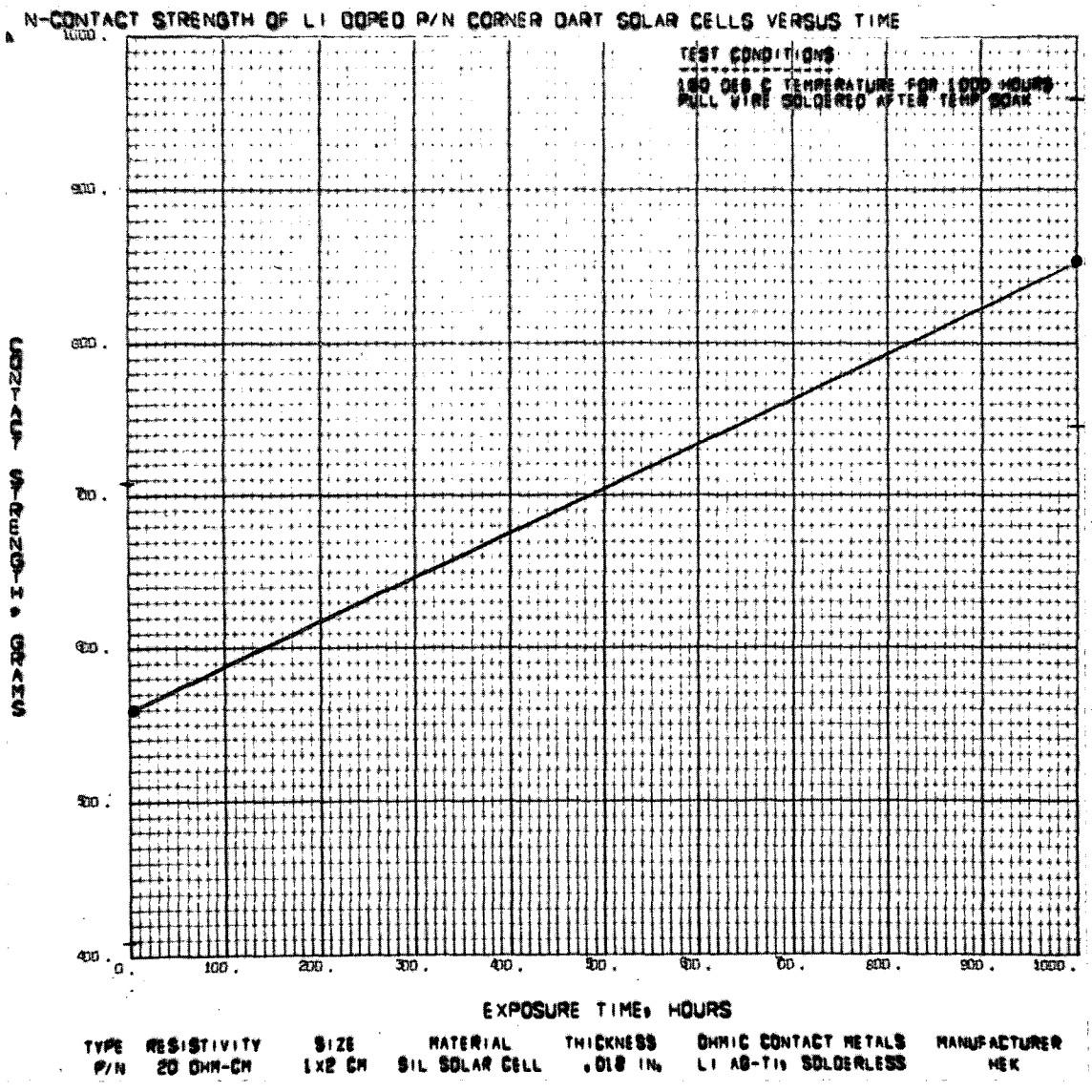


Fig. 7. Bottom-contact strength, cell type HL, as a function of time, 150 °C storage

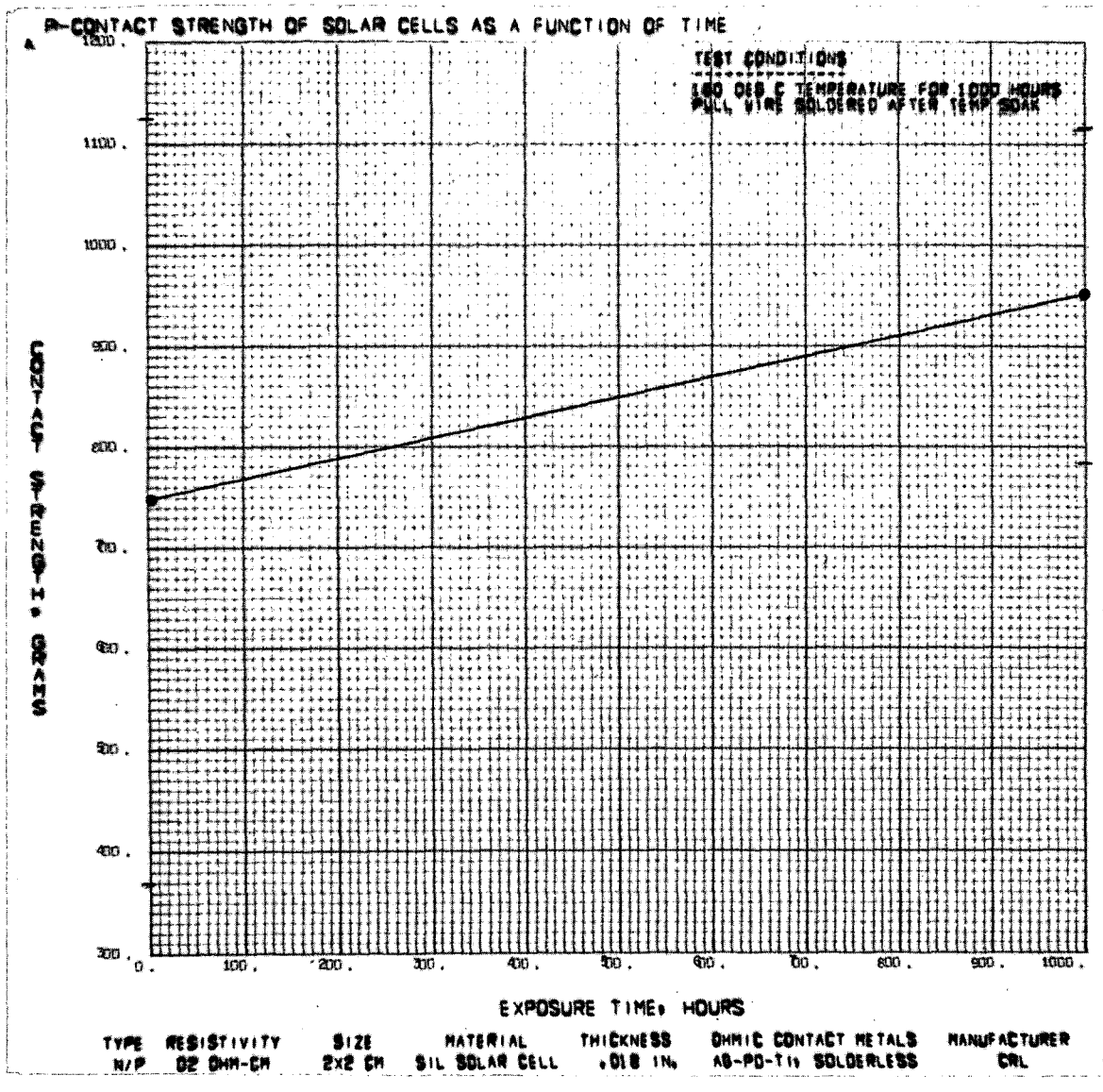


Fig. 8. Bottom-contact strength, cell type CP, as a function of time, 150 °C storage

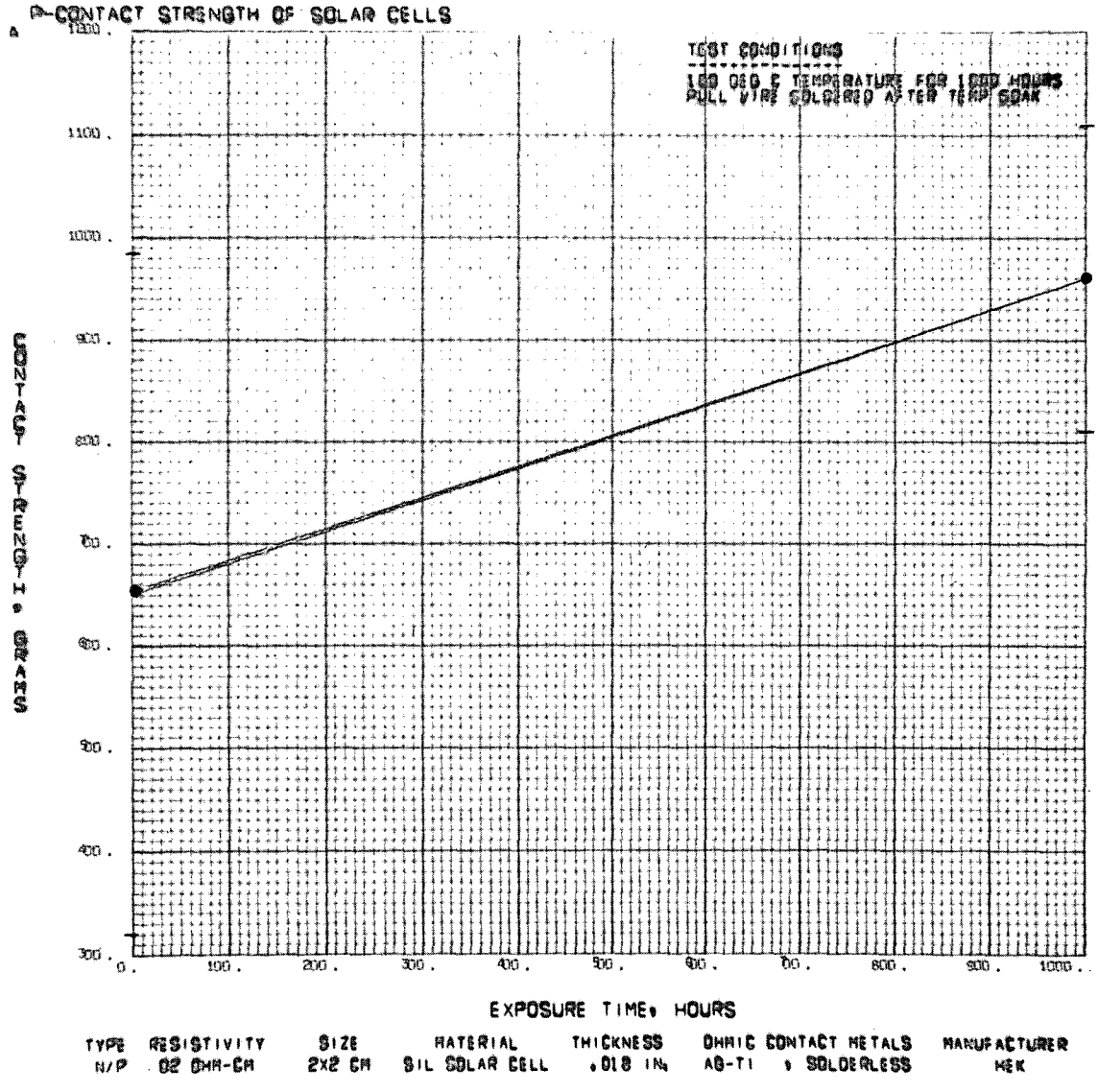


Fig. 9. Bottom-contact strength, cell type H, as a function of time, 150 °C storage

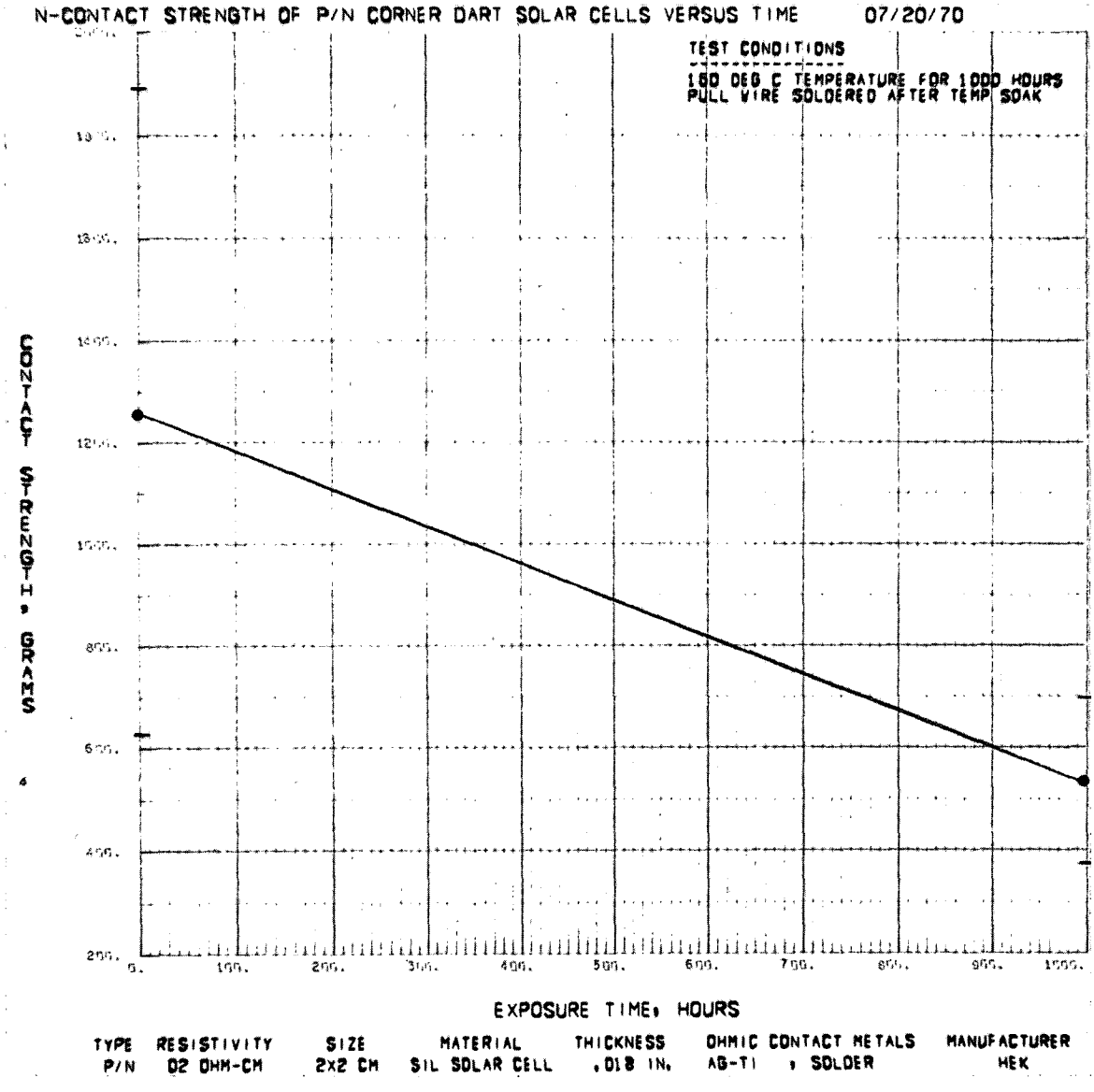


Fig. 10. Bottom-contact strength, cell type H-17, as a function of time, 150 °C storage

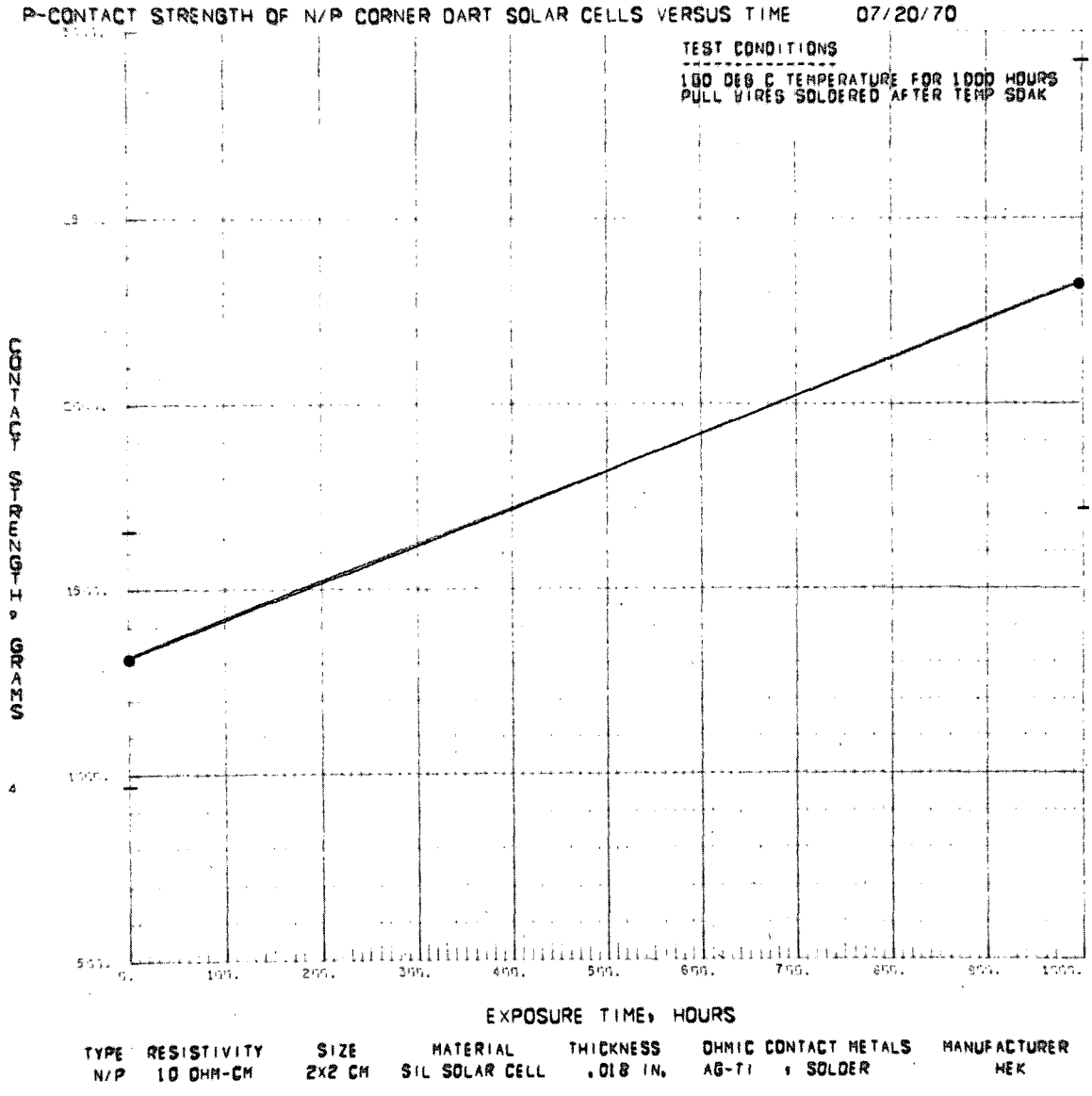


Fig. 11. Bottom-contact strength, cell type H-11, as a function of time, 150 °C storage

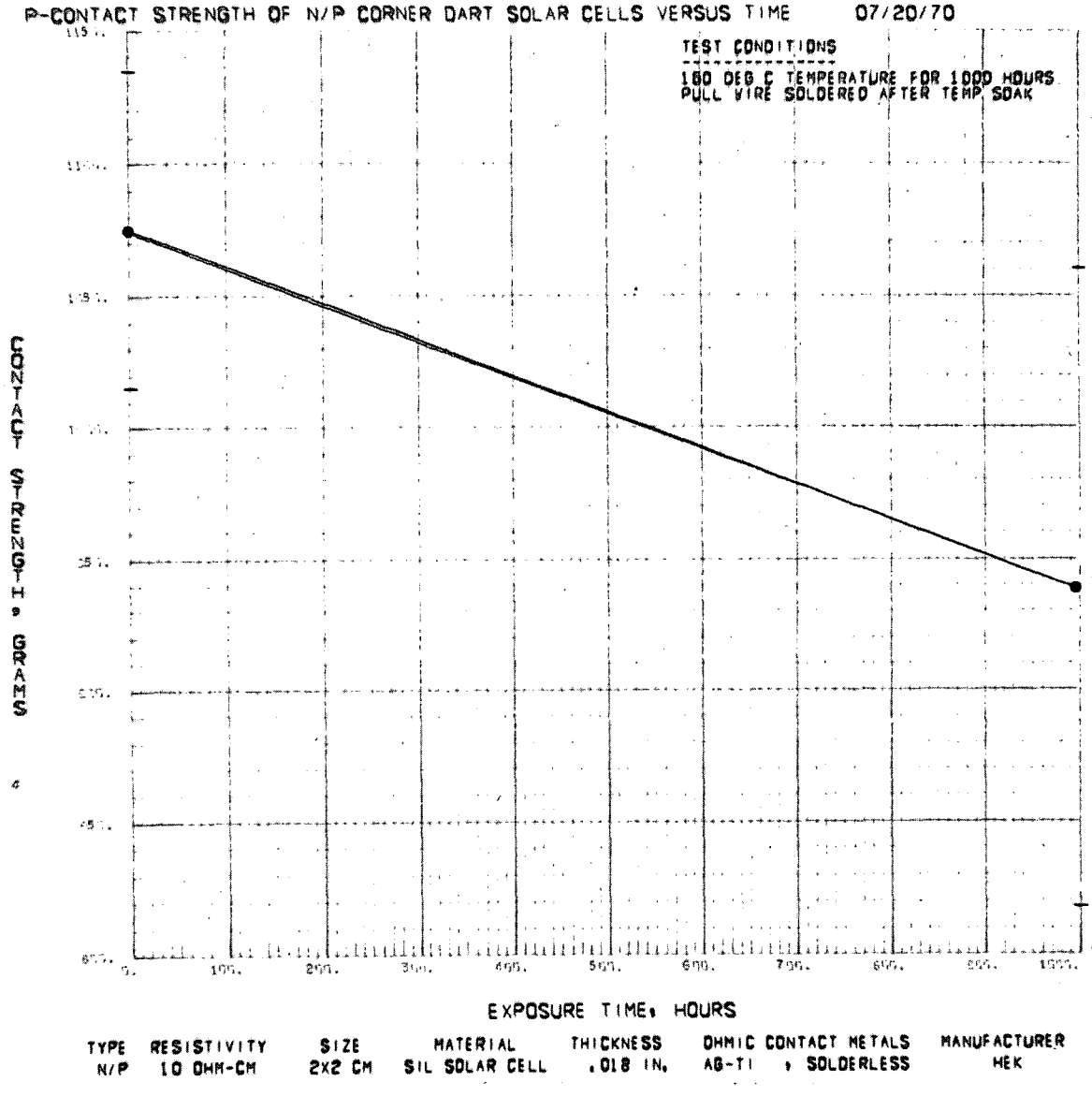


Fig. 12. Bottom-contact strength, cell type H-13, as a function of time, 150°C storage

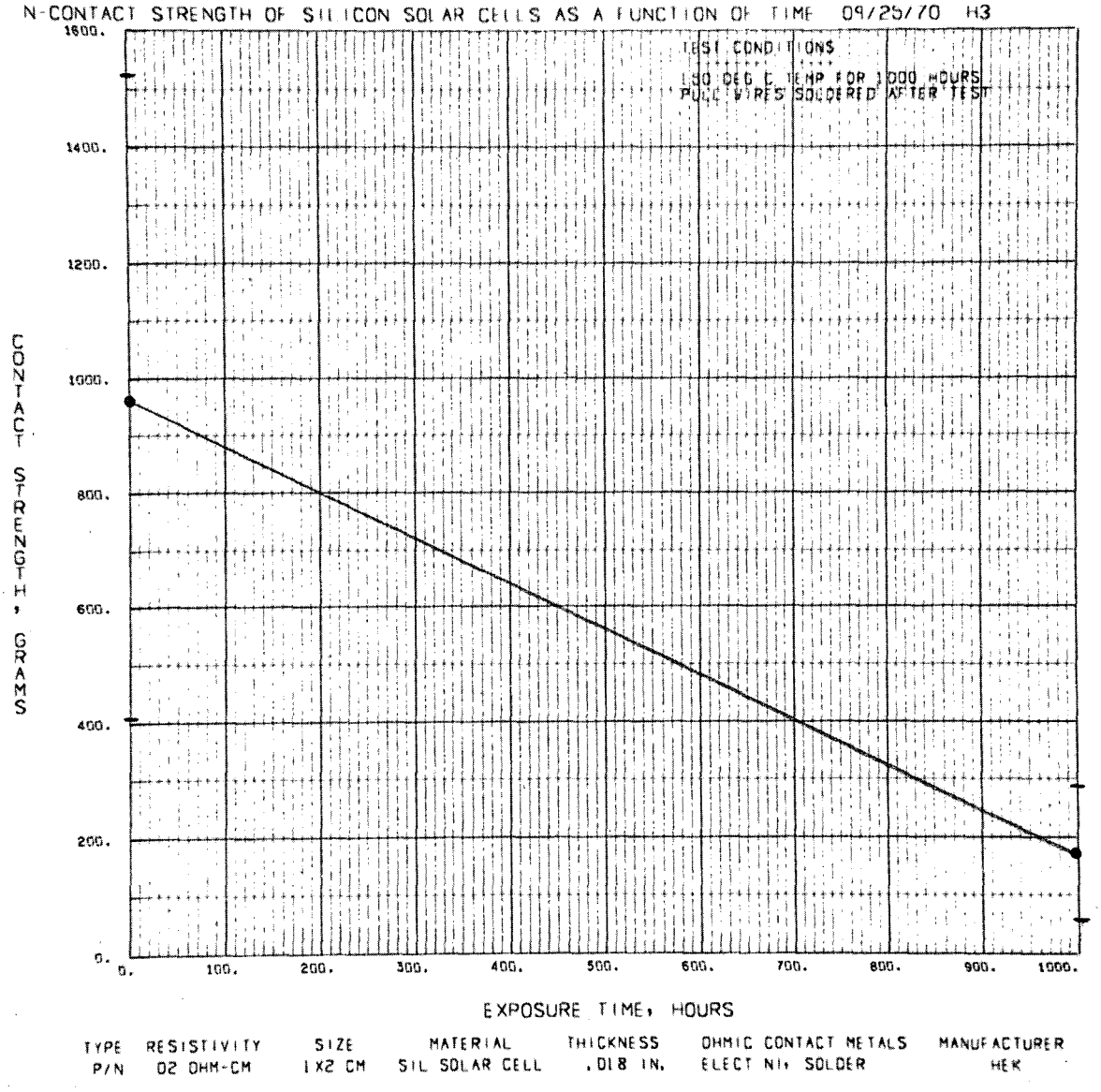


Fig. 13. Bottom-contact strength, cell type H-3, as a function of time, 150 °C storage

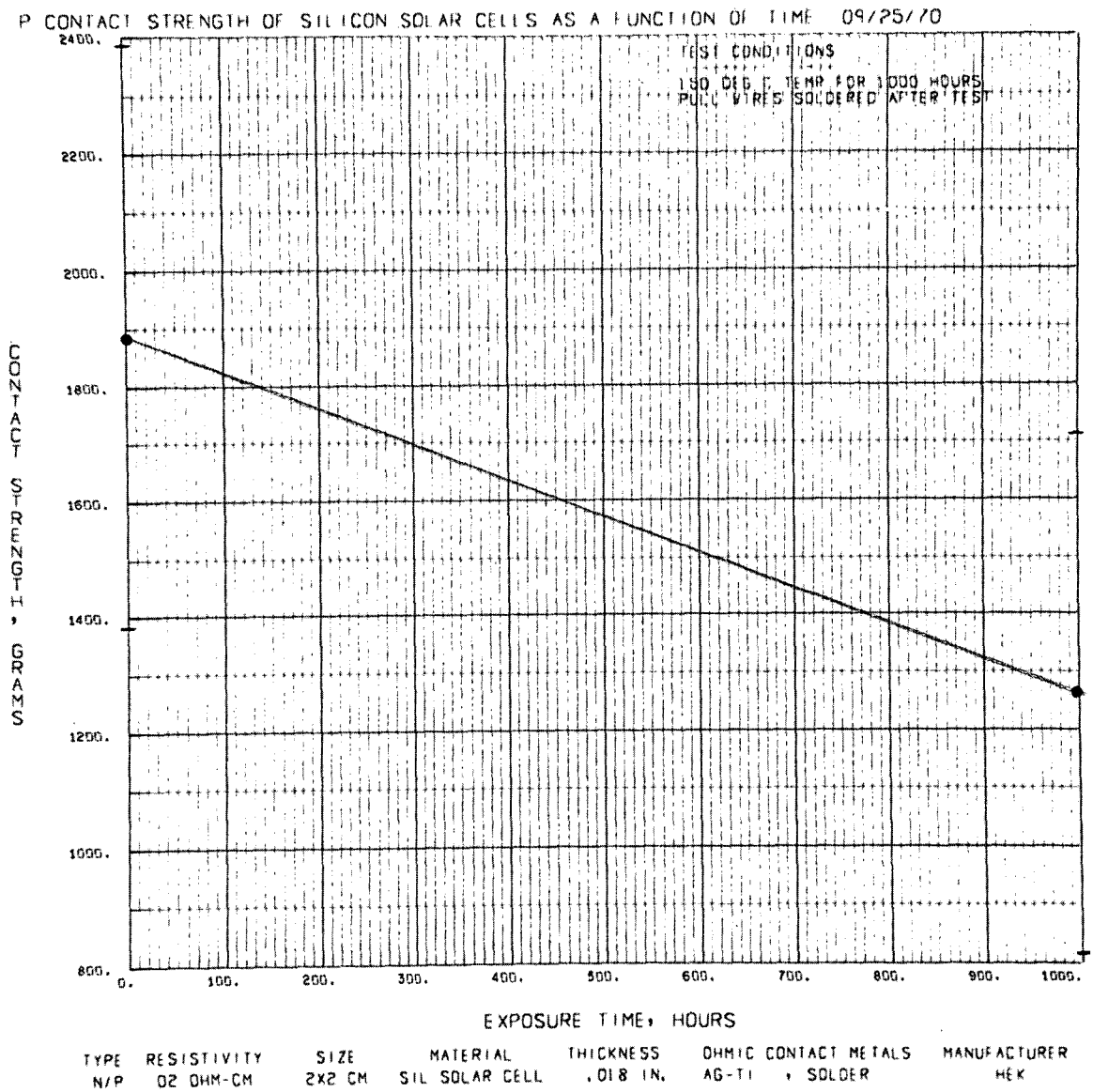


Fig. 14. Bottom-contact strength, cell type M, as a function of time, 150 °C storage

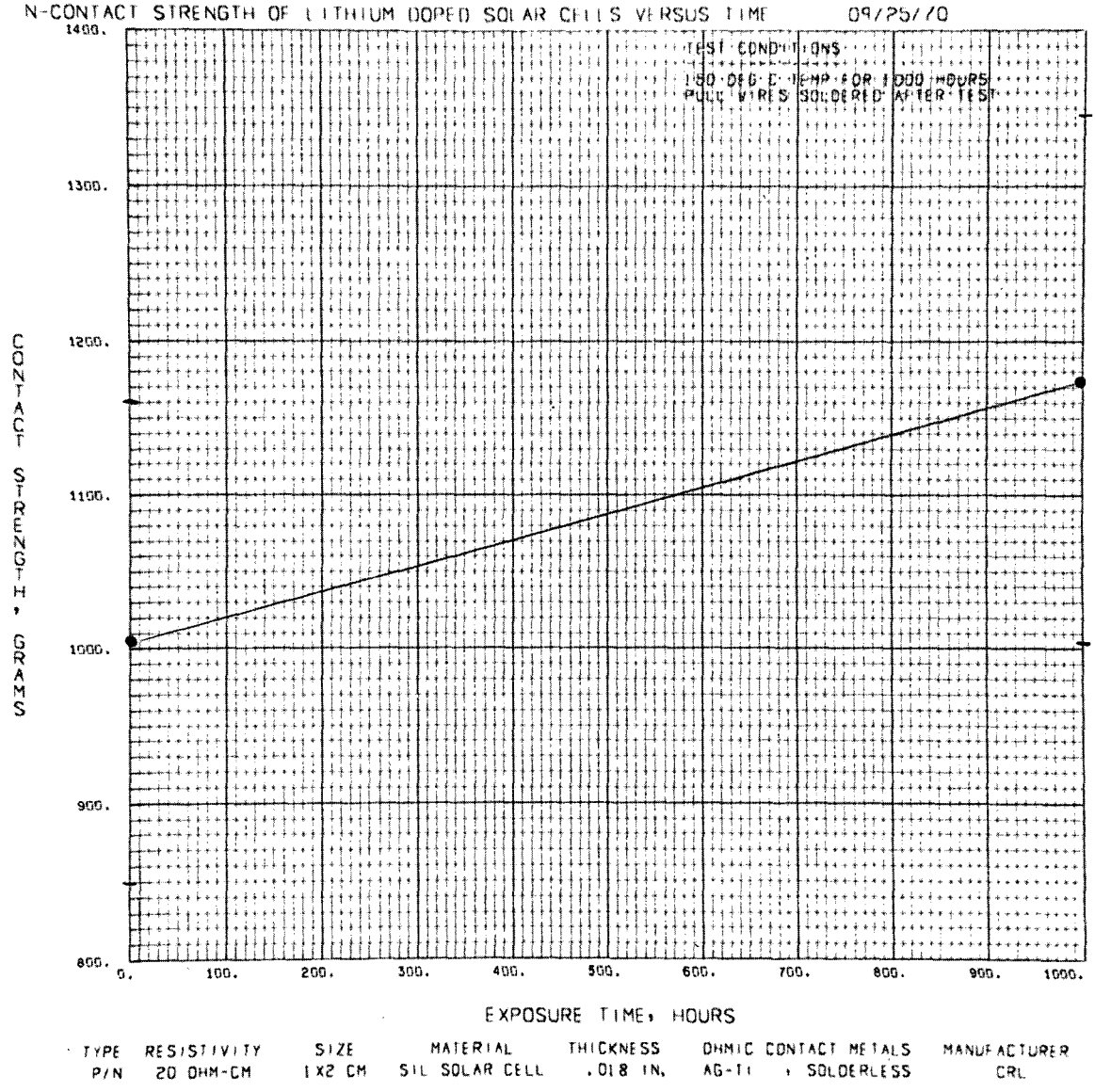


Fig. 15. Bottom-contact strength, cell type CL, as a function of time, 150 °C storage

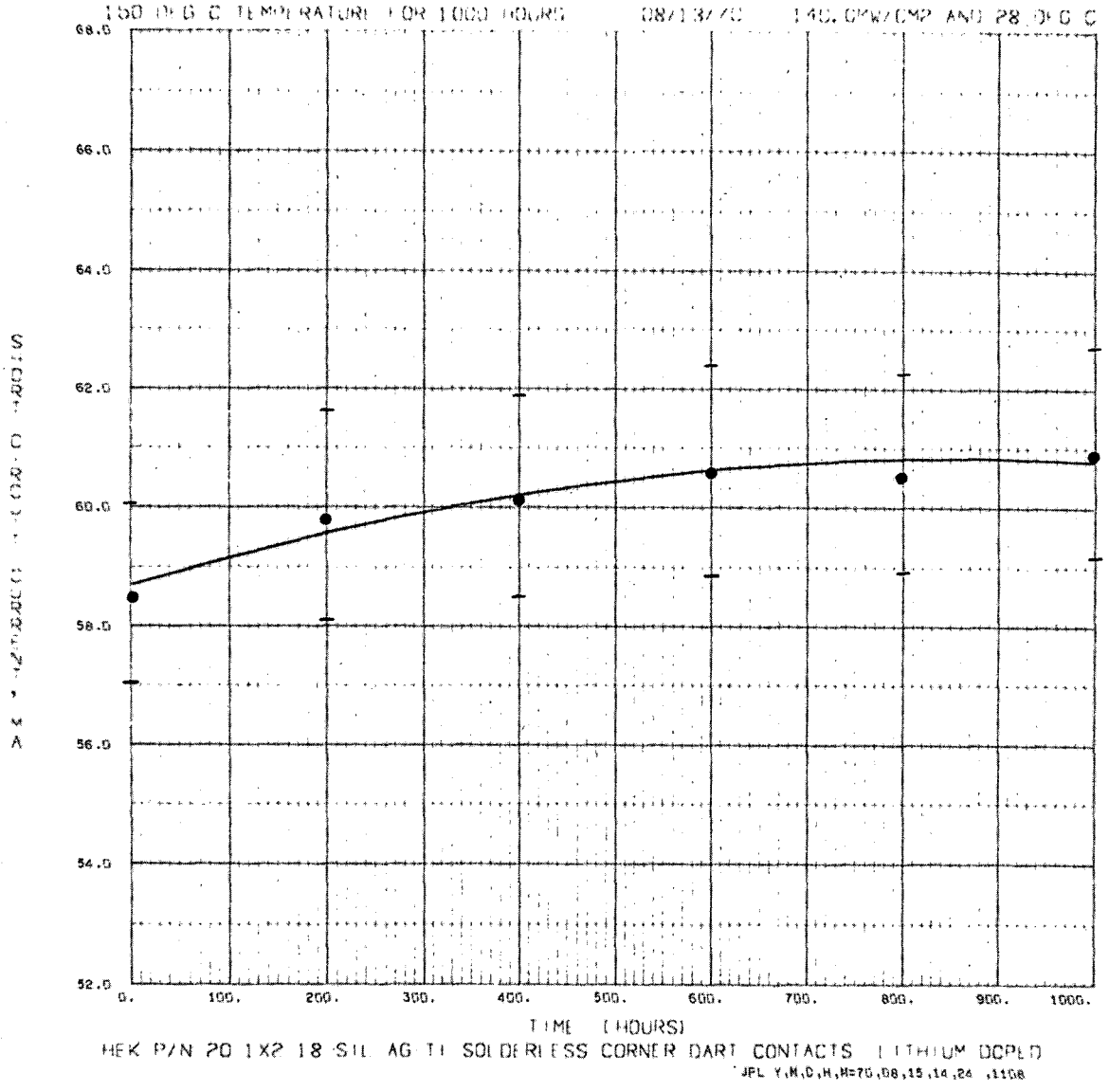


Fig. 16. Short-circuit current, cell type HL, as a function of time, 150°C storage

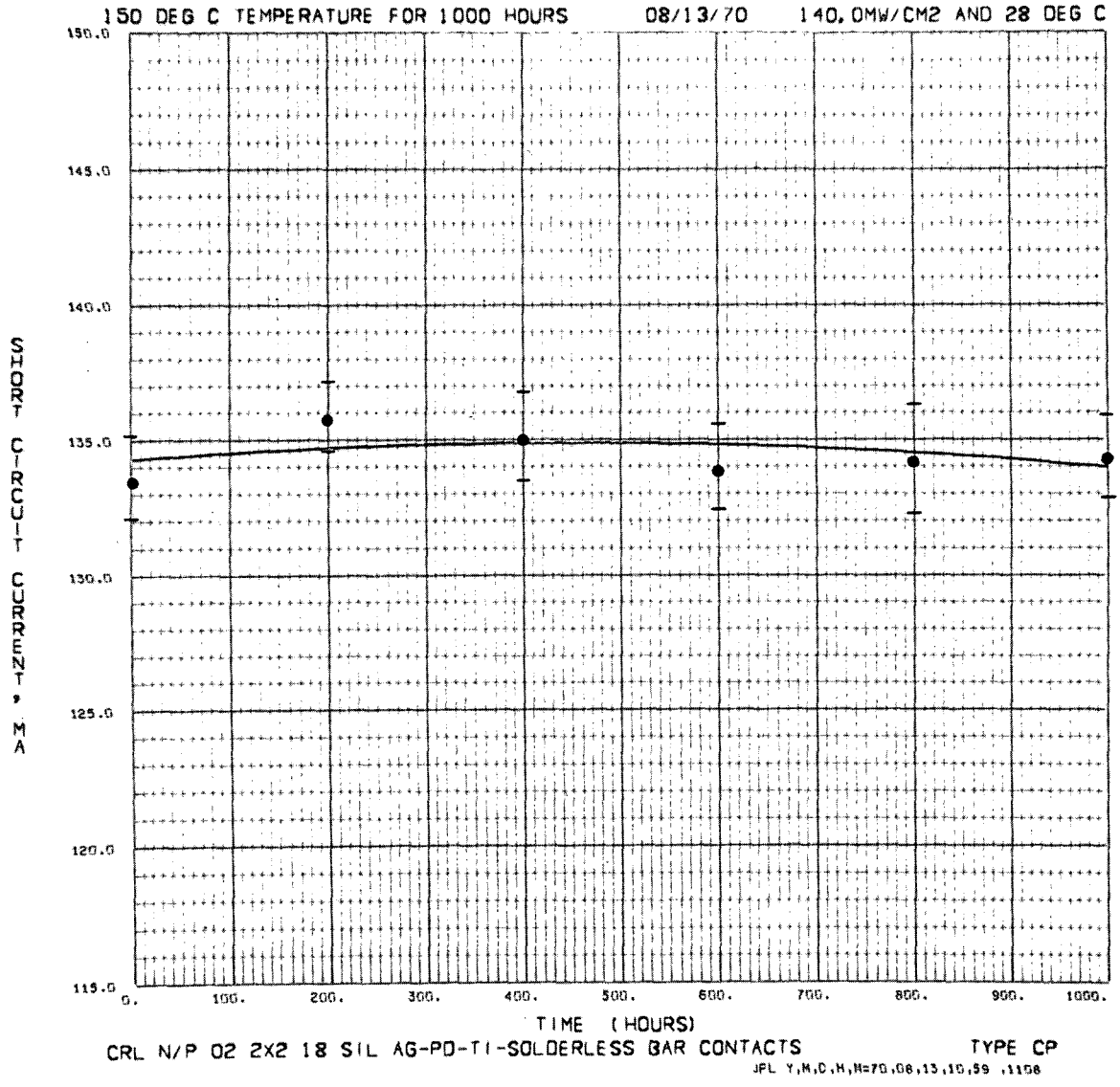


Fig. 17. Short-circuit current, cell type CP, as a function of time, 150 °C storage

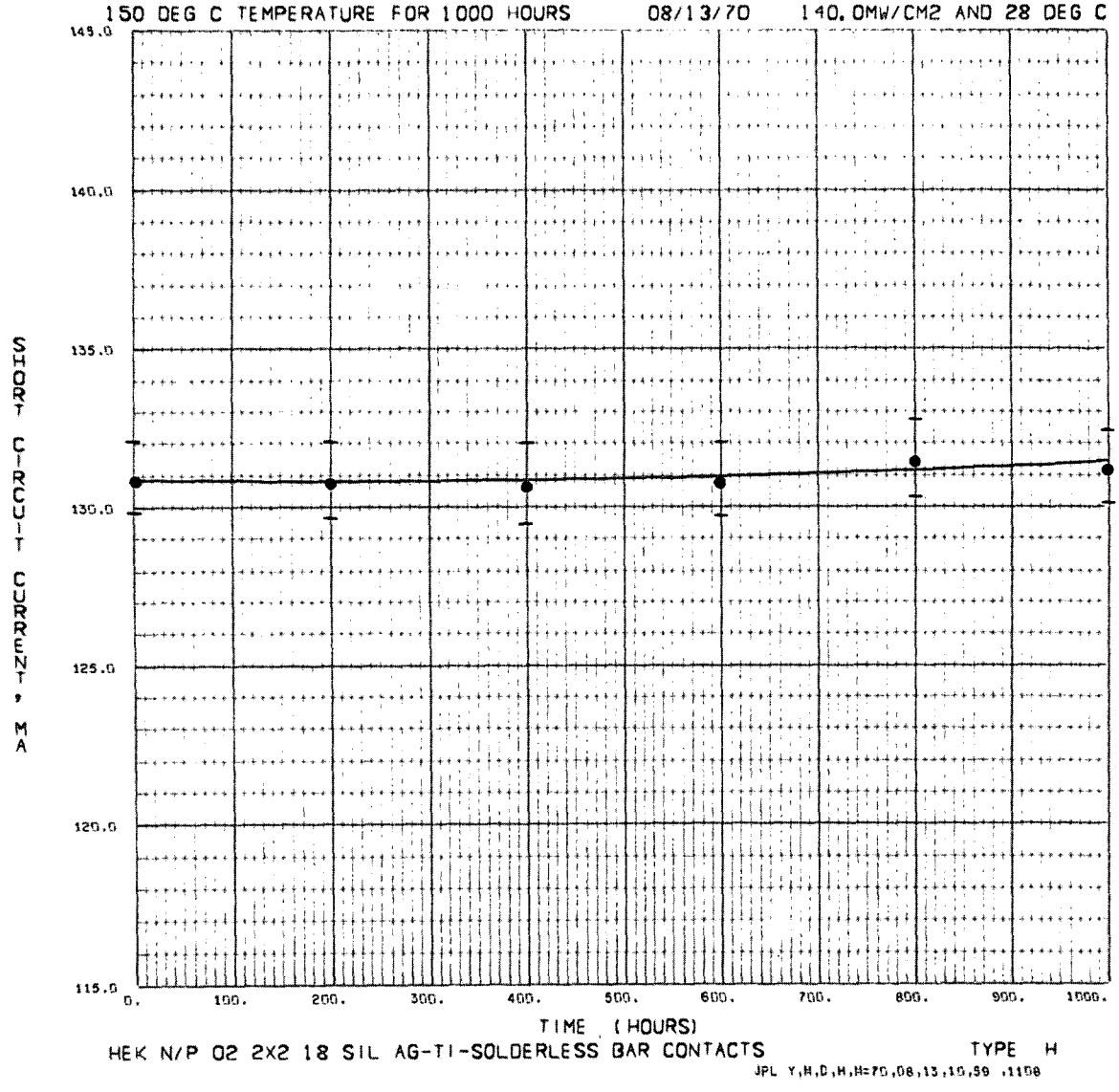


Fig. 18. Short-circuit current, cell type H, as a function of time, 150°C storage

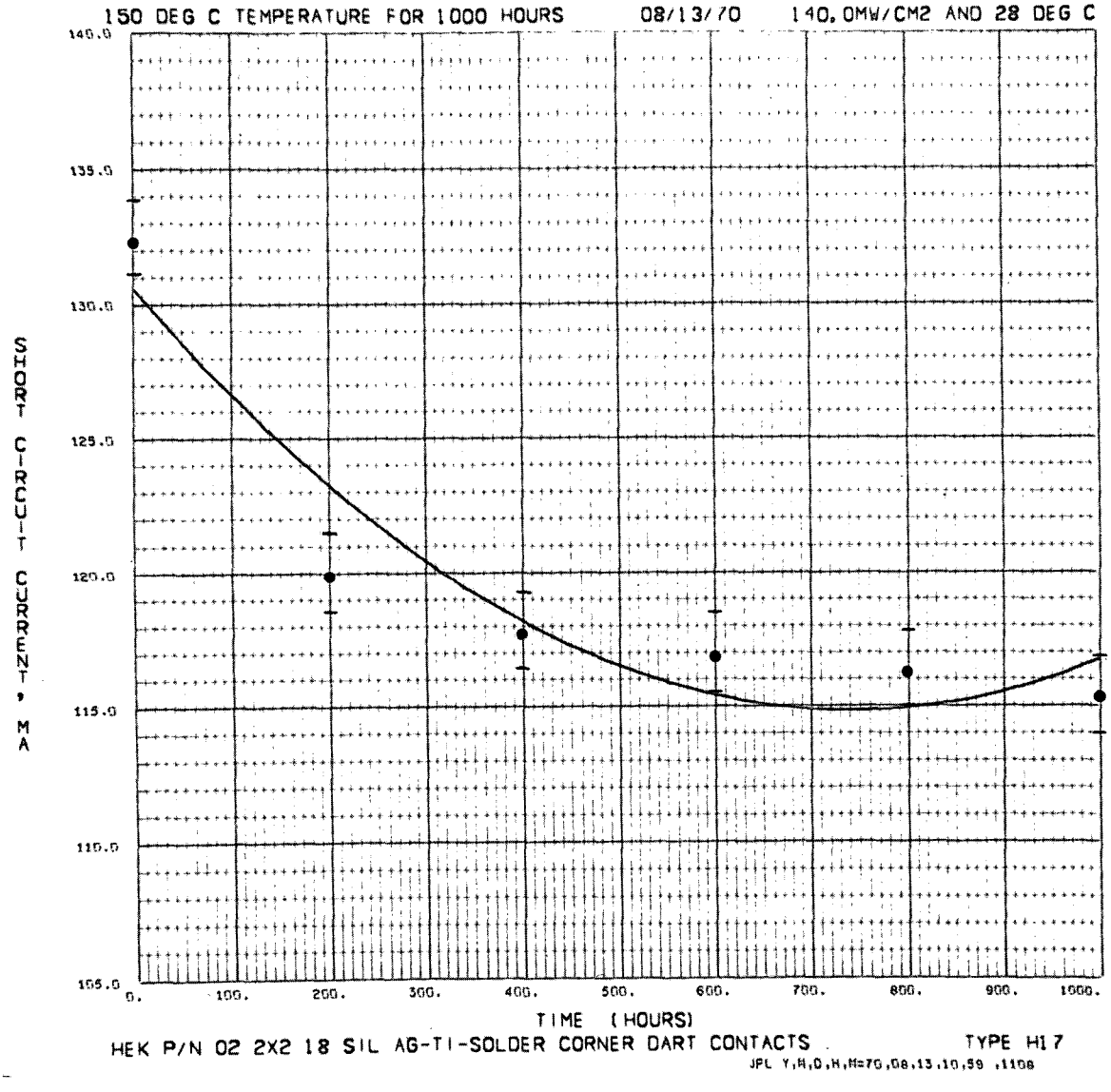


Fig. 19. Short-circuit current, cell type H-17, as a function of time, 150 °C storage

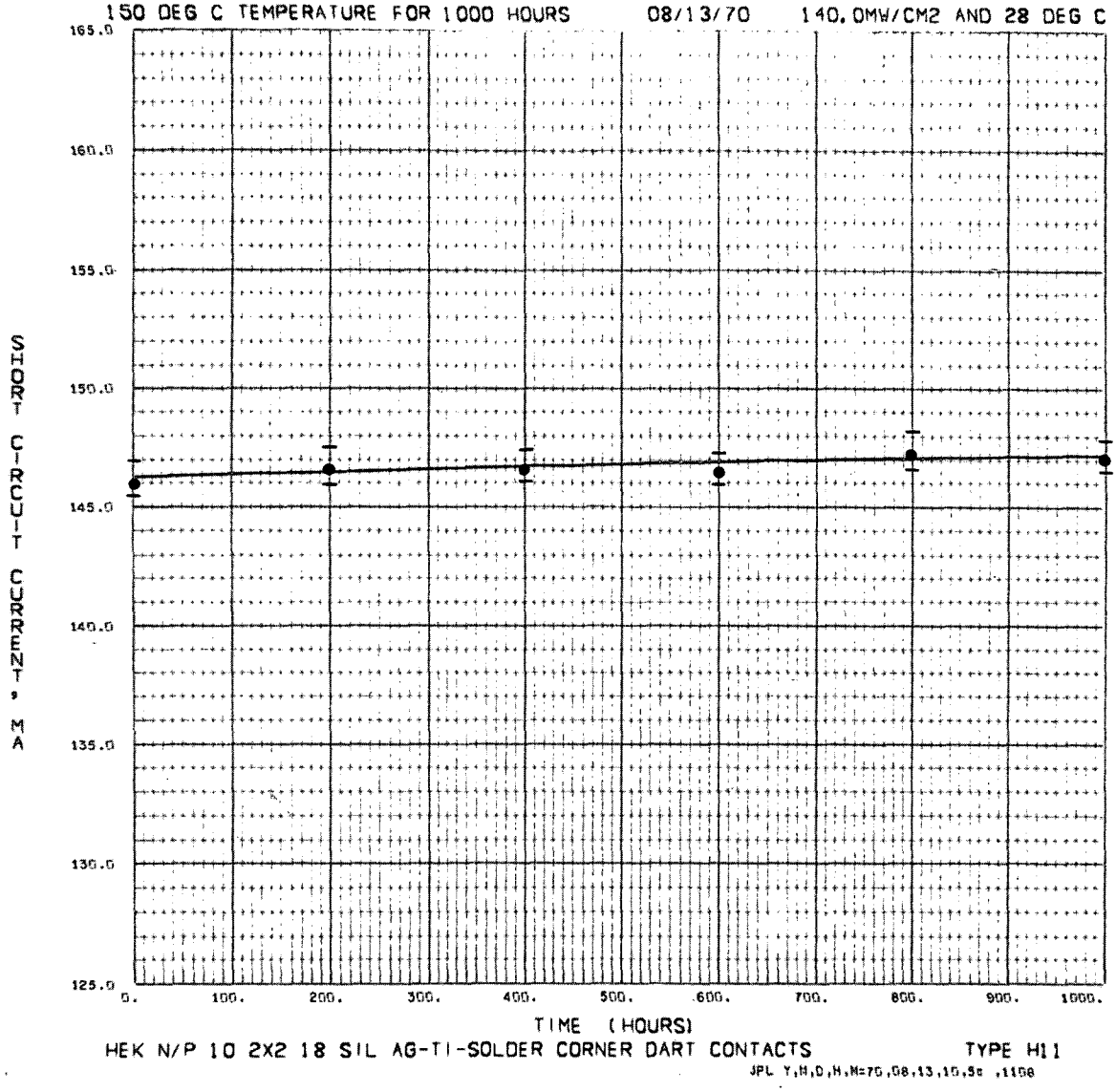


Fig. 20. Short-circuit current, cell type H-11, as a function of time, 150 °C storage

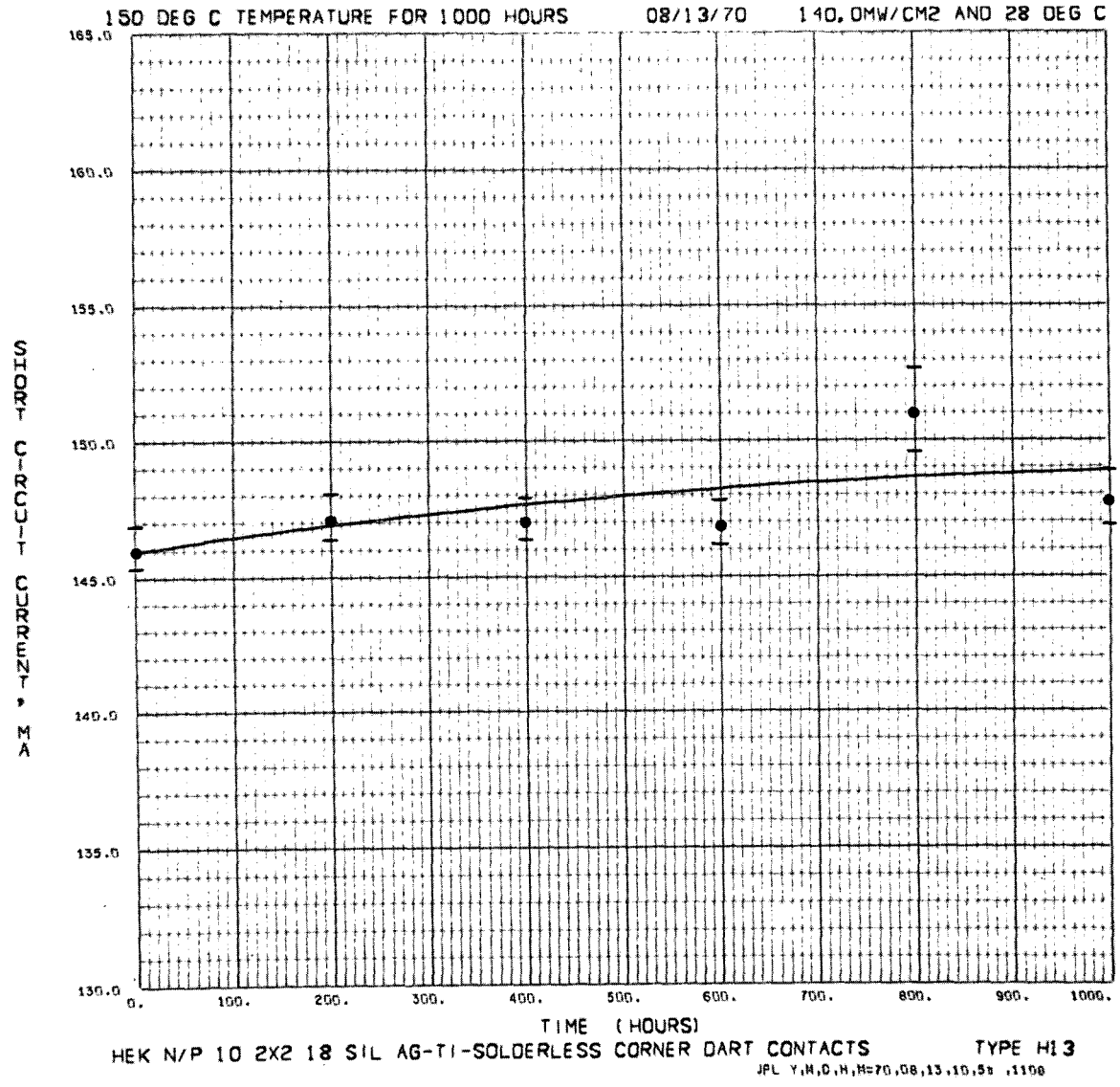


Fig. 21. Short-circuit current, cell type H-13, as a function of time, 150 °C storage

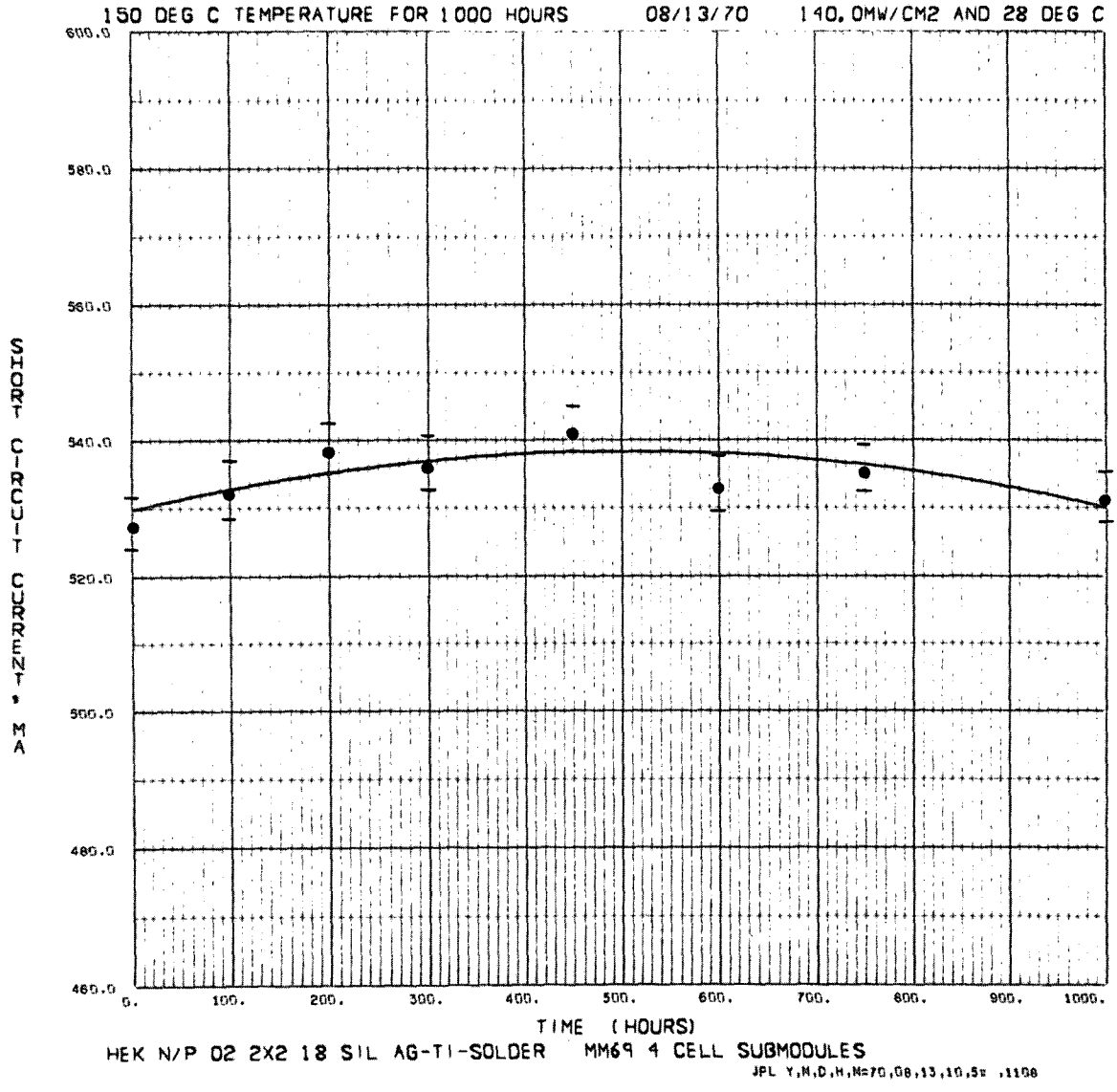


Fig. 22. Short-circuit current, cell type M69 module, as a function of time, 150 °C storage

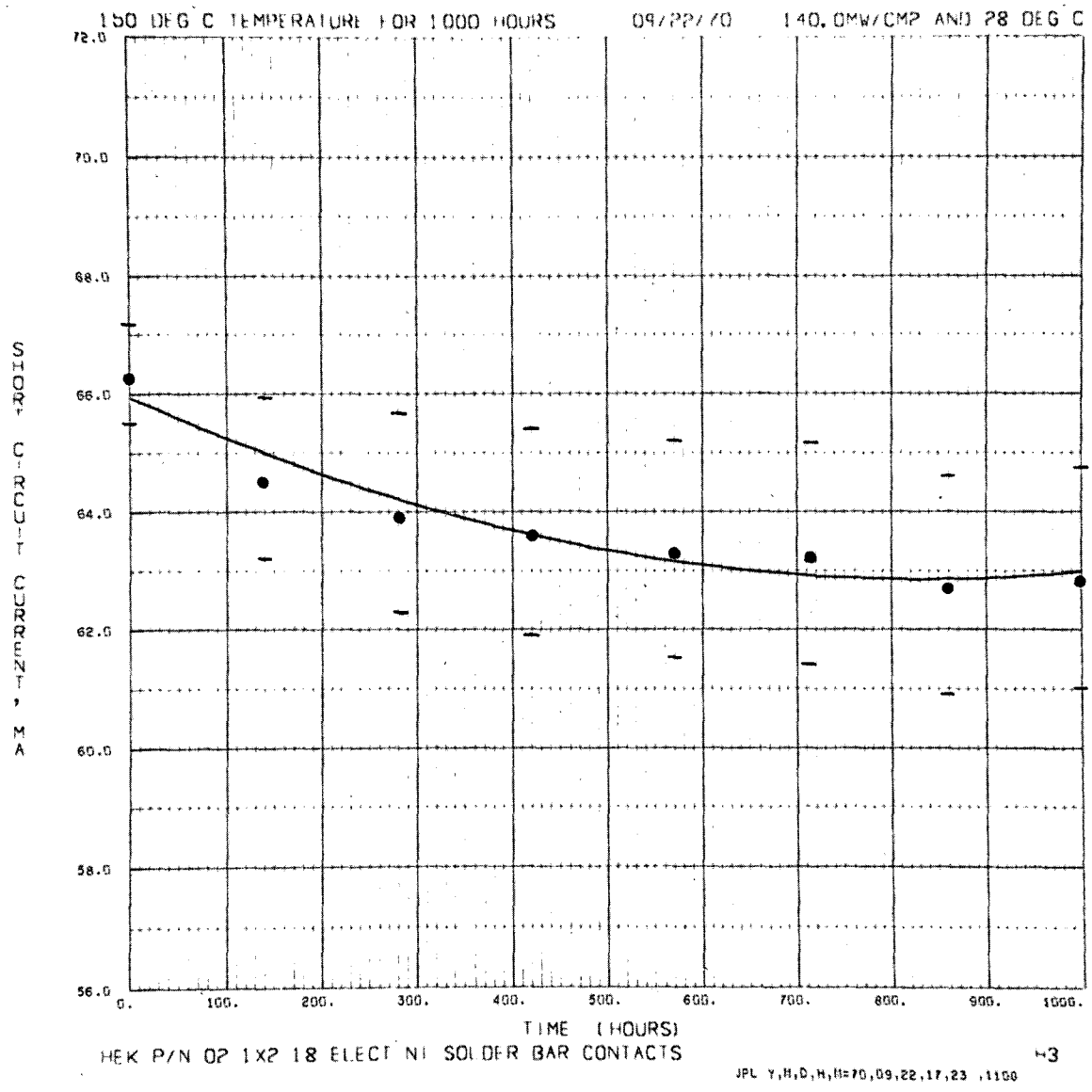


Fig. 23. Short-circuit current, cell type H-3, as a function of time, 150 °C storage

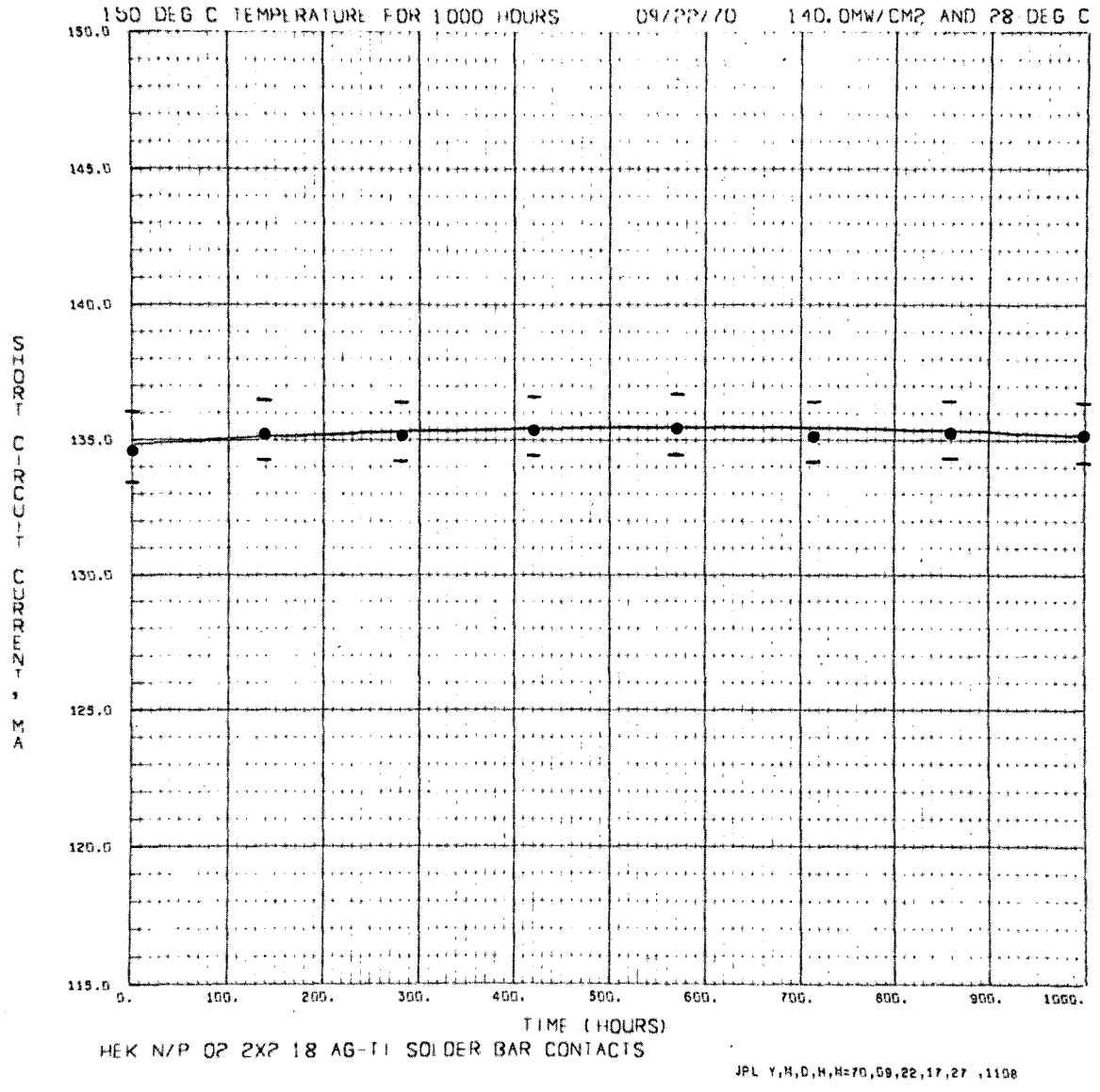


Fig. 24. Short-circuit current, cell type M, as a function of time, 150 °C storage

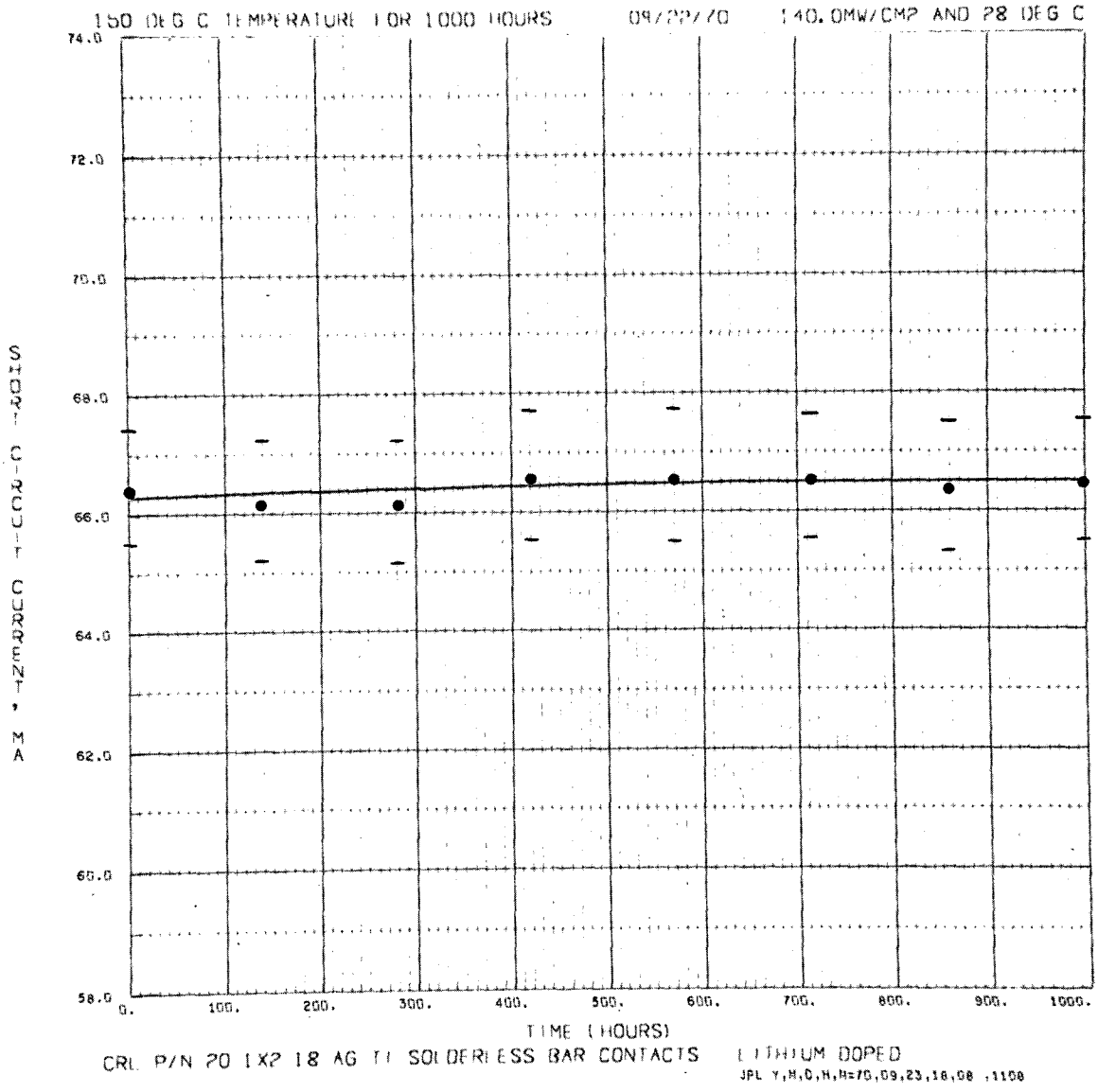


Fig. 25. Short-circuit current, cell type CL, as a function of time, 150 °C storage

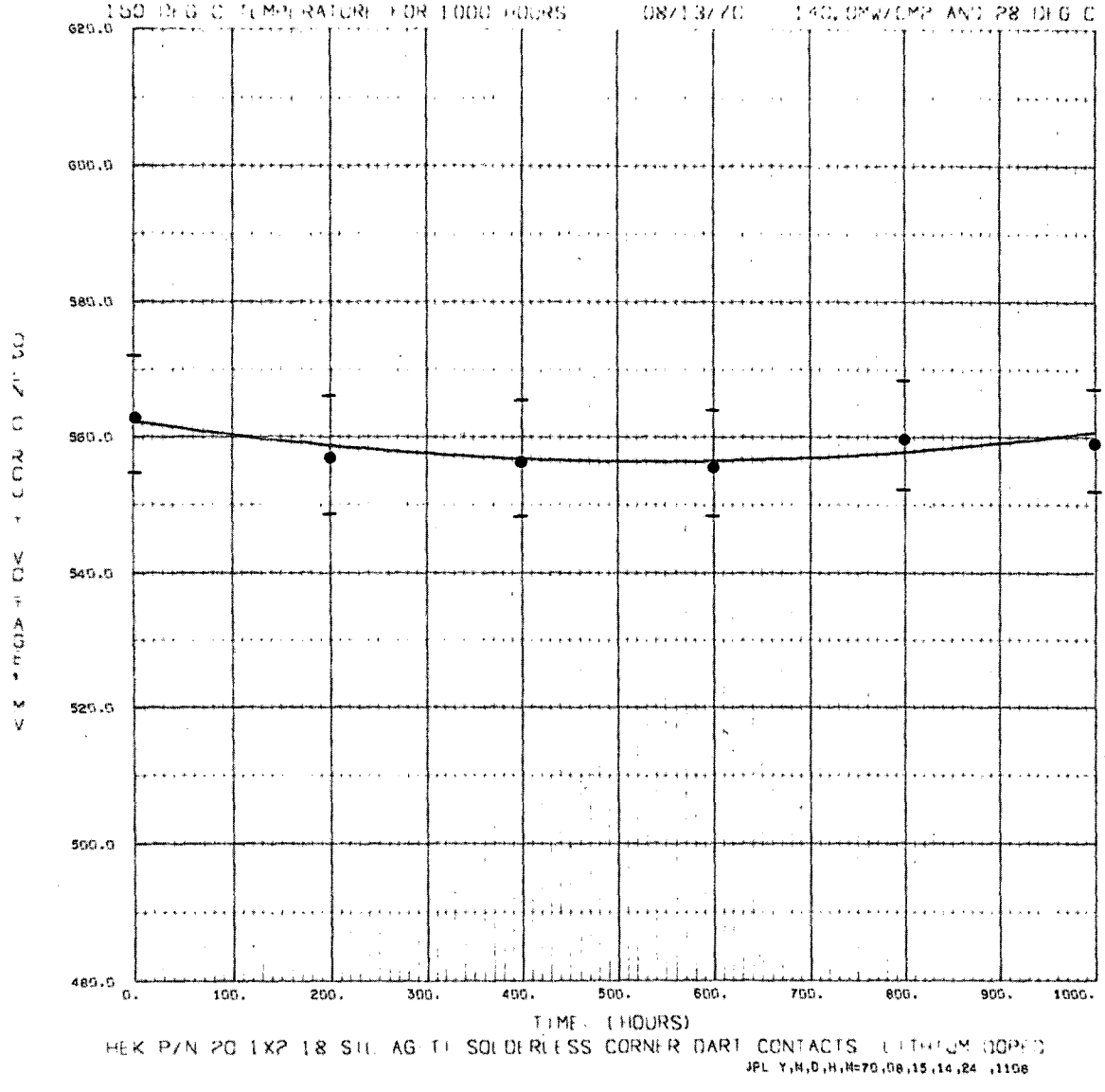


Fig. 26. Open-circuit voltage, cell type HL, as a function of time, 150 °C storage

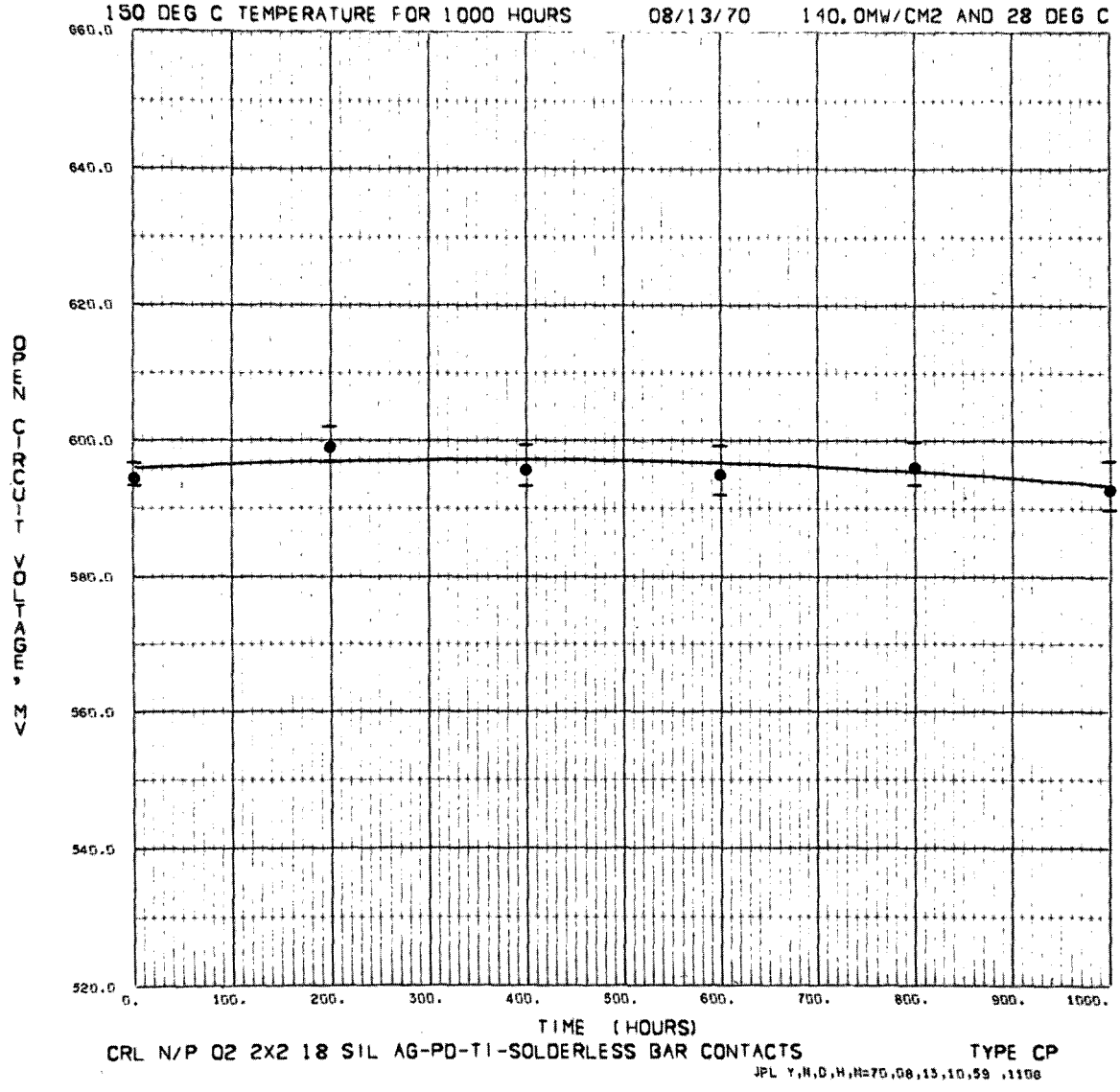


Fig. 27. Open-circuit voltage, cell type CP, as a function of time, 150°C storage

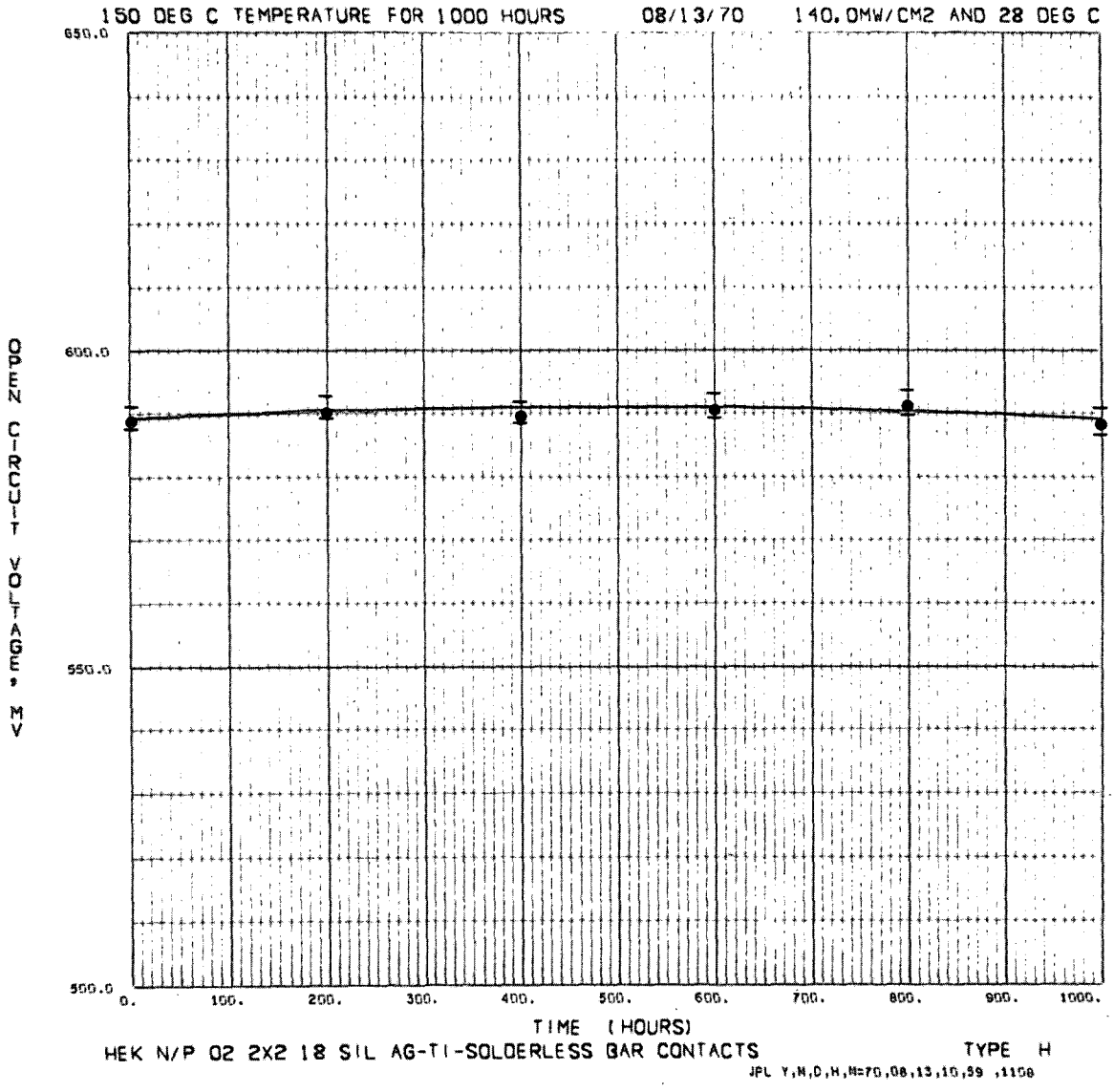


Fig. 28. Open-circuit voltage, cell type H, as a function of time, 150 °C storage

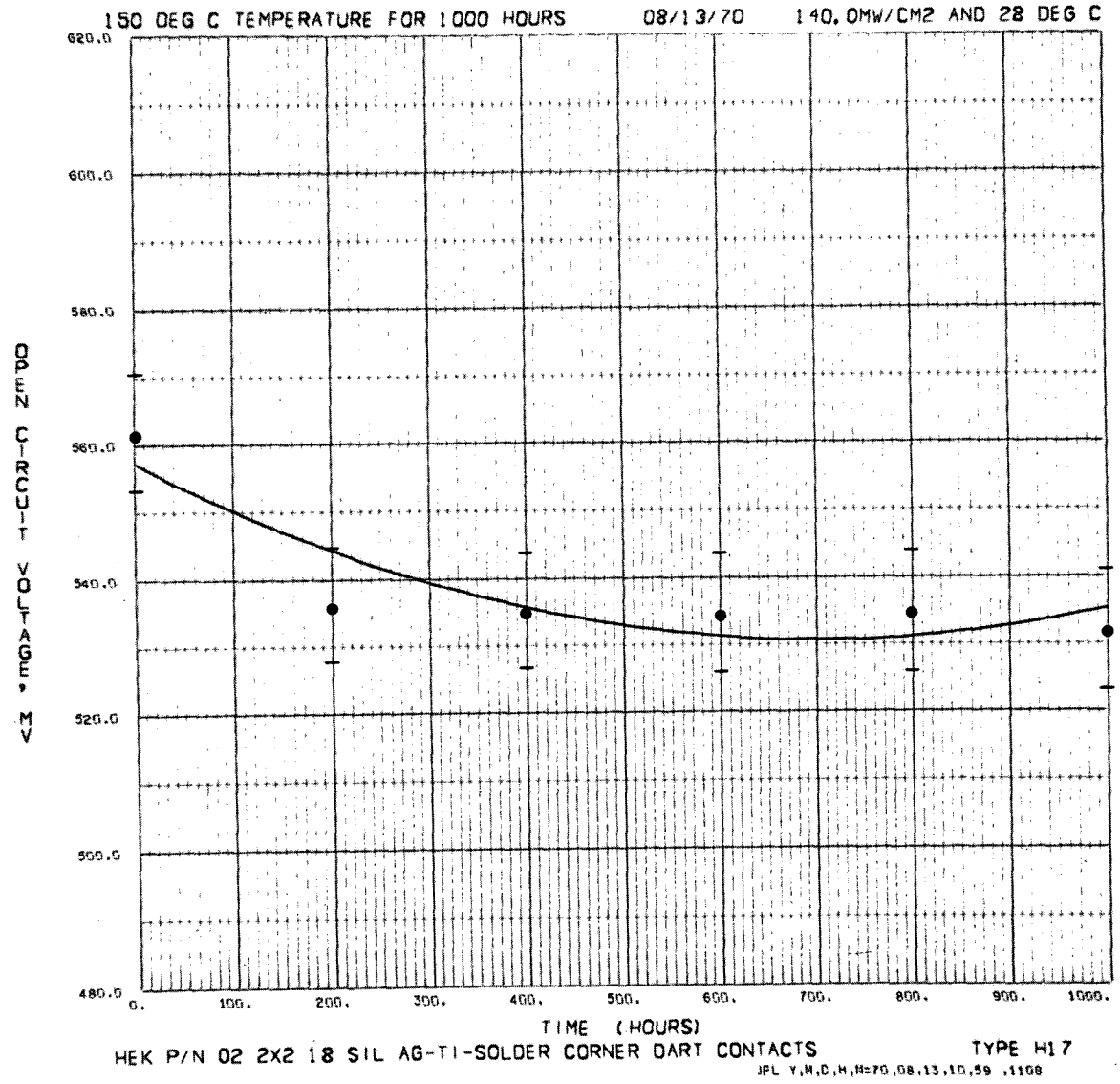


Fig. 29. Open-circuit voltage, cell type H-17, as a function of time, 150 °C storage

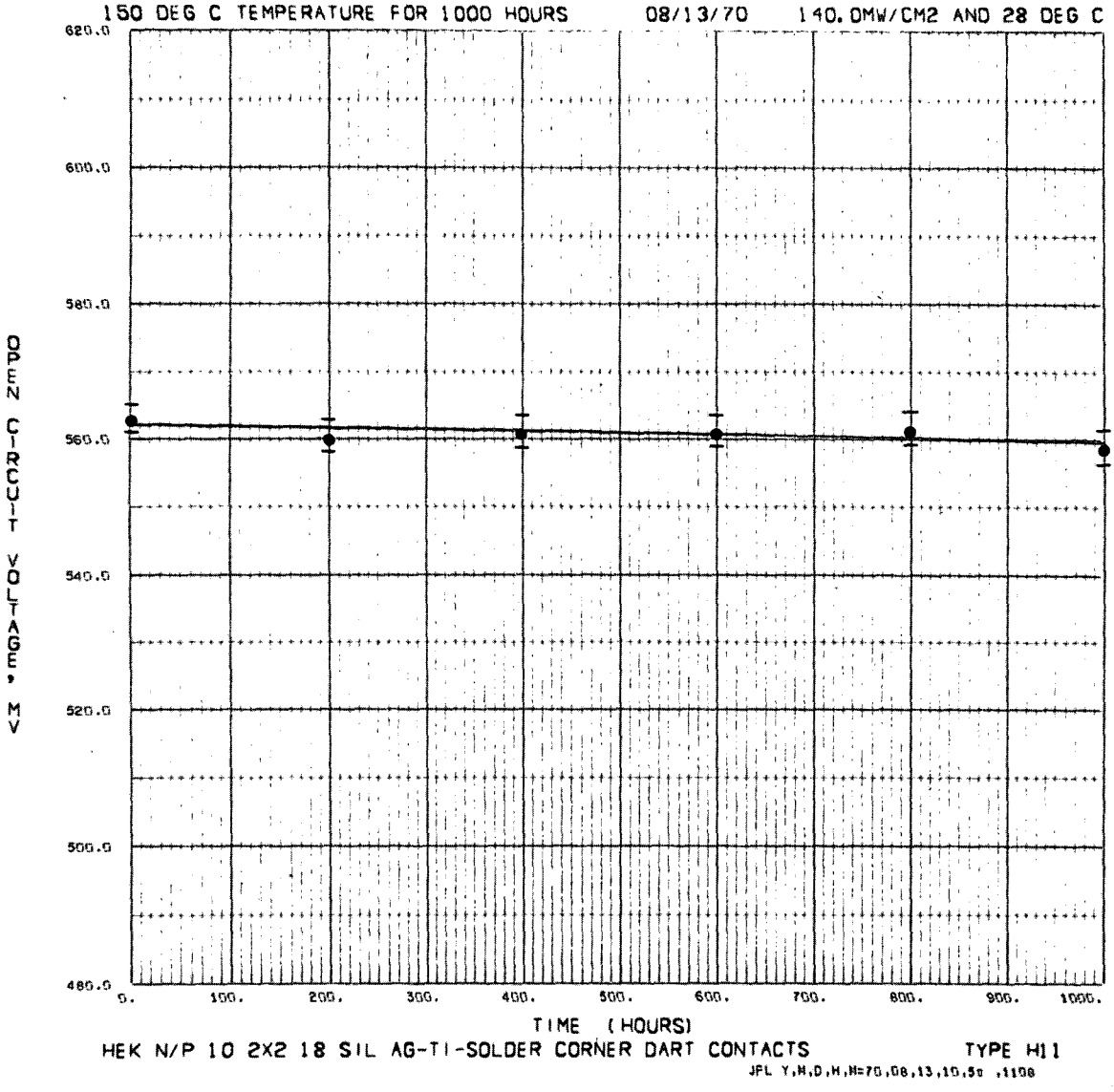


Fig. 30. Open-circuit voltage, cell type H-11, as a function of time, 150°C storage

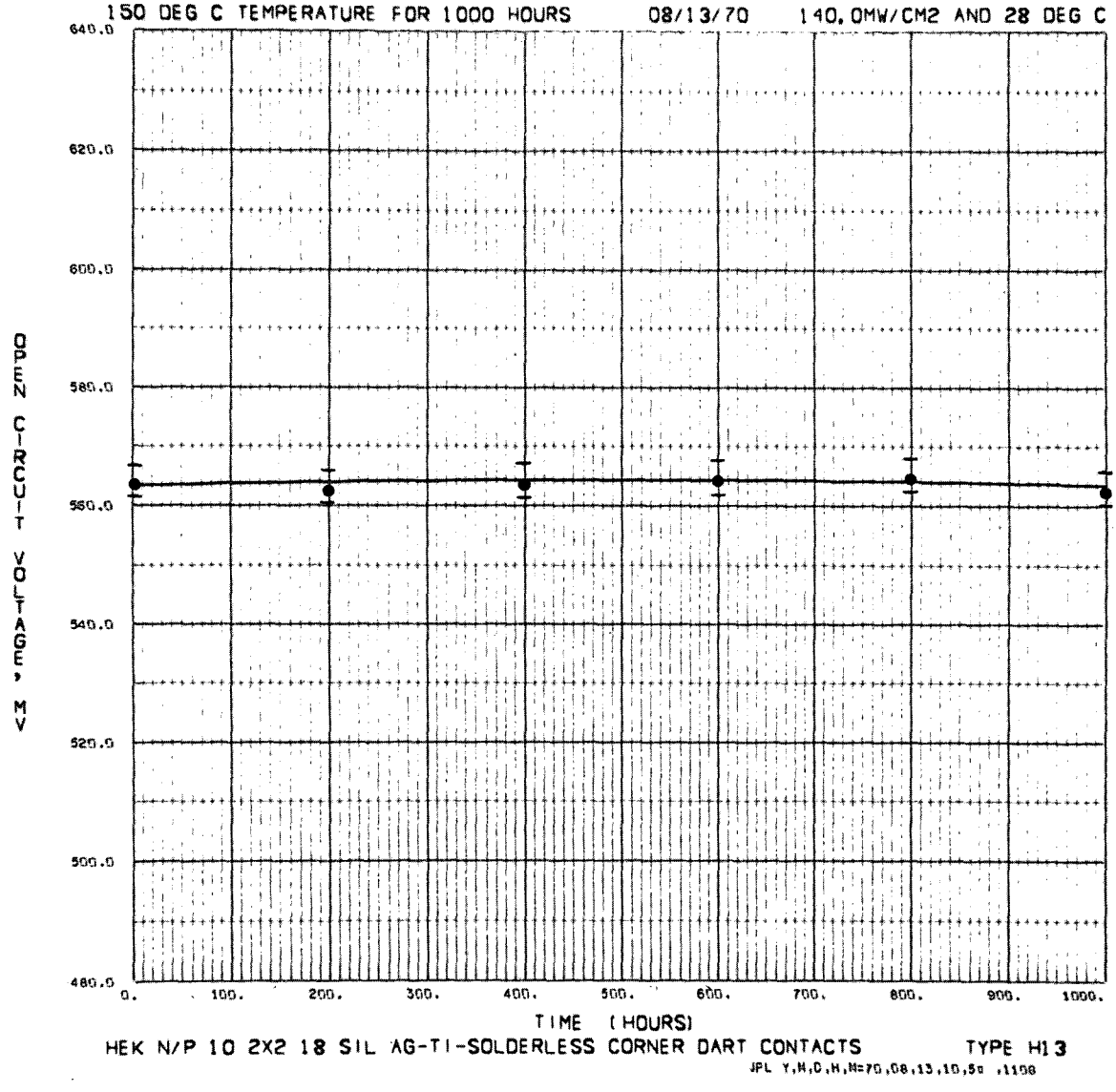


Fig. 31. Open-circuit voltage, cell type H-13, as a function of time, 150°C storage

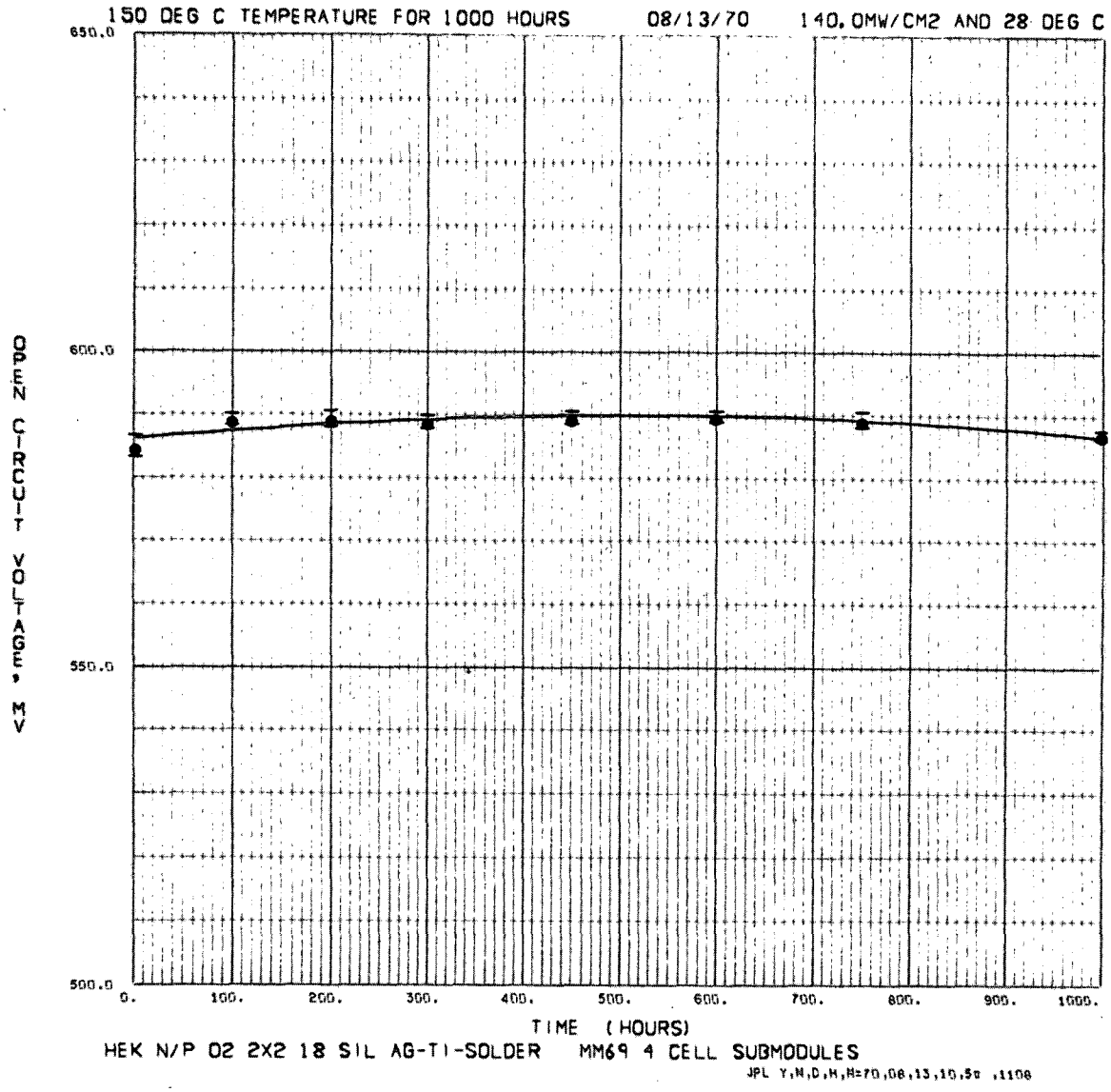


Fig. 32. Open-circuit voltage, cell type M69 module, as a function of time, 150 °C storage

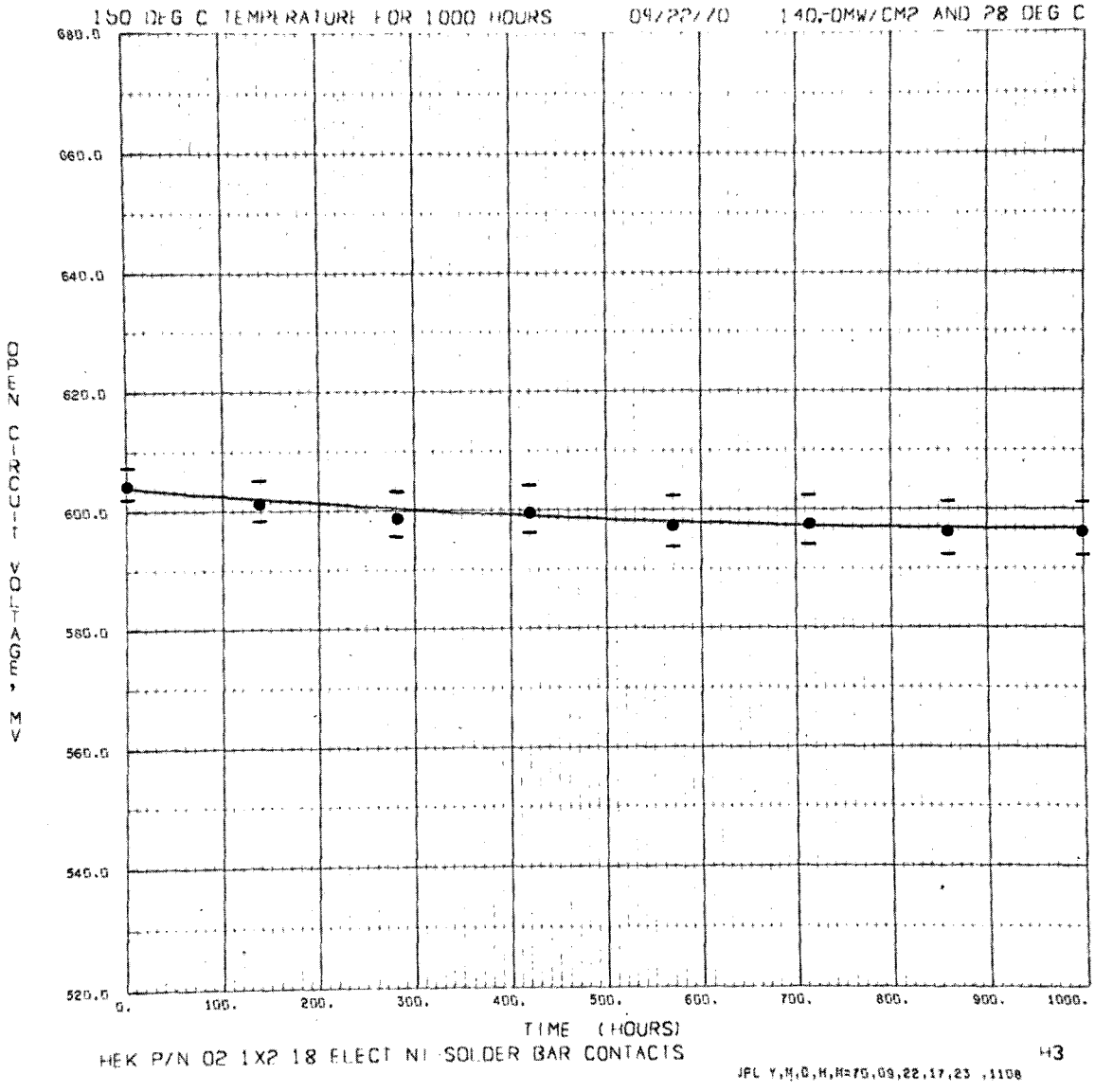


Fig. 33. Open-circuit voltage, cell type H-3, as a function of time, 150 °C storage

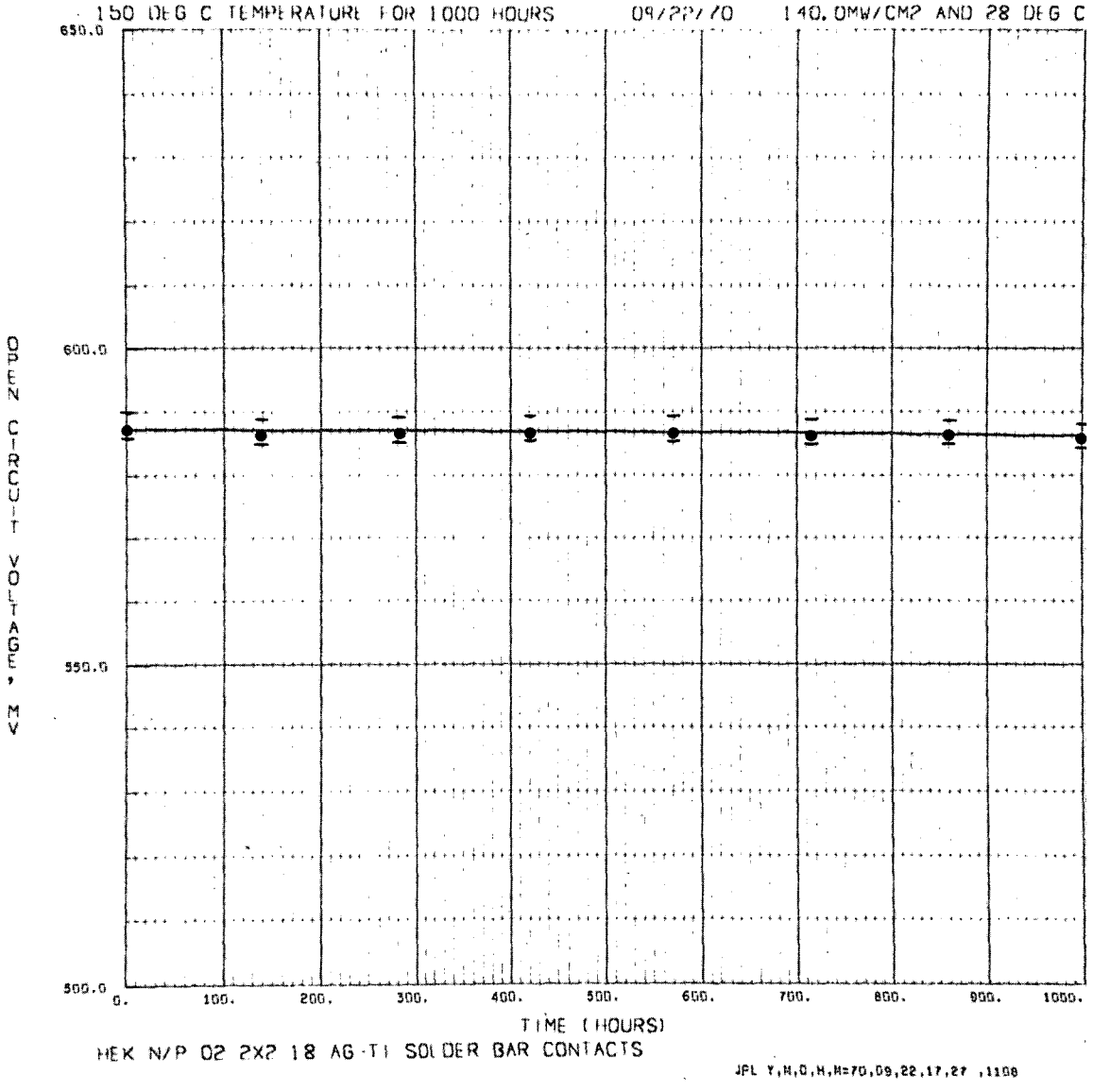


Fig. 34. Open-circuit voltage, cell type M, as a function of time, 150 °C storage

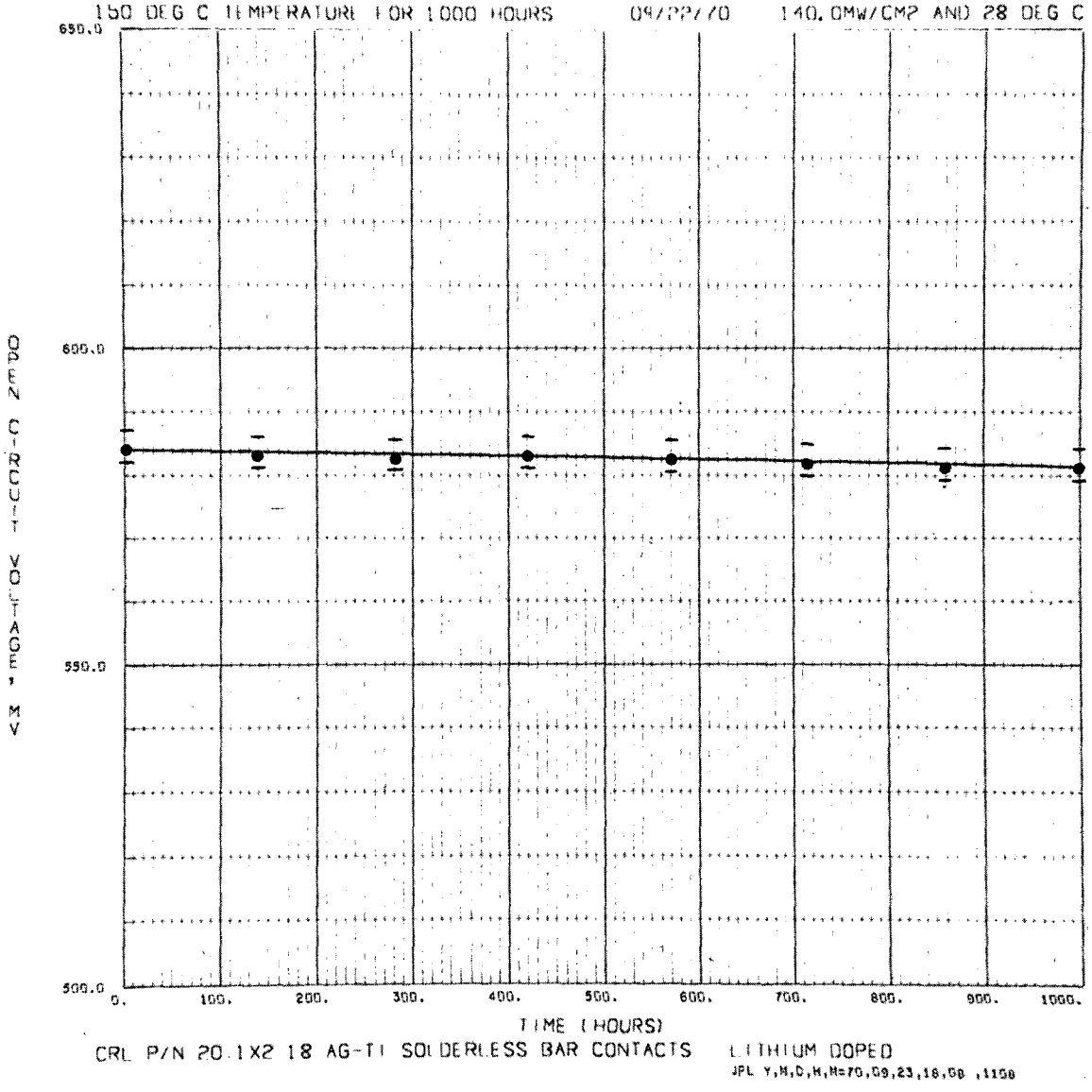


Fig. 35. Open-circuit voltage, cell type CL, as a function of time, 150 °C storage

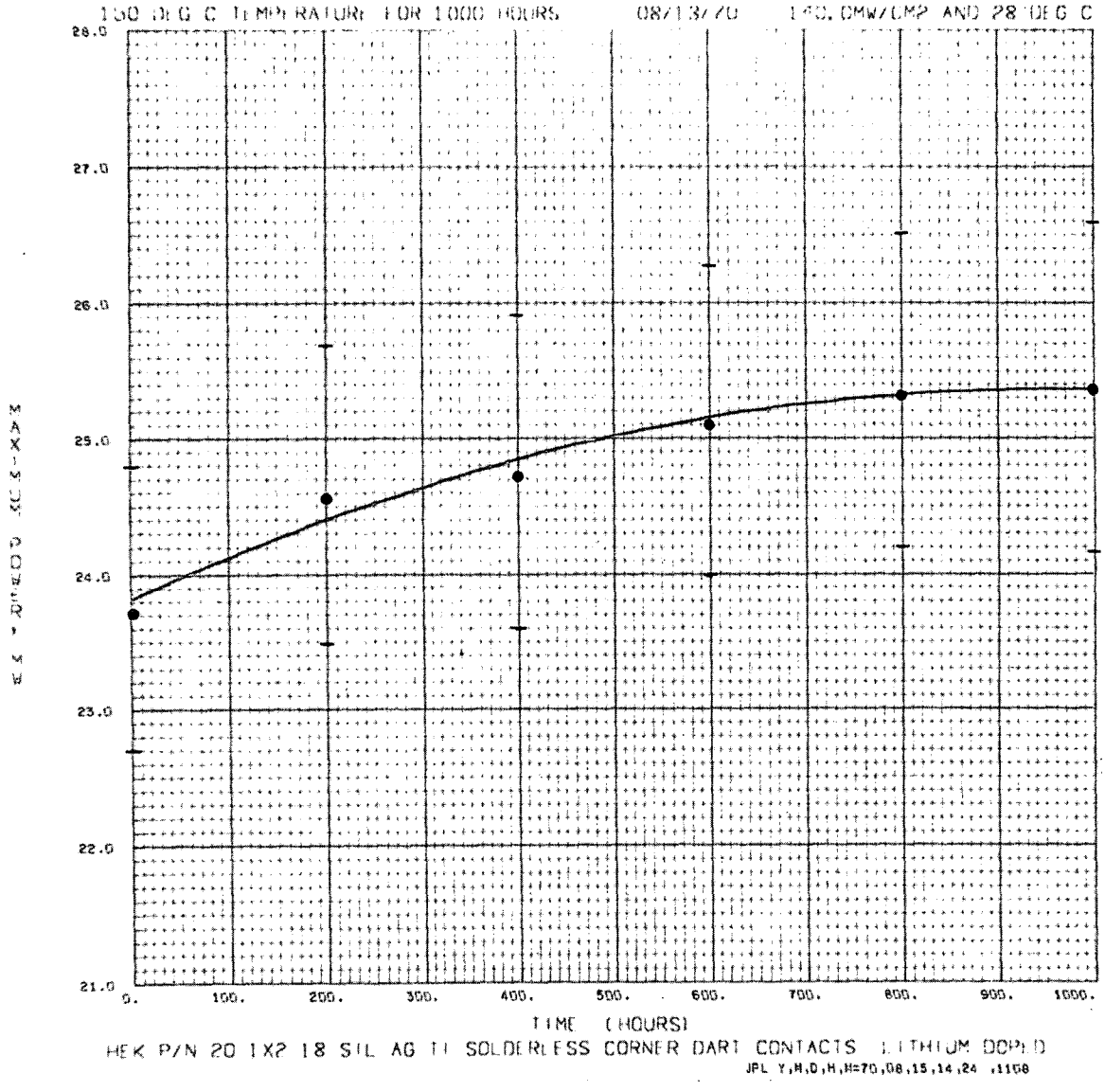


Fig. 36. Maximum-power voltage, cell type HL, as a function of time, 150 °C storage

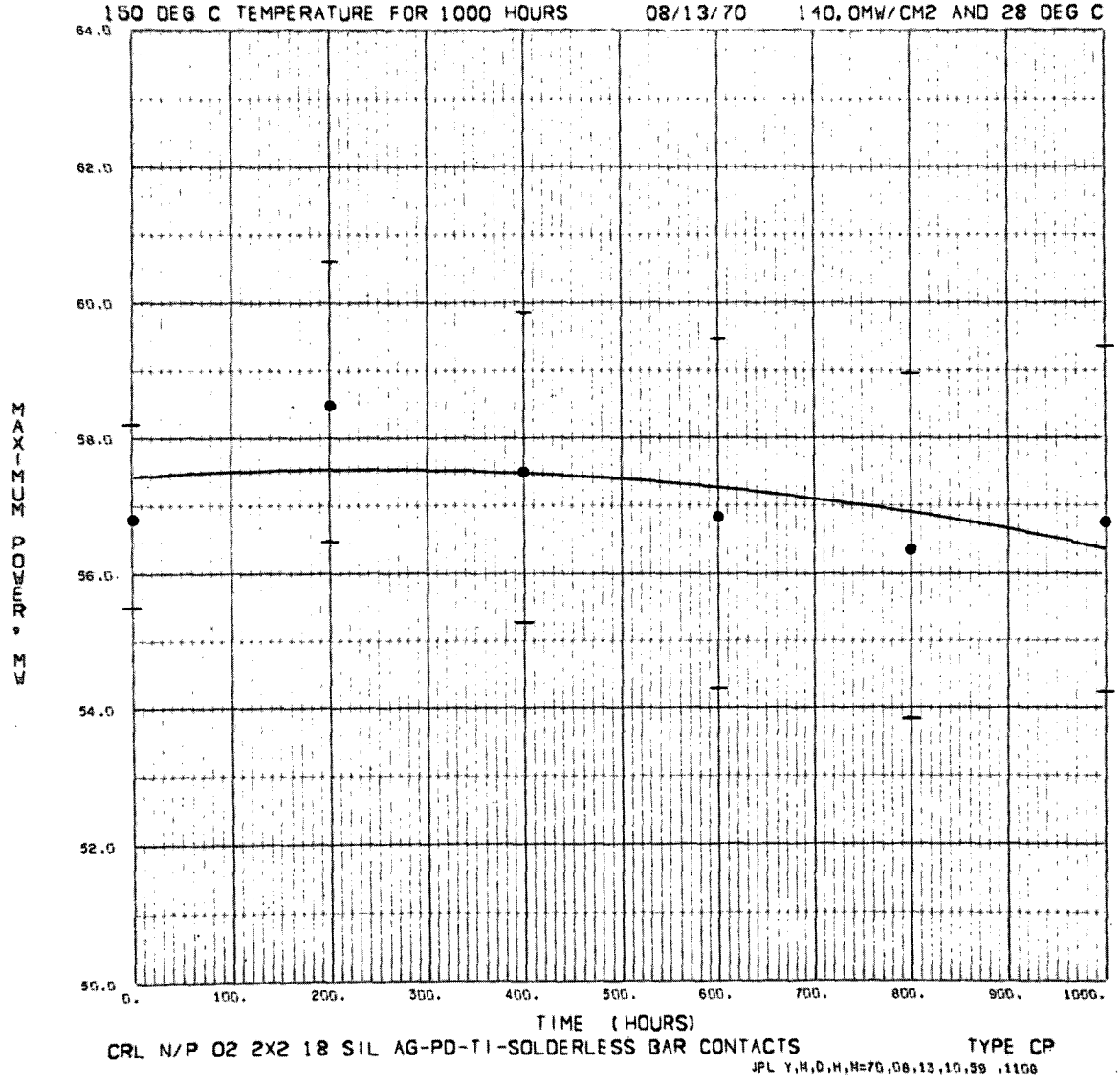


Fig. 37. Maximum-power voltage, cell type CP, as a function of time, 150 °C storage

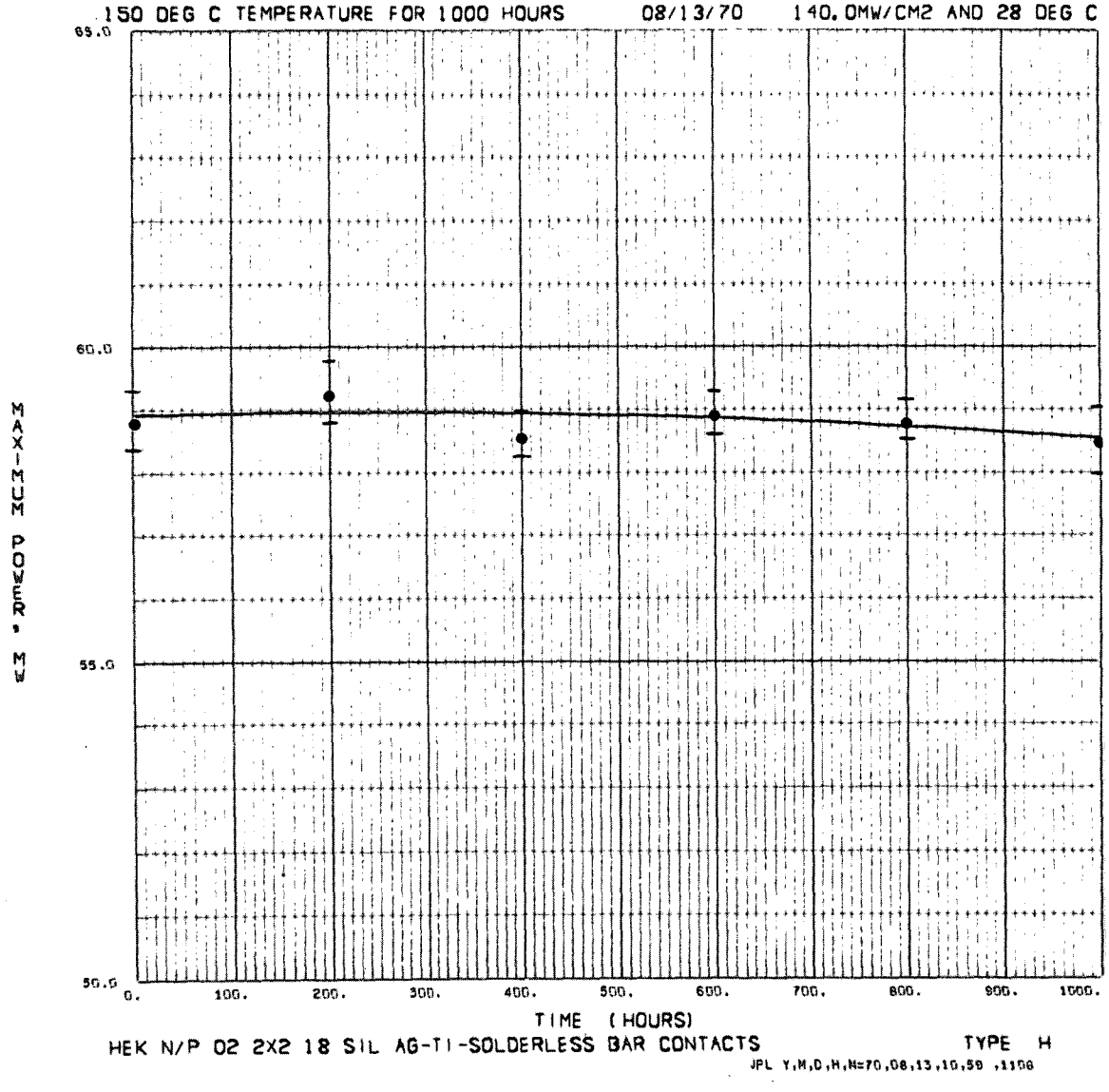


Fig. 38. Maximum-power voltage, cell type H, as a function of time, 150°C storage

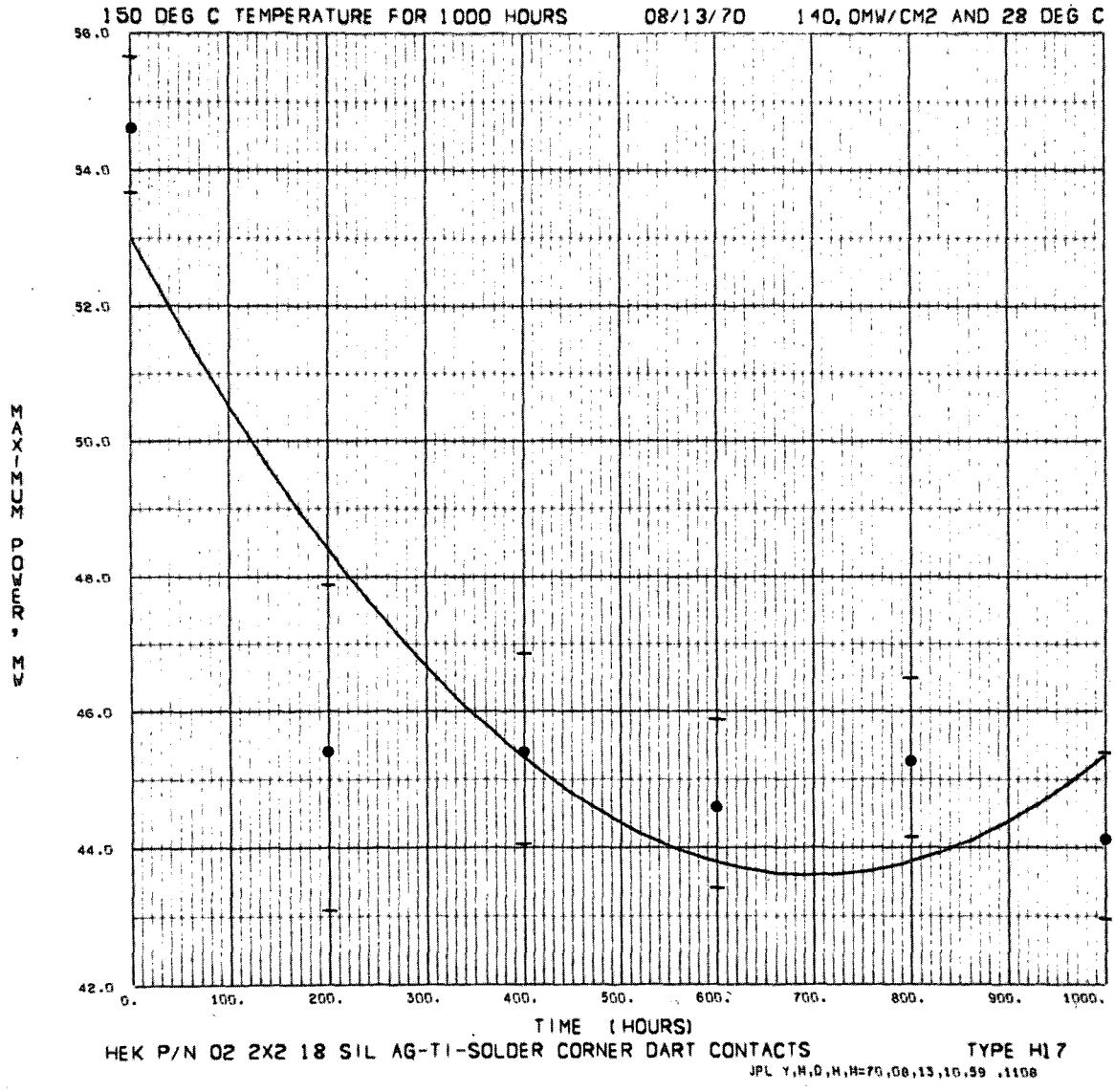


Fig. 39. Maximum-power voltage, cell type H-17, as a function of time, 150 °C storage

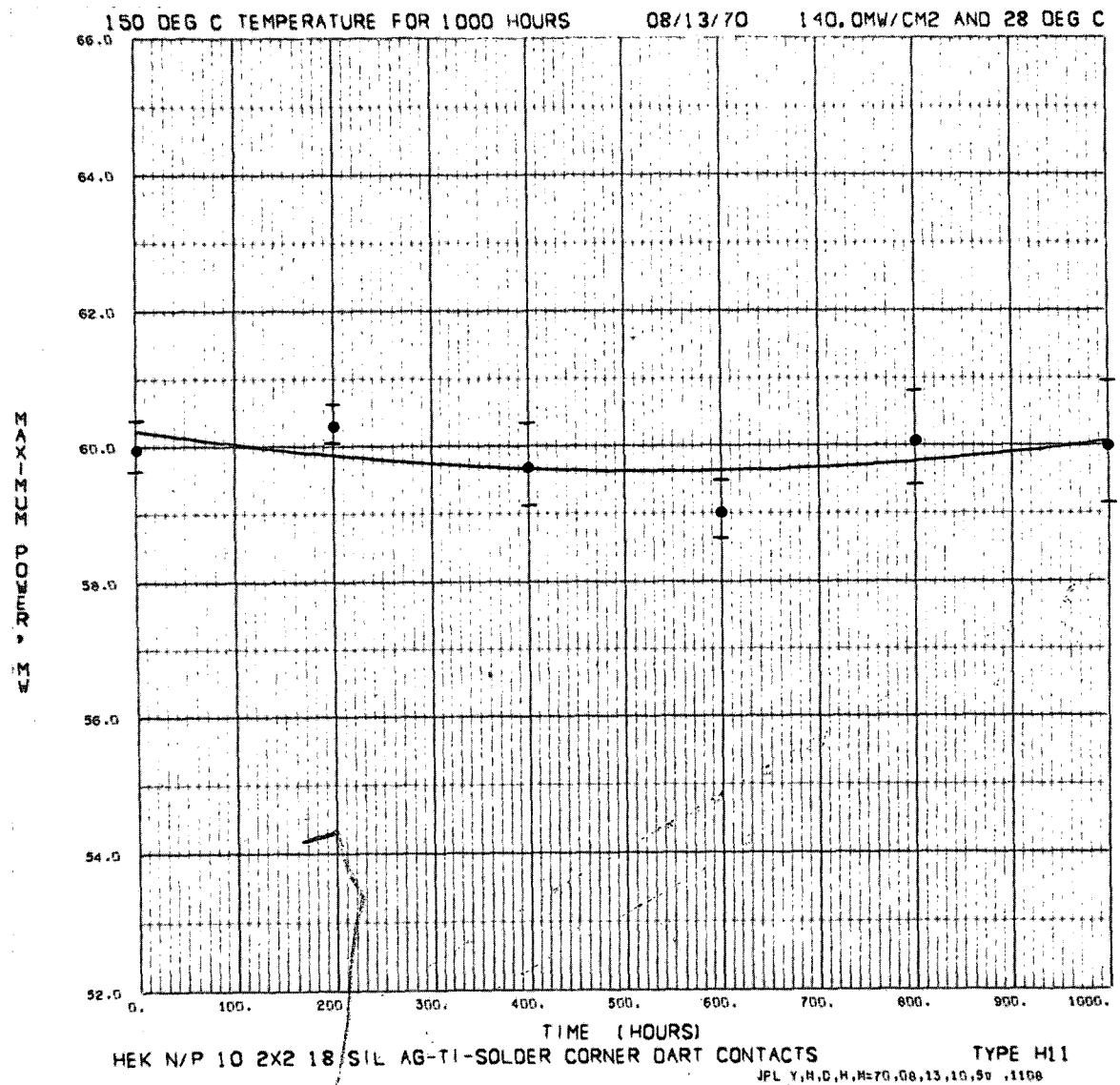


Fig. 40. Maximum-power voltage, cell type H-11, as a function of time, 150 °C storage

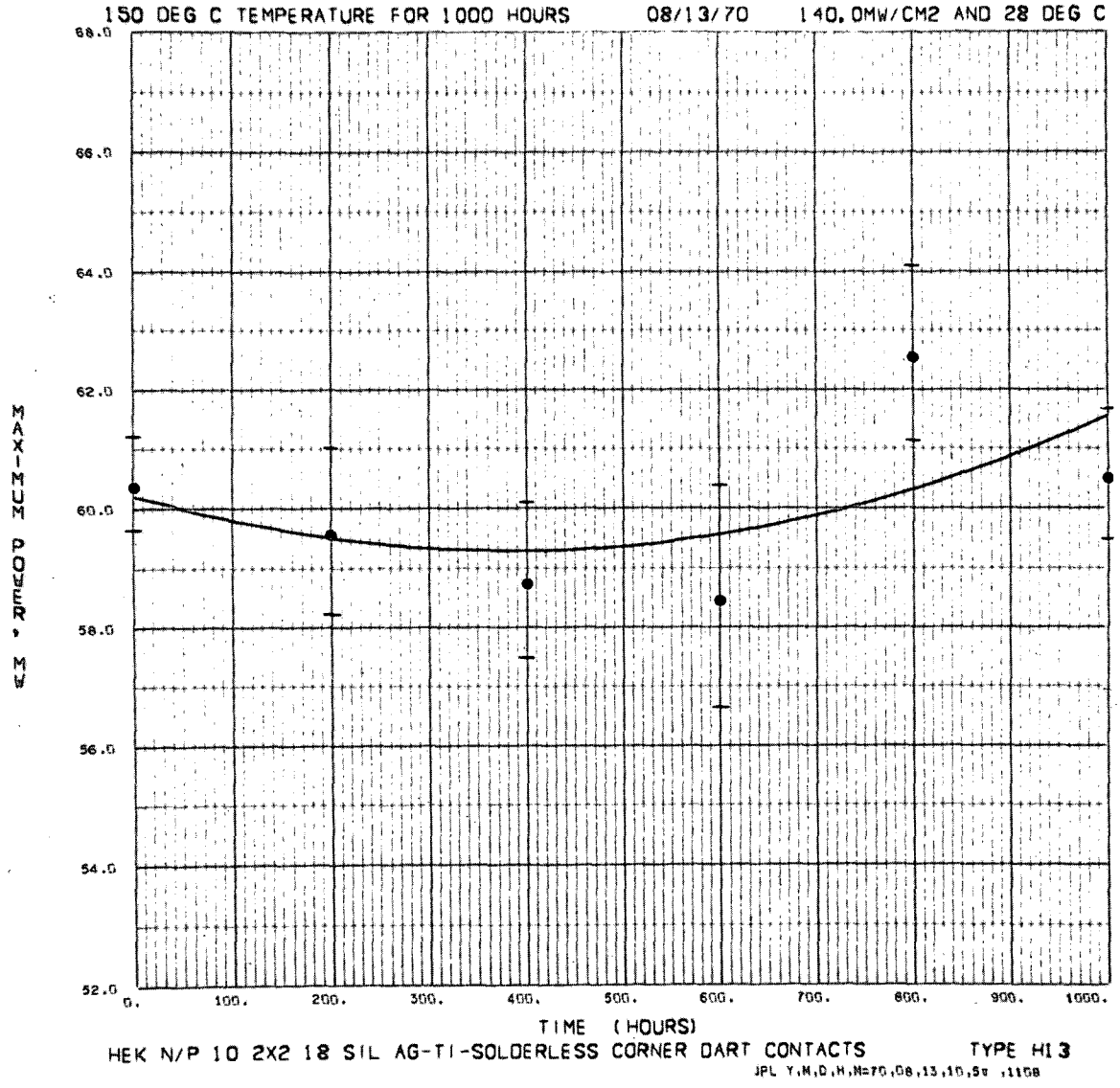


Fig. 41. Maximum-power voltage, cell type H-13, as a function of time, 150°C storage

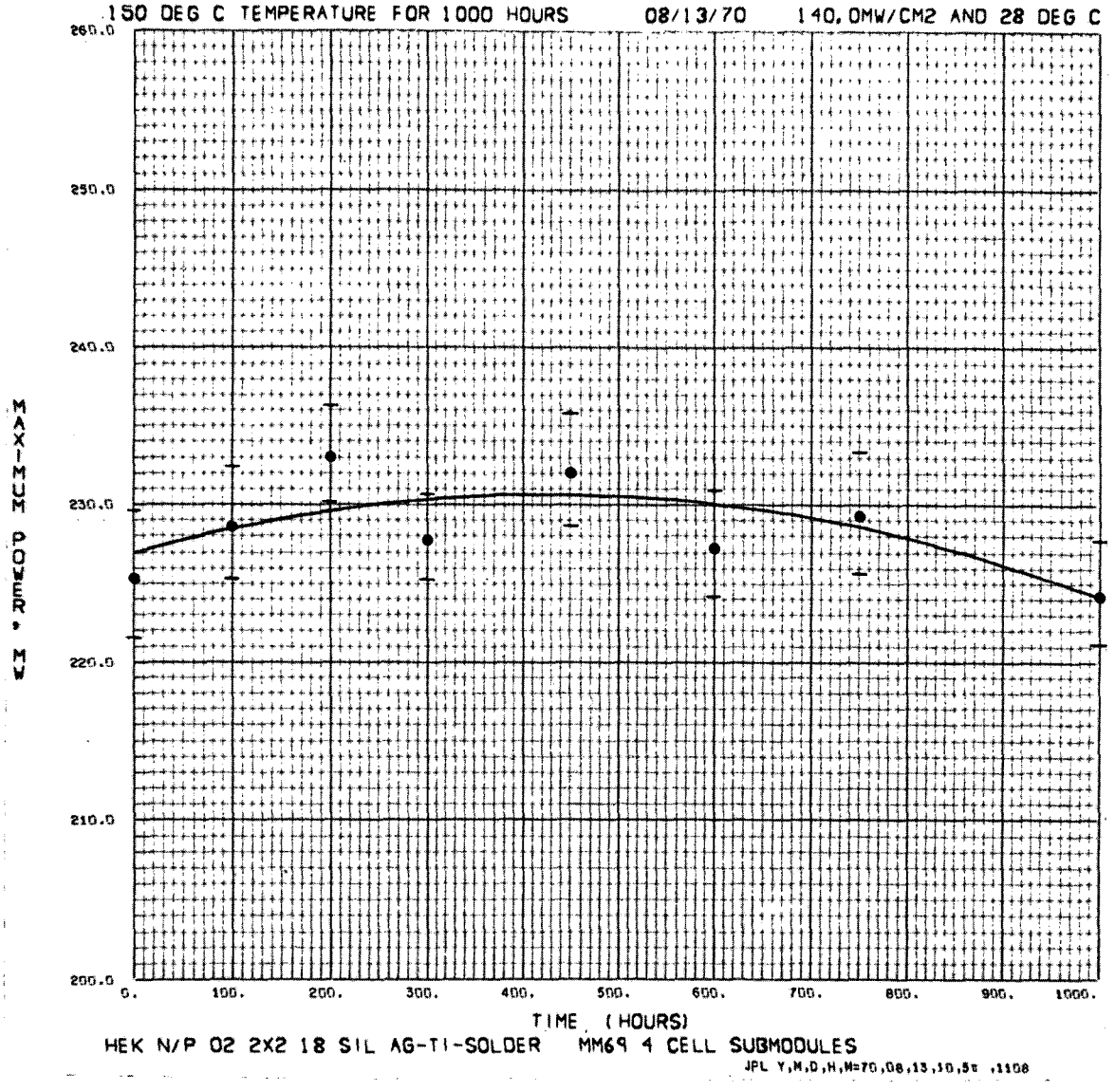


Fig. 42. Maximum-power voltage, cell type M69 module, as a function of time, 150°C storage

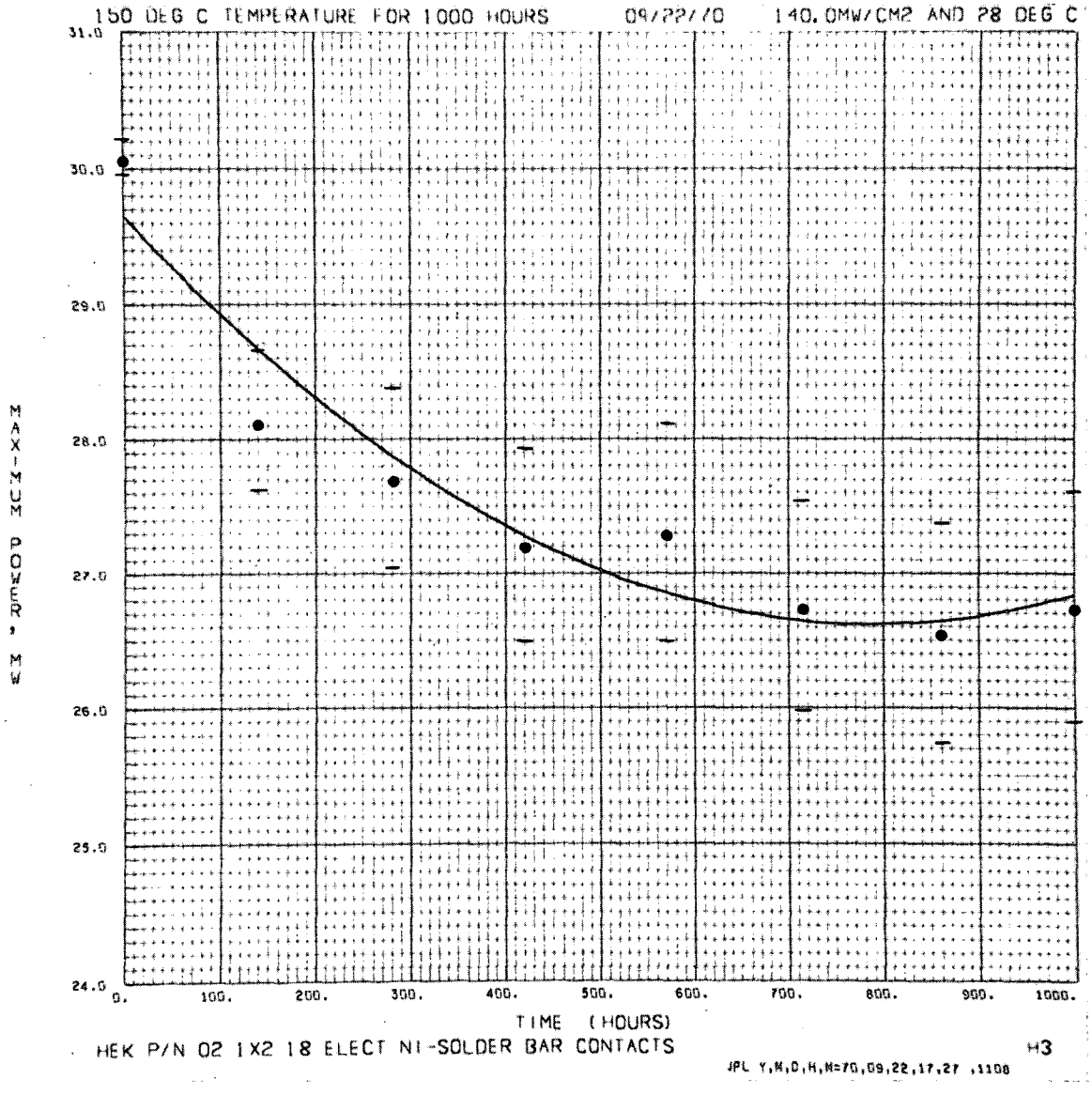


Fig. 43. Maximum-power voltage, cell type H-3, as a function of time, 150 °C storage

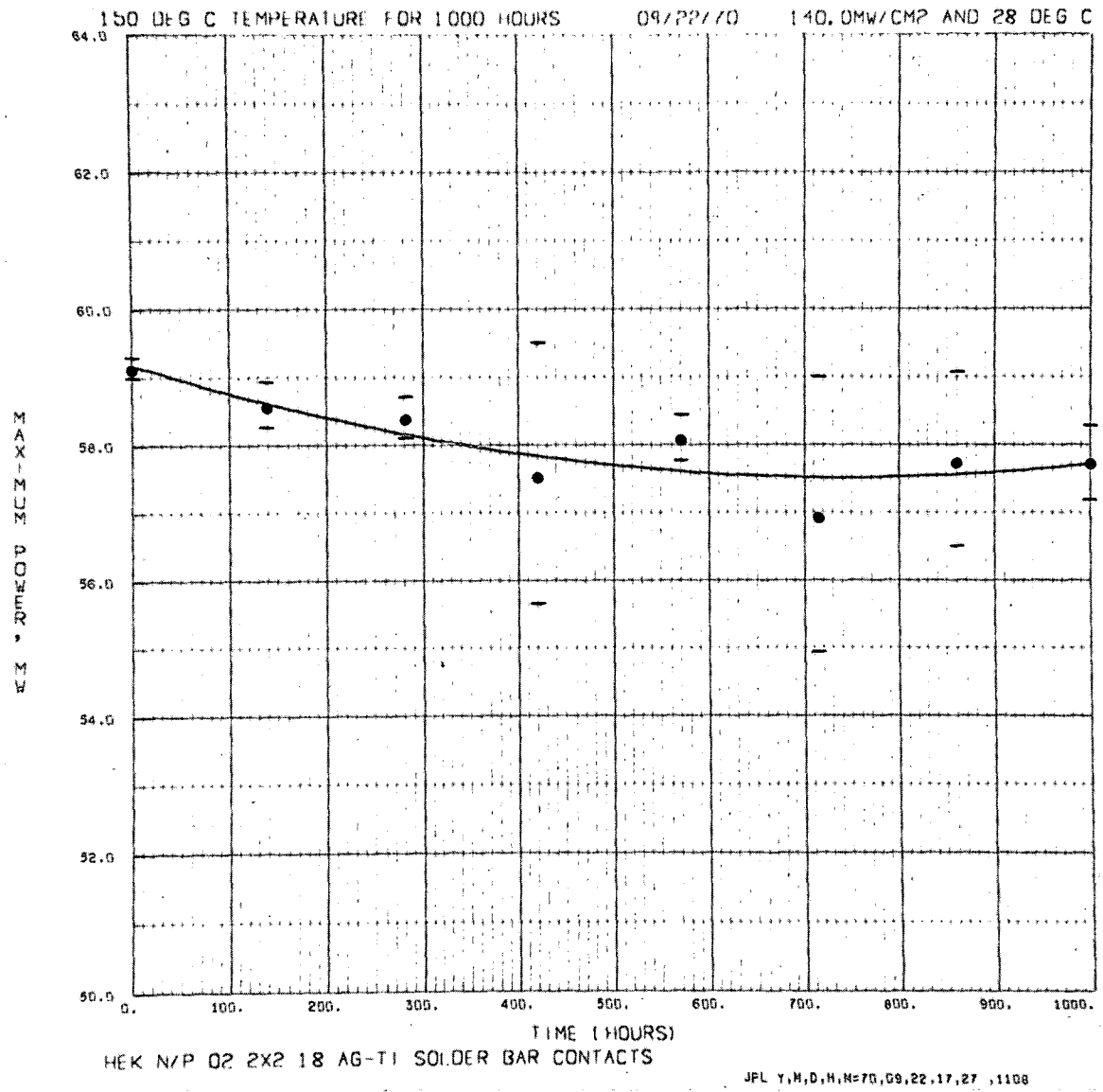


Fig. 44. Maximum-power voltage, cell type M, as a function of time, 150 °C storage

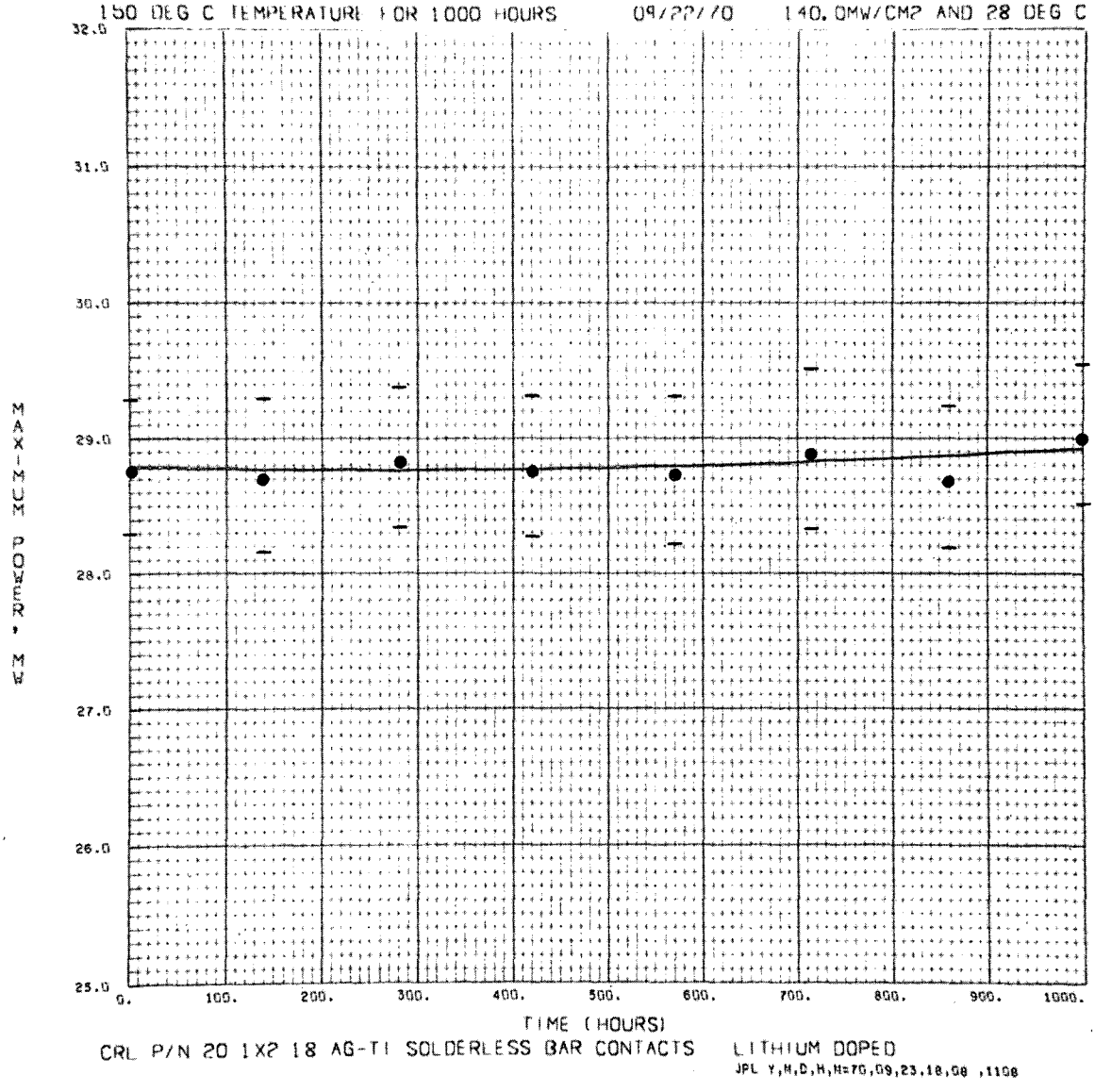


Fig. 45. Maximum-power voltage, cell type CL, as a function of time, 150 °C storage

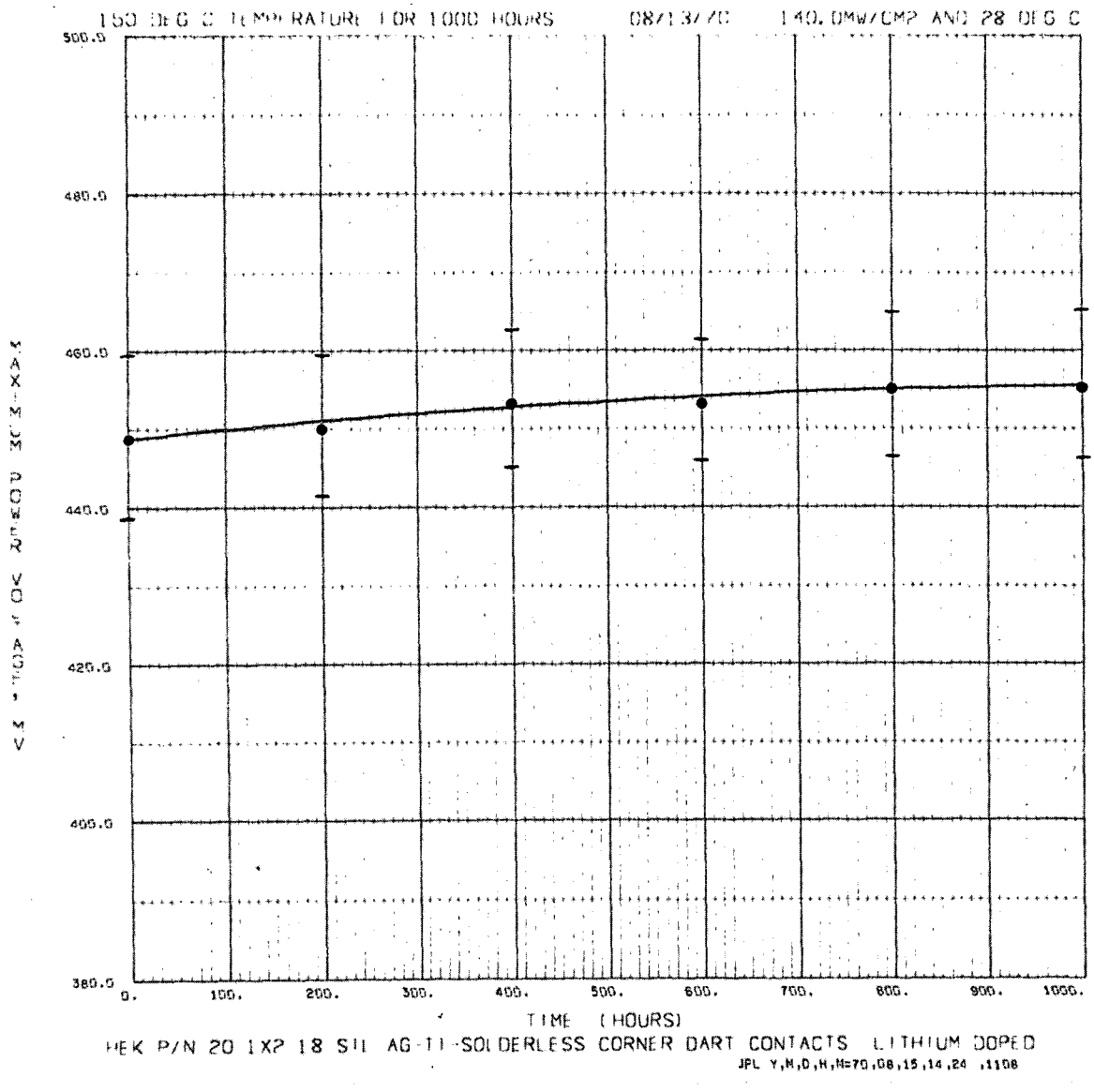


Fig. 46. Maximum-power voltage, cell type HL, as a function of time, 150°C storage

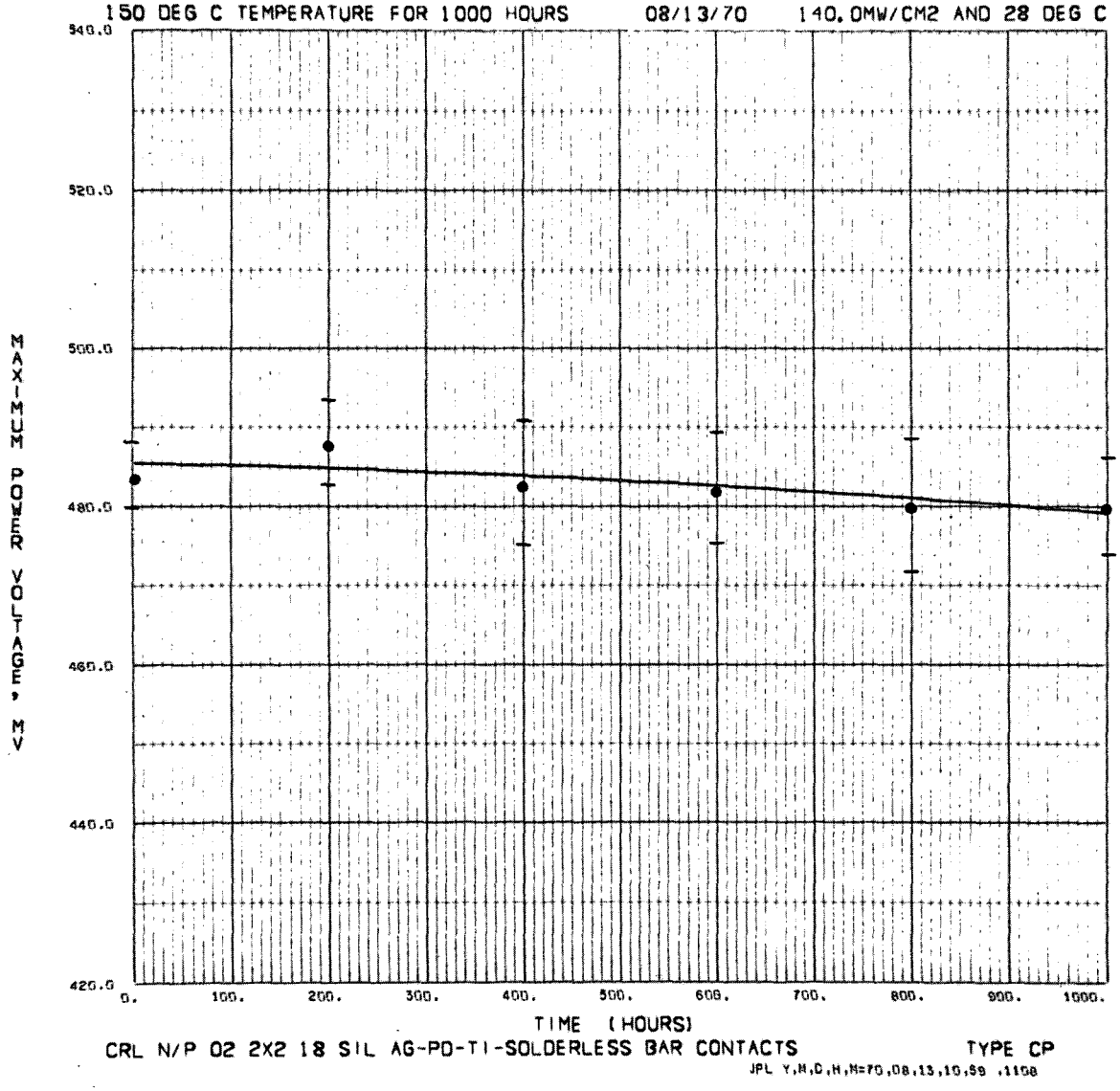


Fig. 47. Maximum-power voltage, cell type CP, as a function of time, 150 °C storage

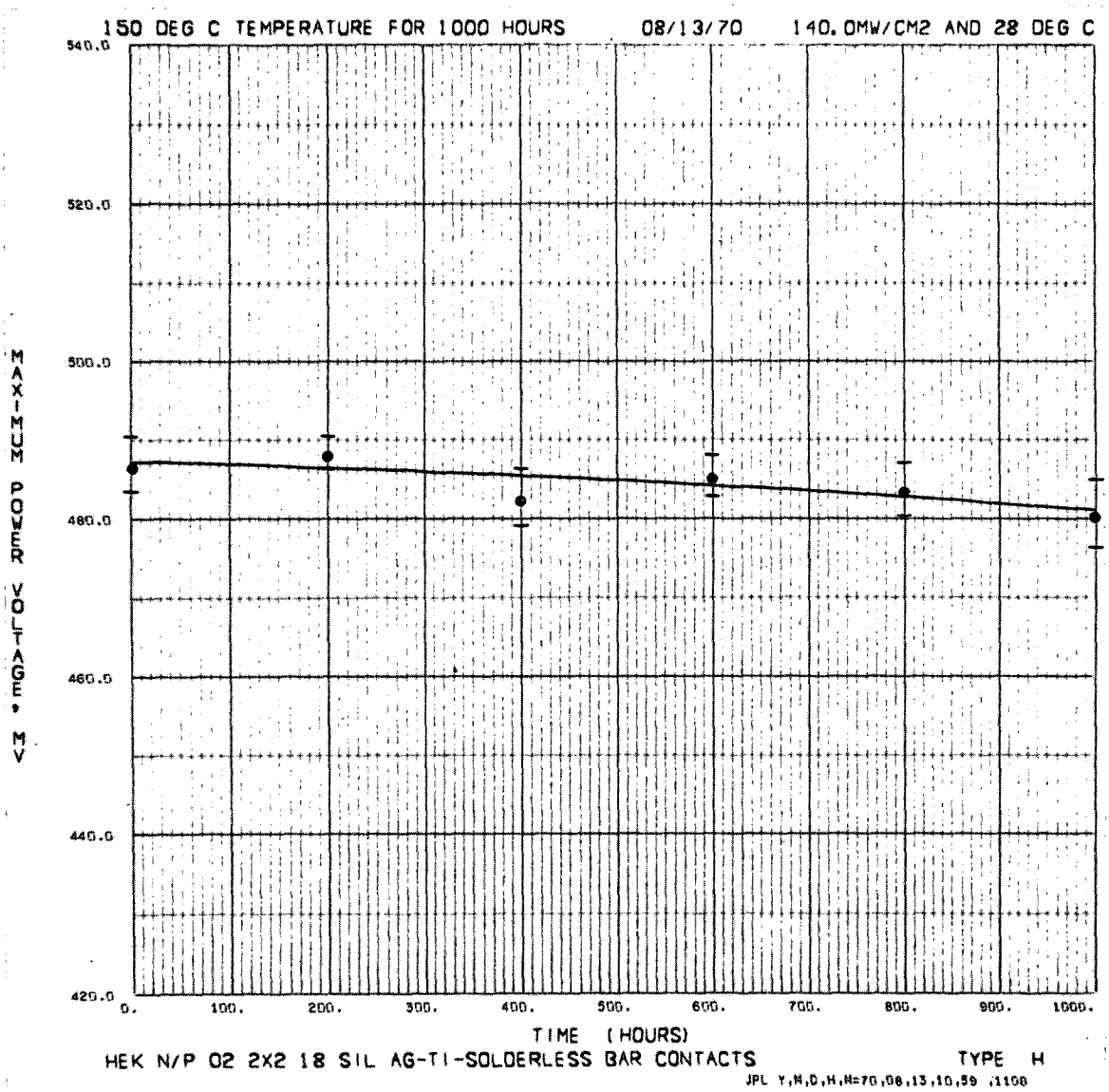


Fig. 48. Maximum-power voltage, cell type H, as a function of time, 150 °C storage

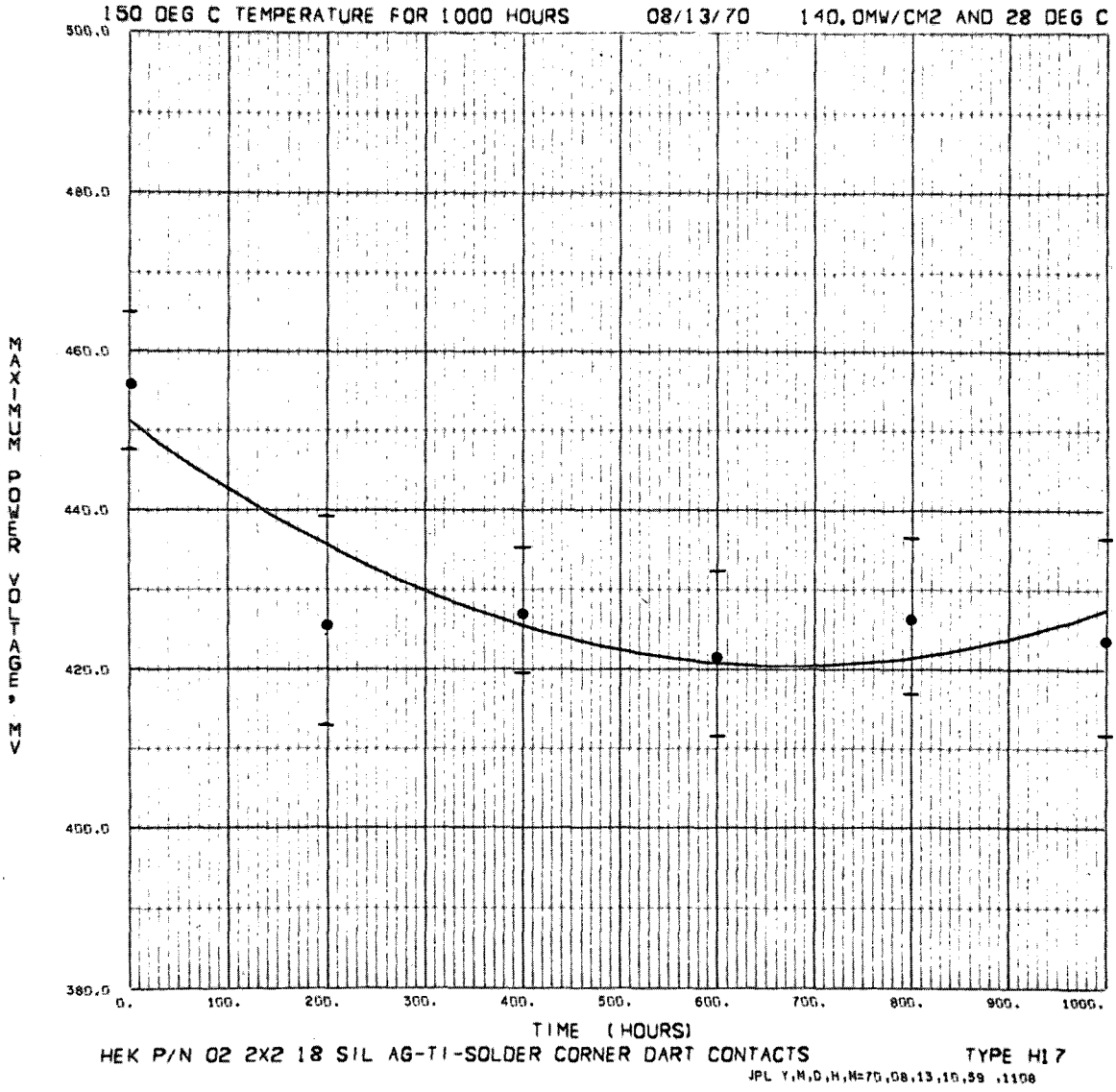


Fig. 49. Maximum-power voltage, cell type H-17, as a function of time, 150 °C storage

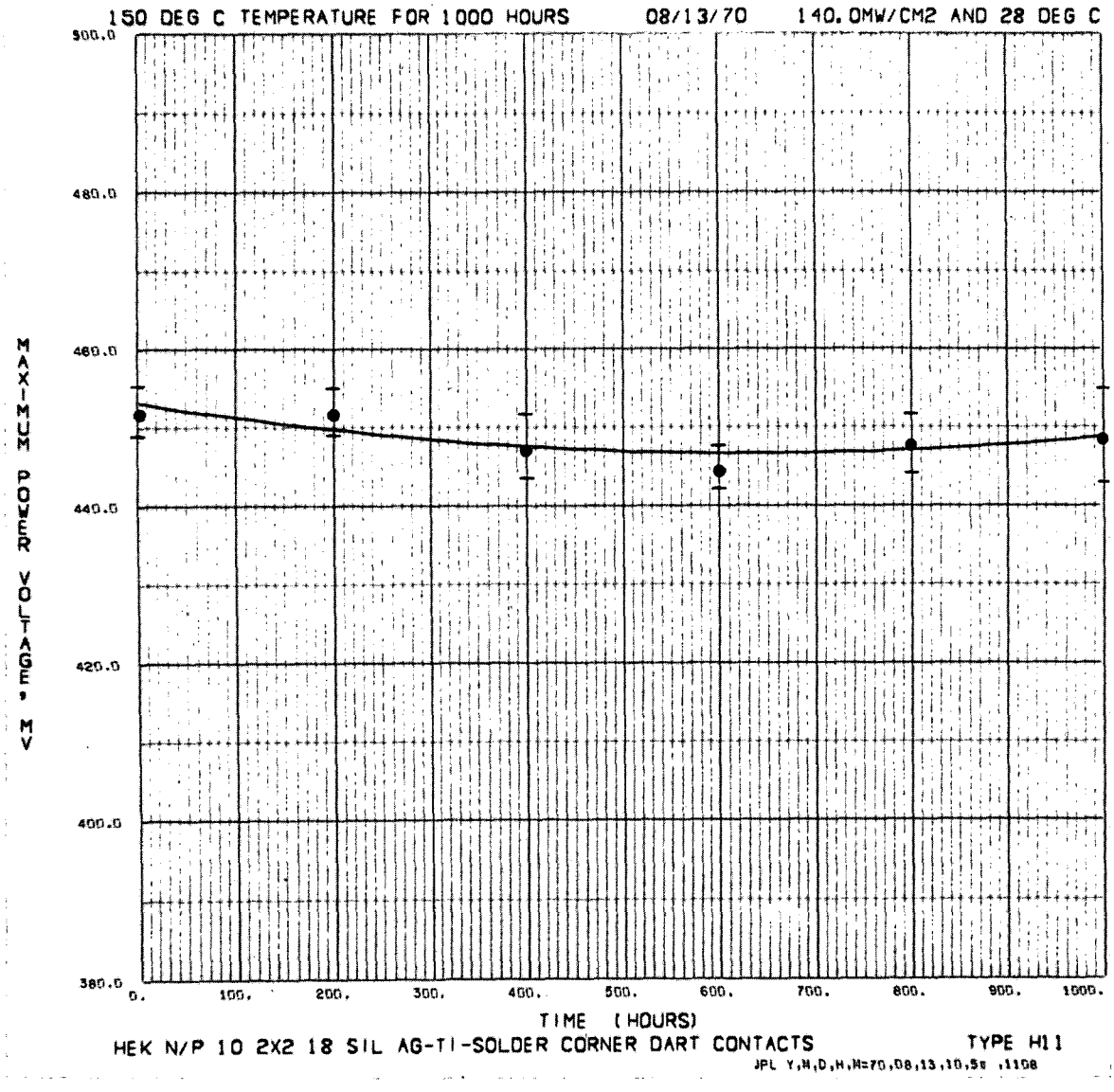


Fig. 50. Maximum-power voltage, cell type H-11, as a function of time, 150 °C storage

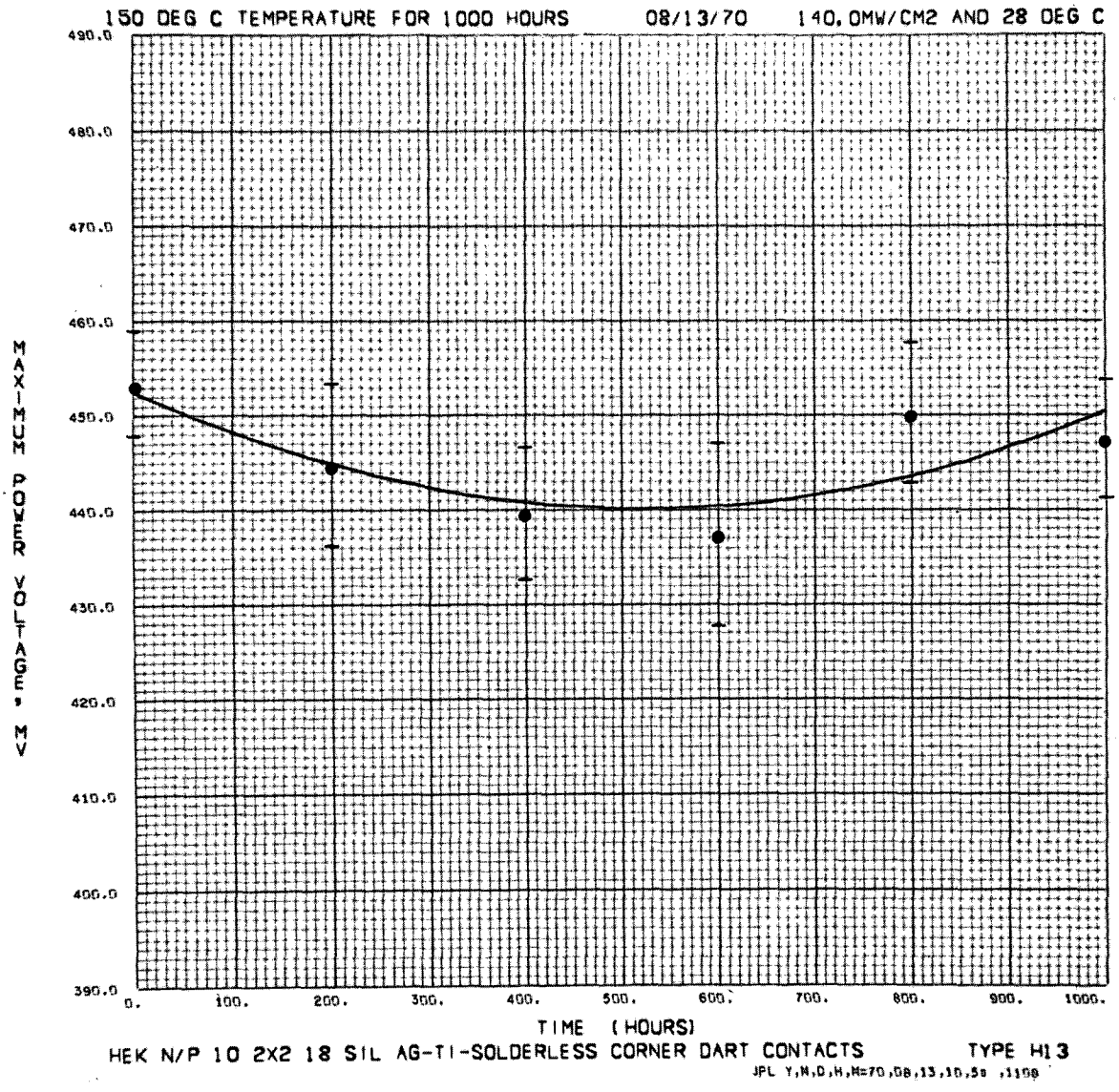


Fig. 51. Maximum-power voltage, cell type H-13, as a function of time, 150 °C storage

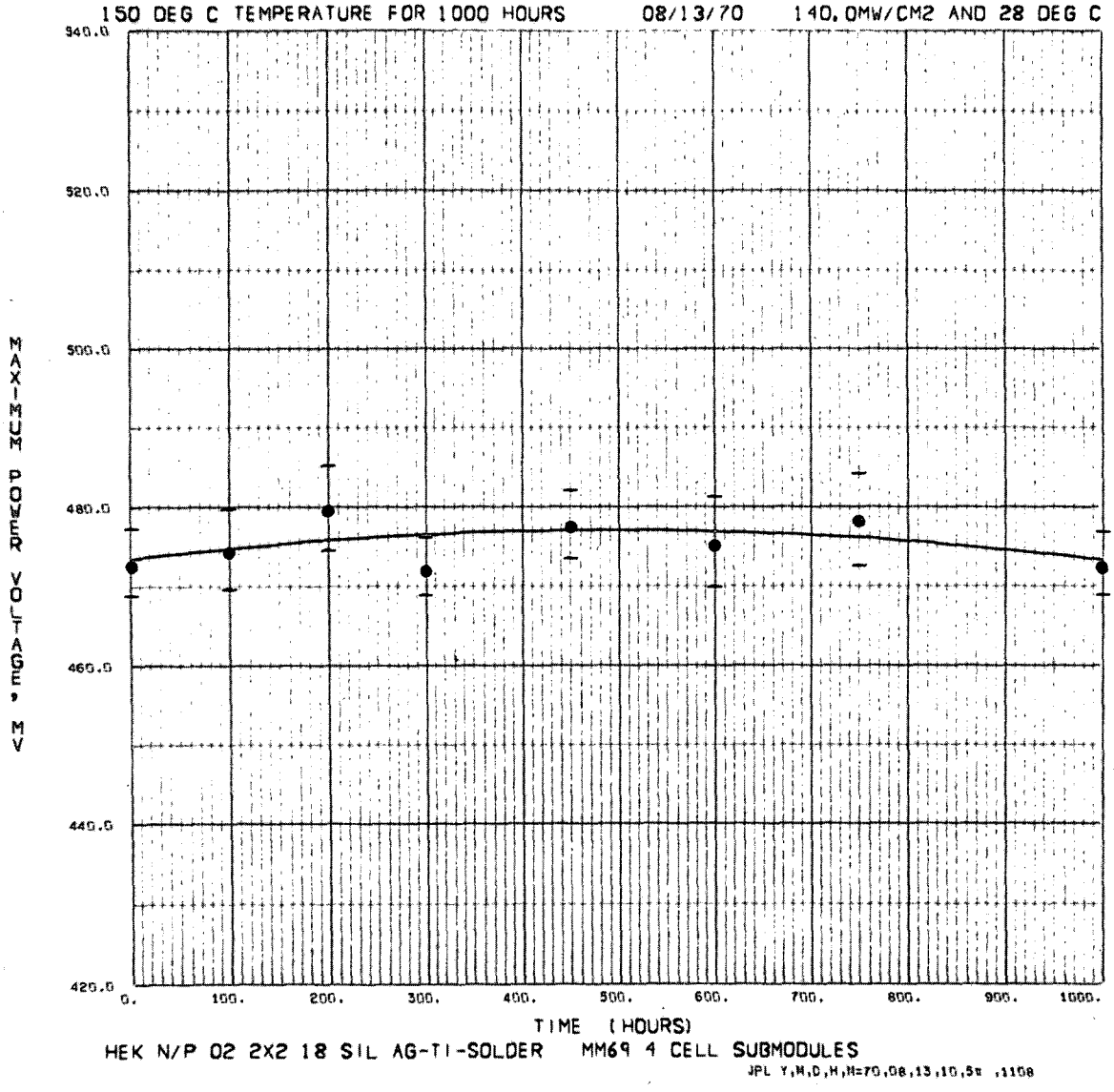


Fig. 52. Maximum-power voltage, cell type M69 module, as a function of time, 150 °C storage

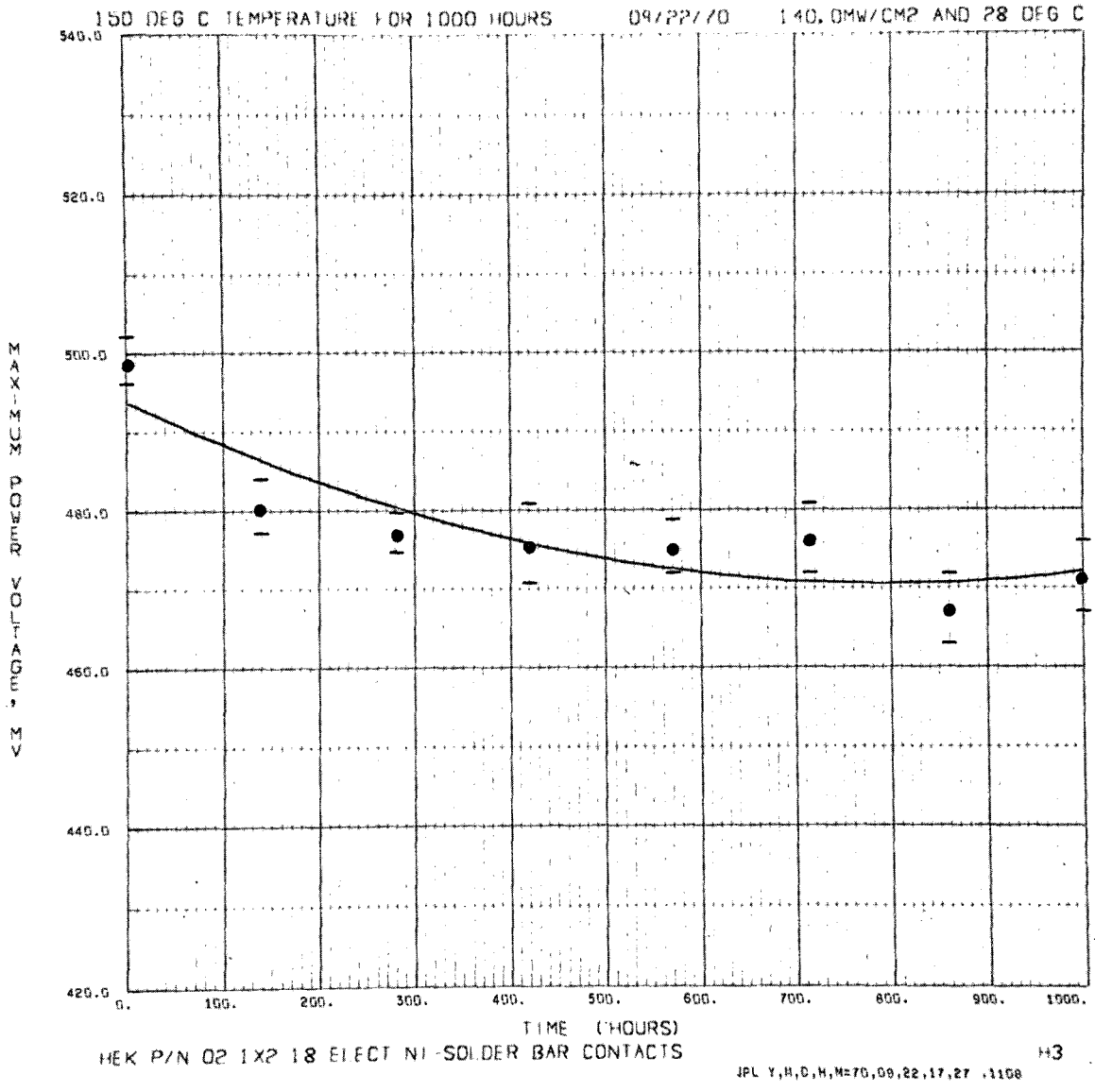


Fig. 53. Maximum-power voltage, cell type H-3, as a function of time, 150 °C storage

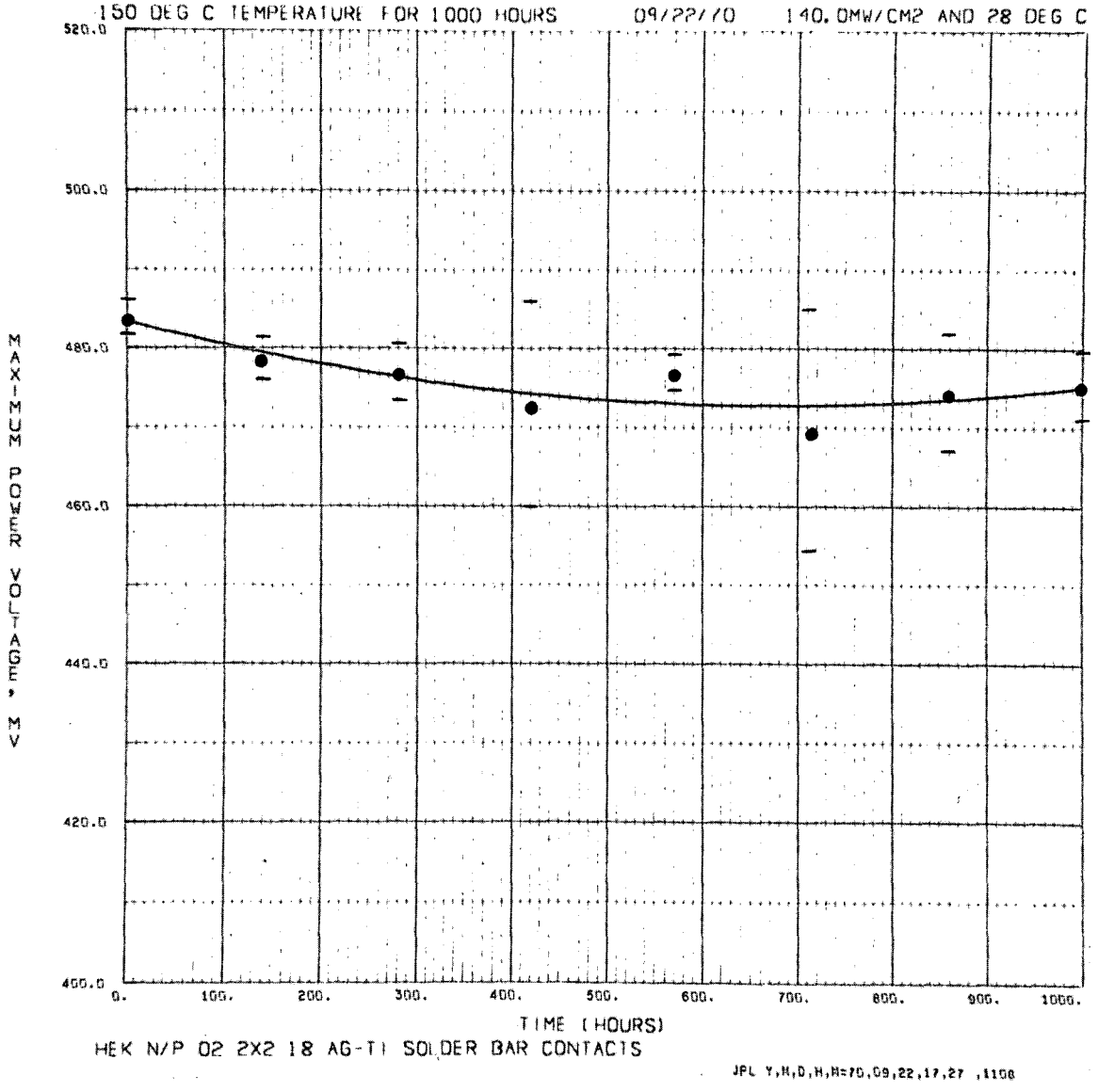


Fig. 54. Maximum-power voltage, cell type M, as a function of time, 150 °C storage

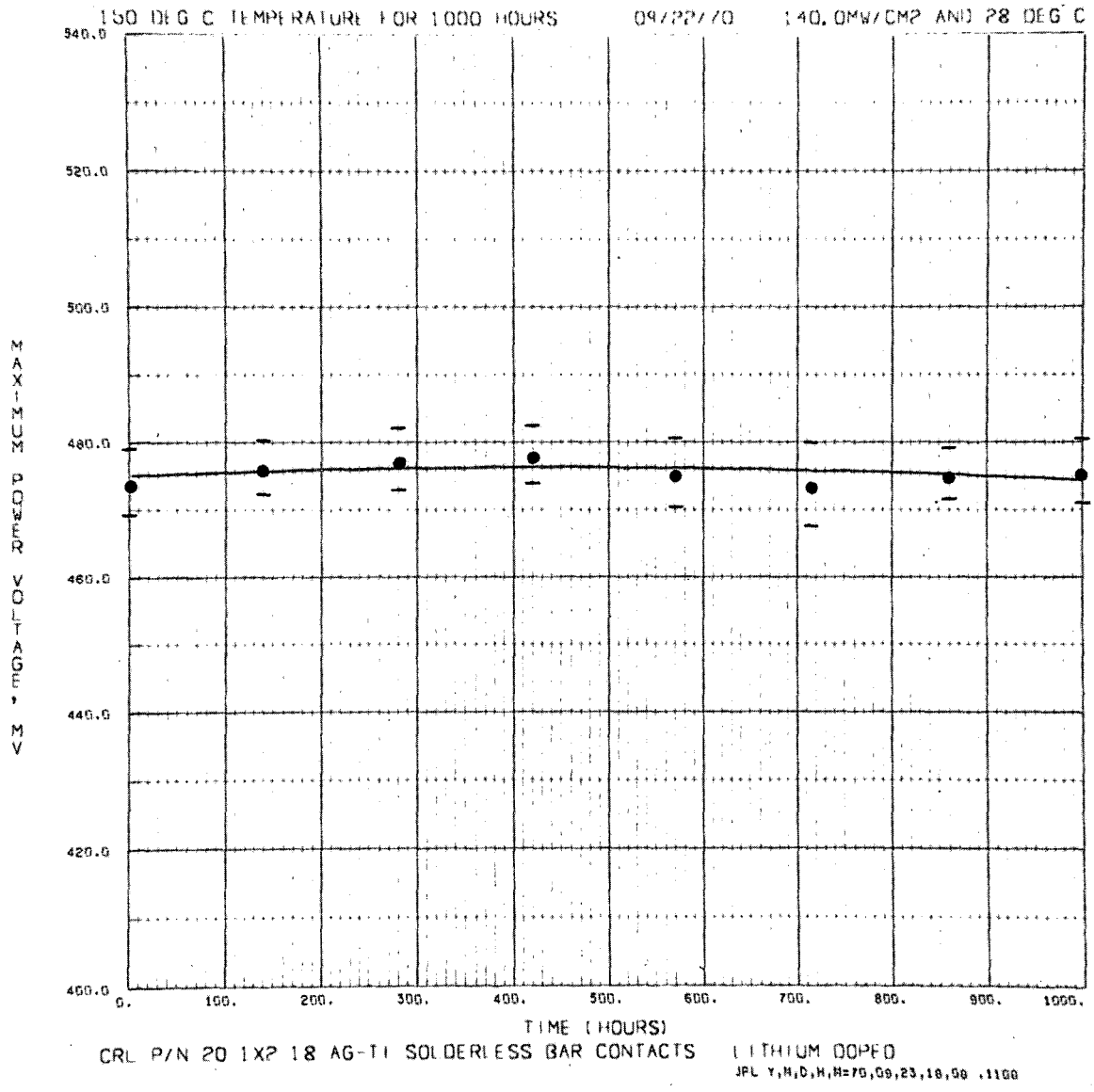


Fig. 55. Maximum-power voltage, cell type CL, as a function of time, 150 °C storage

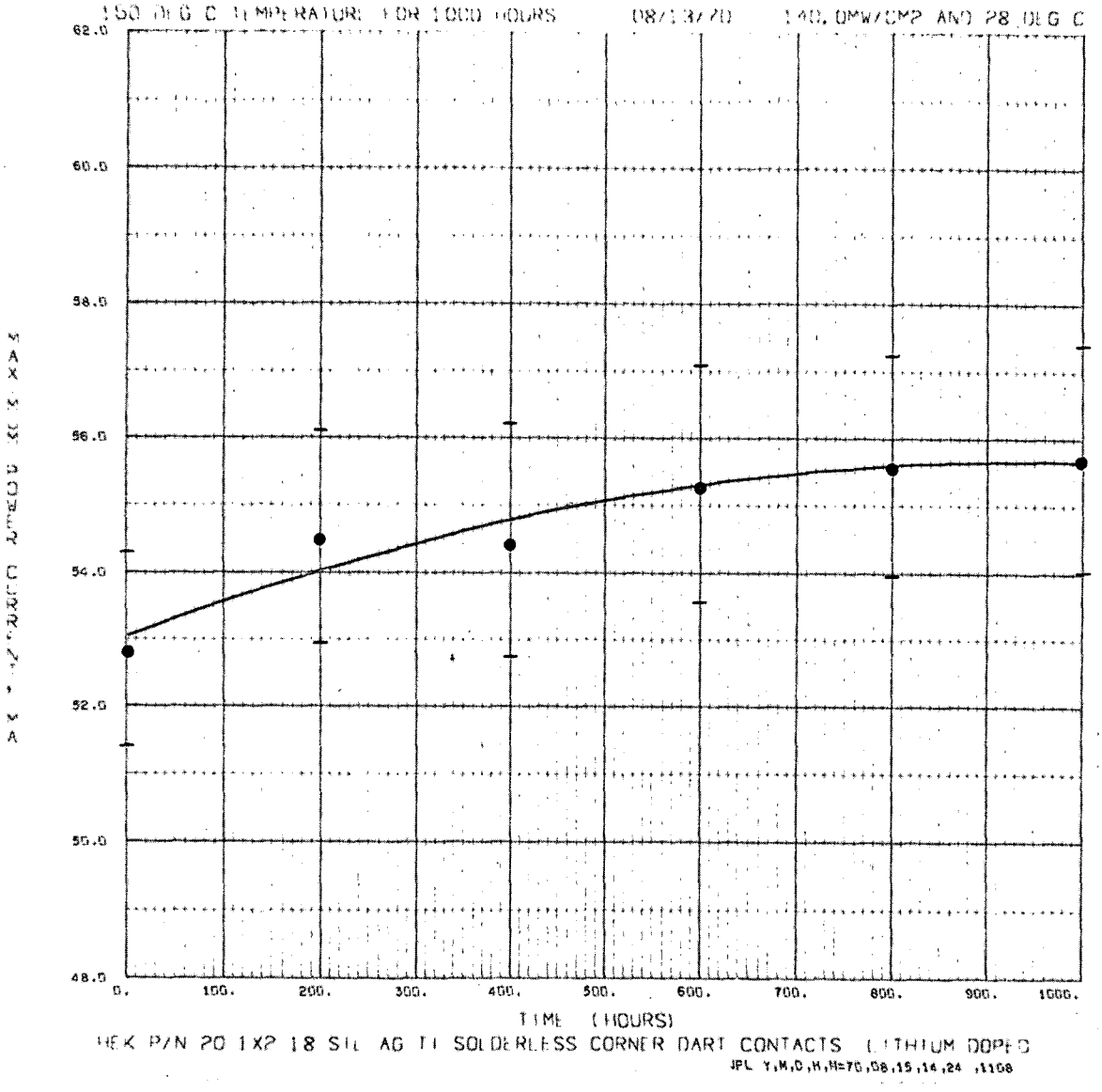


Fig. 56. Maximum-power current, cell type HL, as a function of time, 150 °C storage

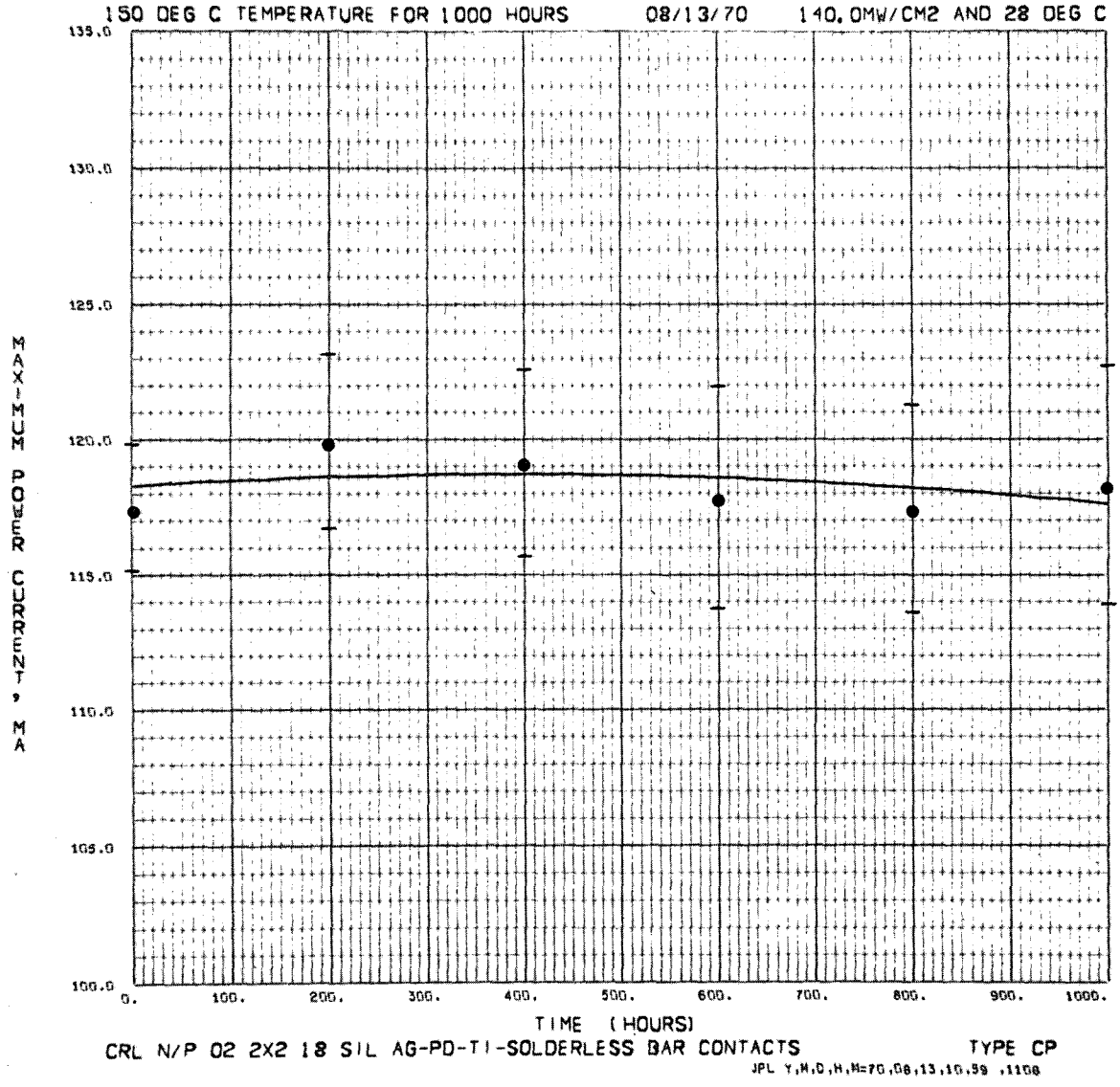


Fig. 57. Maximum-power current, cell type CP, as a function of time, 150 °C storage

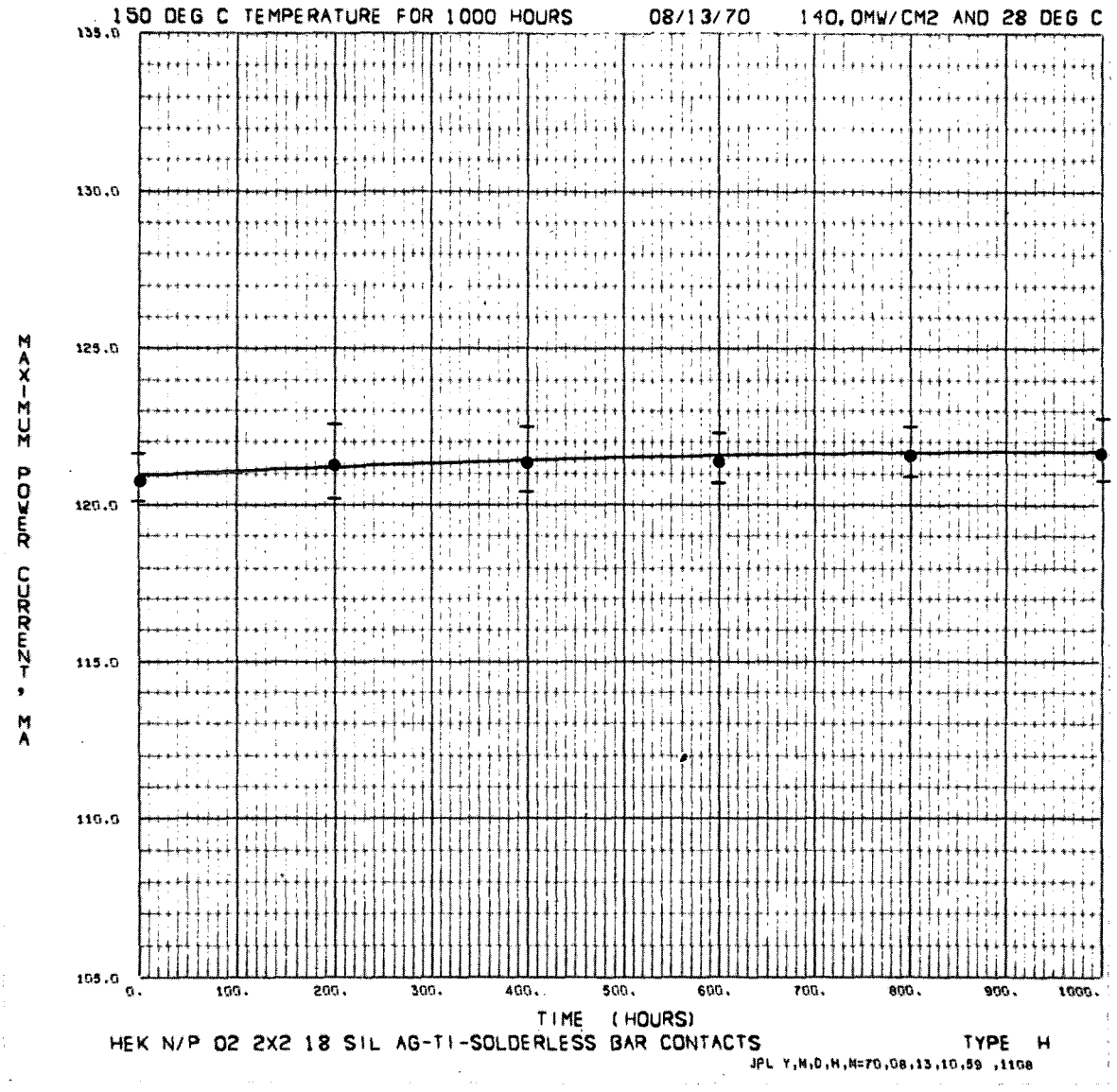


Fig. 58. Maximum-power current, cell type H, as a function of time, 150 °C storage

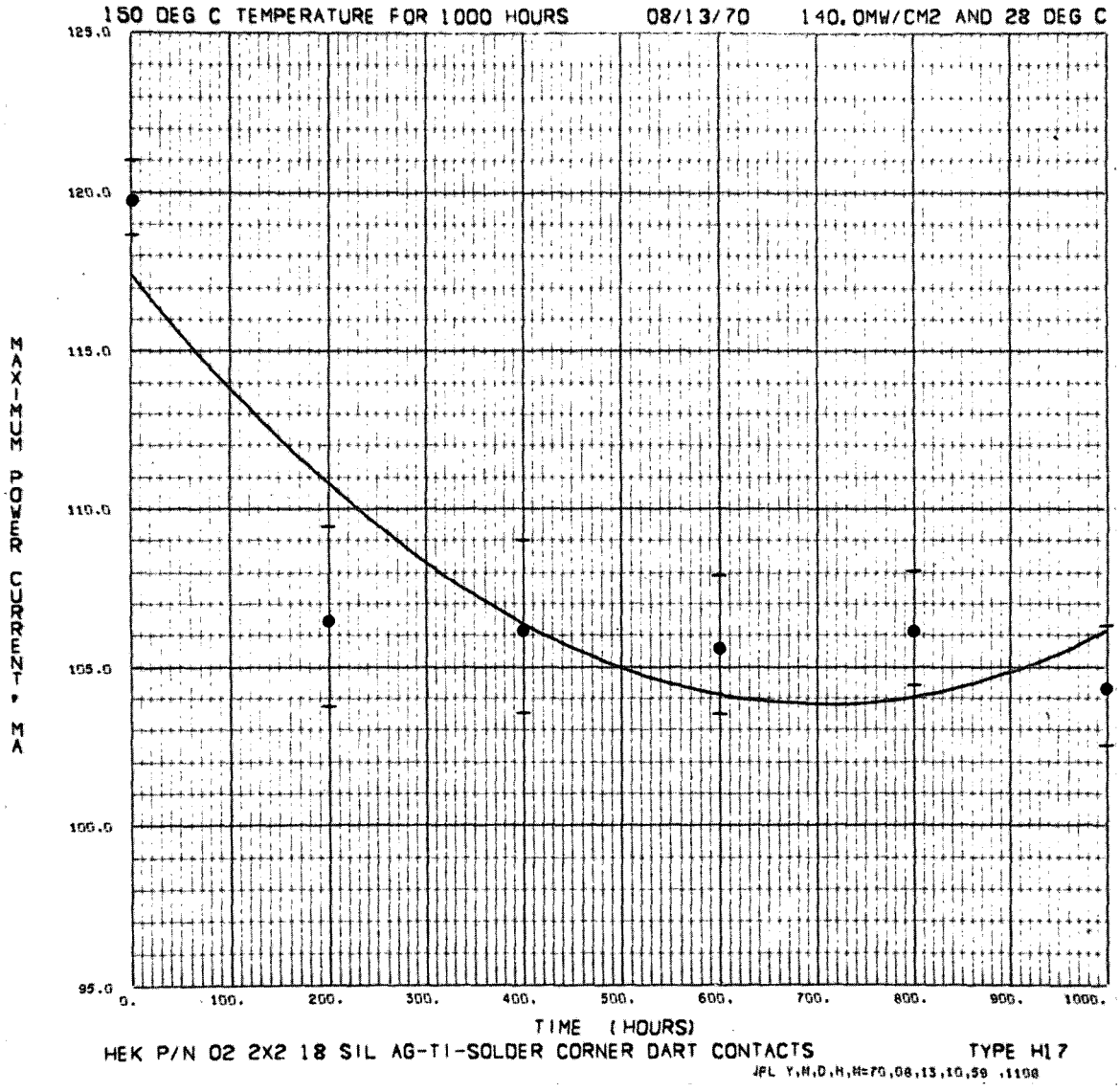


Fig. 59. Maximum-power current, cell type H-17, as a function of time, 150 °C storage

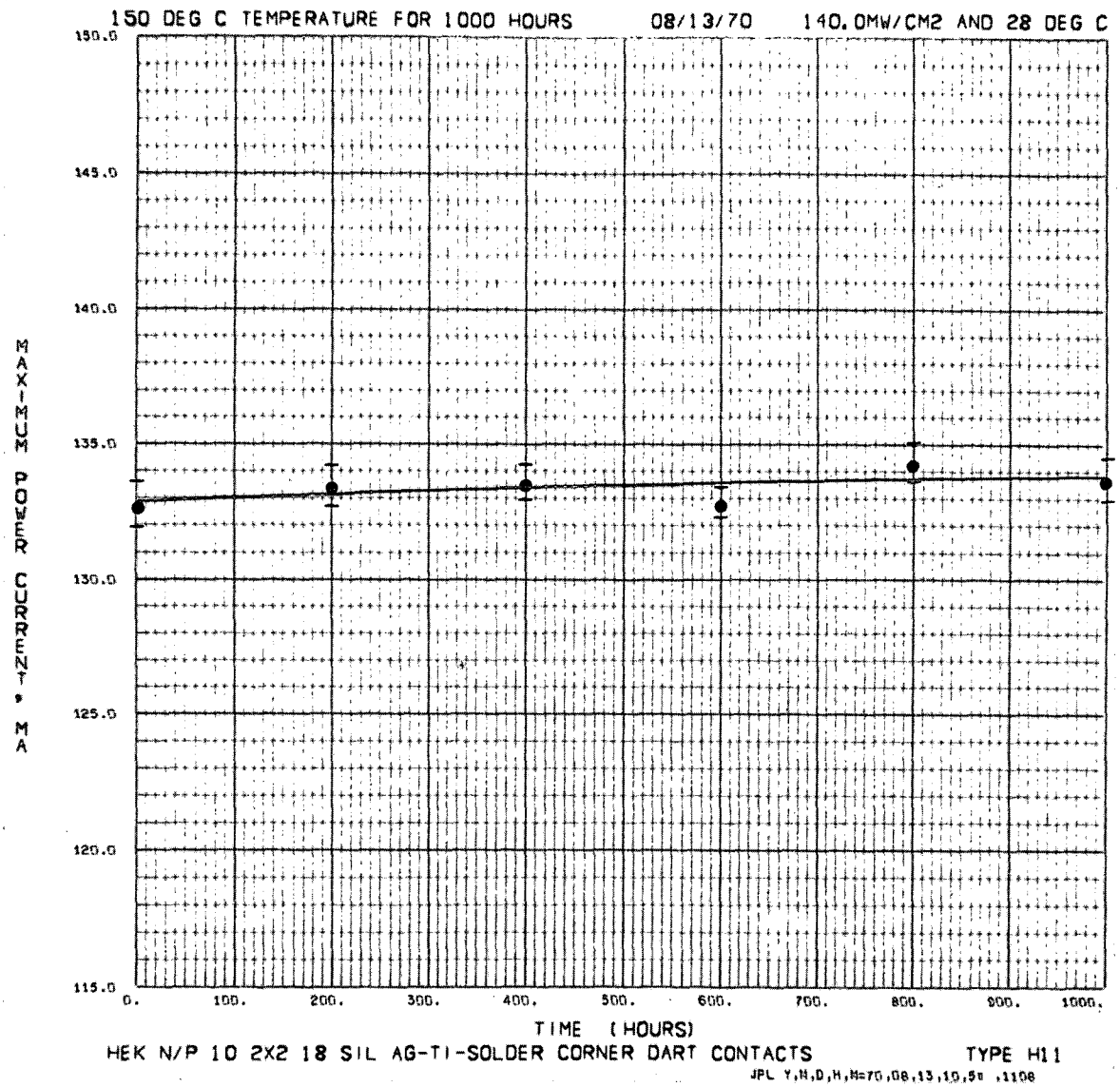


Fig. 60. Maximum-power current, cell type H-11, as a function of time, 150 °C storage

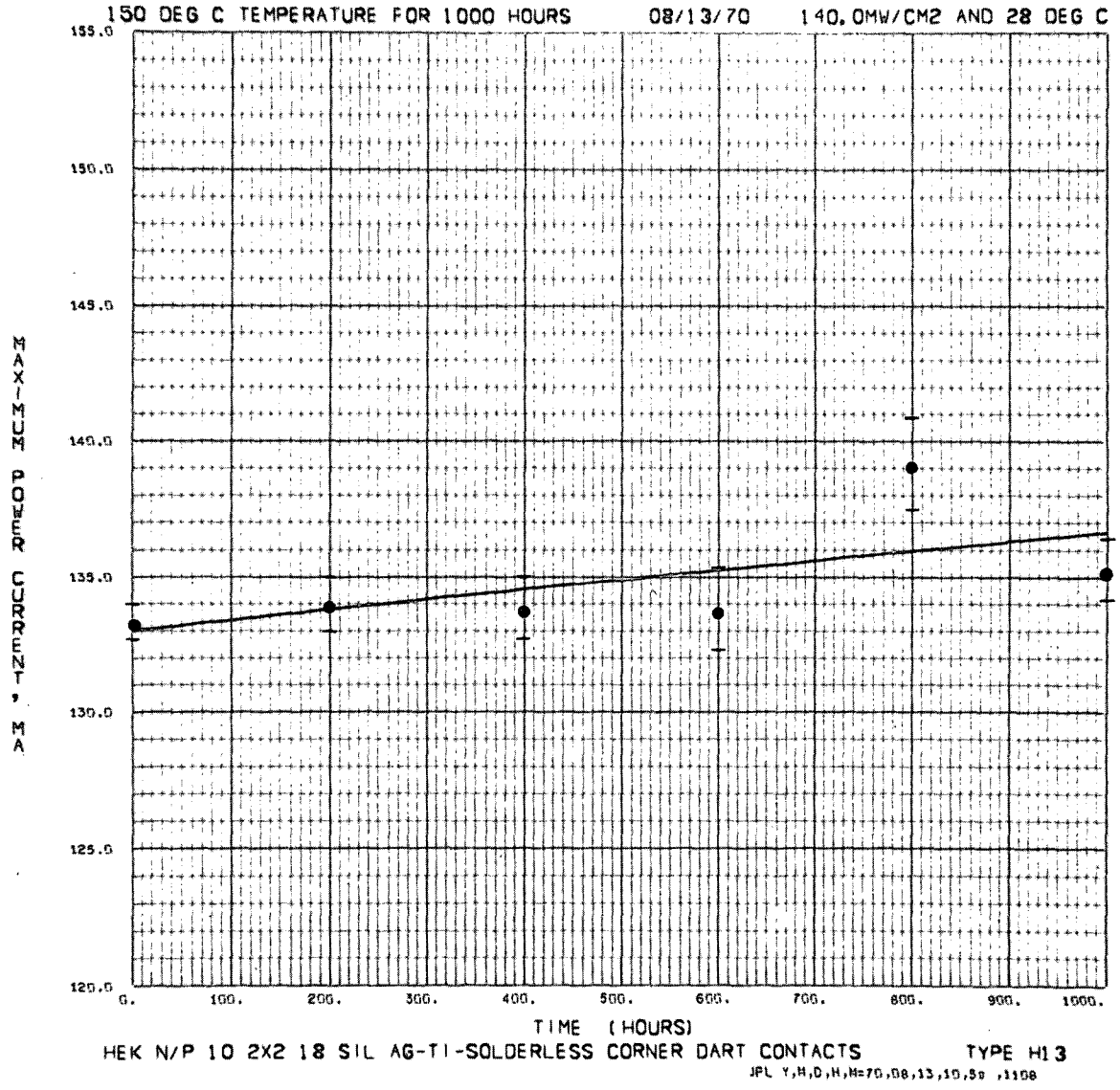


Fig. 61. Maximum-power current, cell type H-13, as a function of time, 150 °C storage

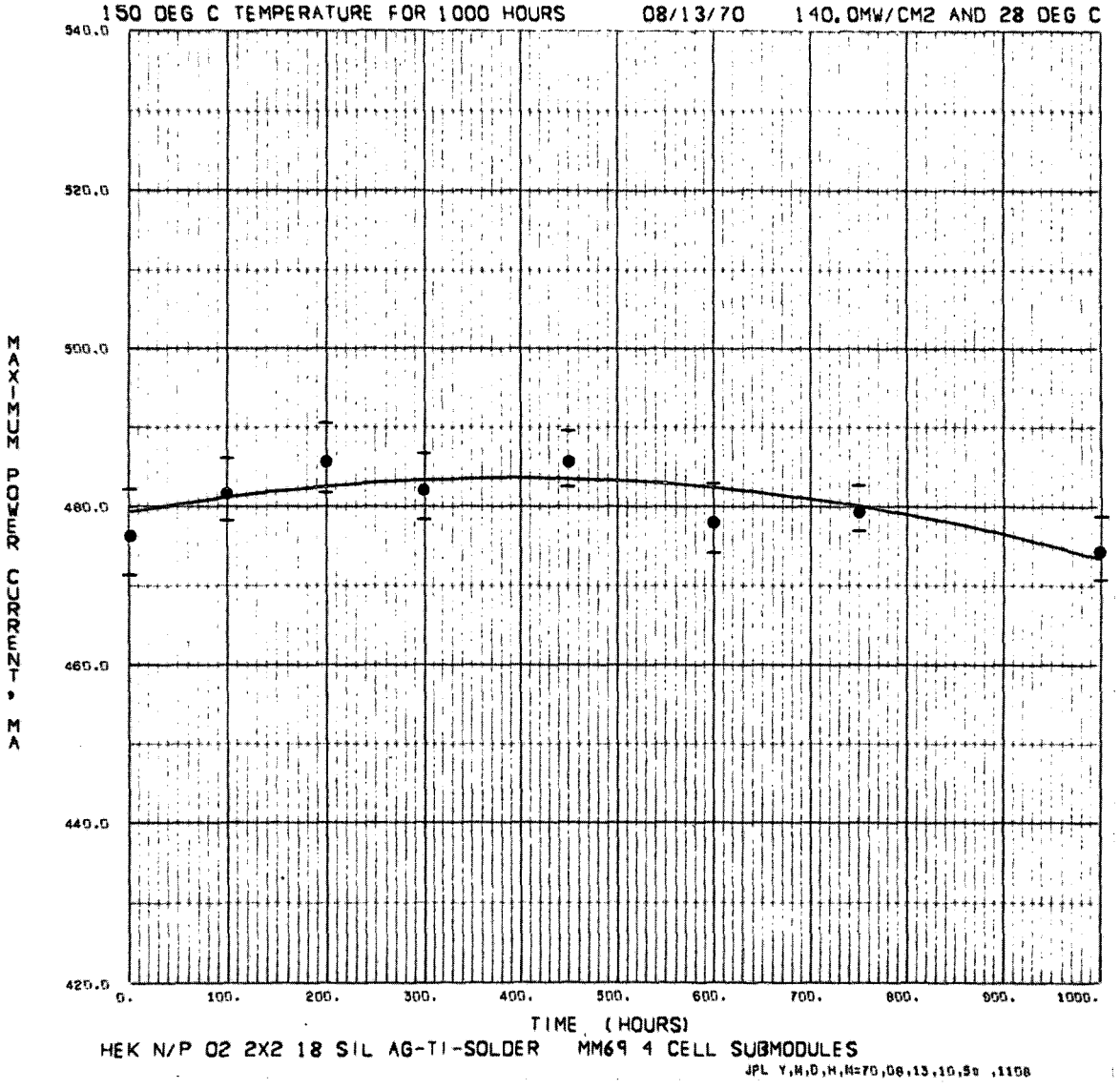


Fig. 62. Maximum-power current, cell type M69 module, as a function of time, 150°C storage

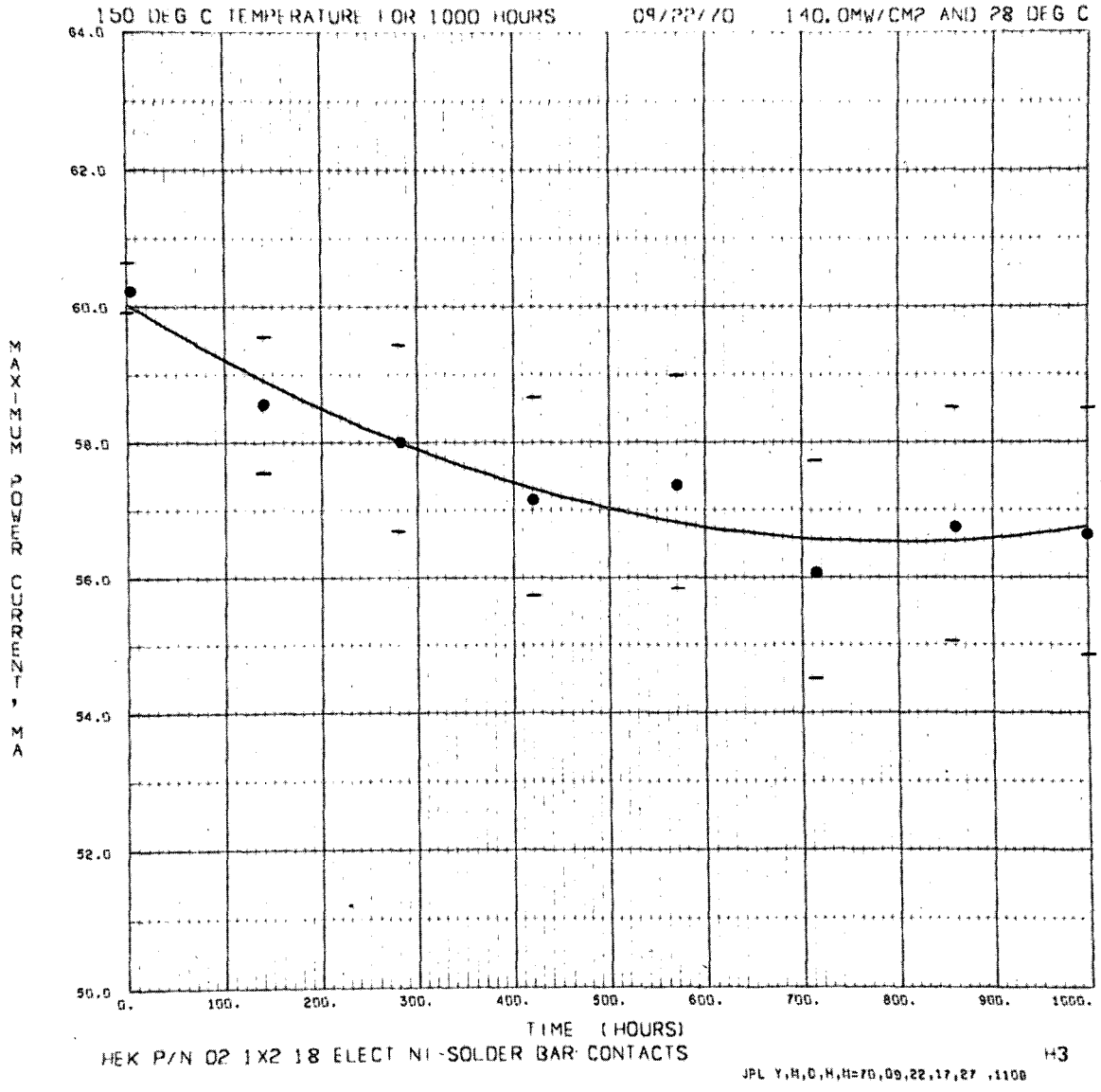


Fig. 63. Maximum-power current, cell type H-3, as a function of time, 150 °C storage

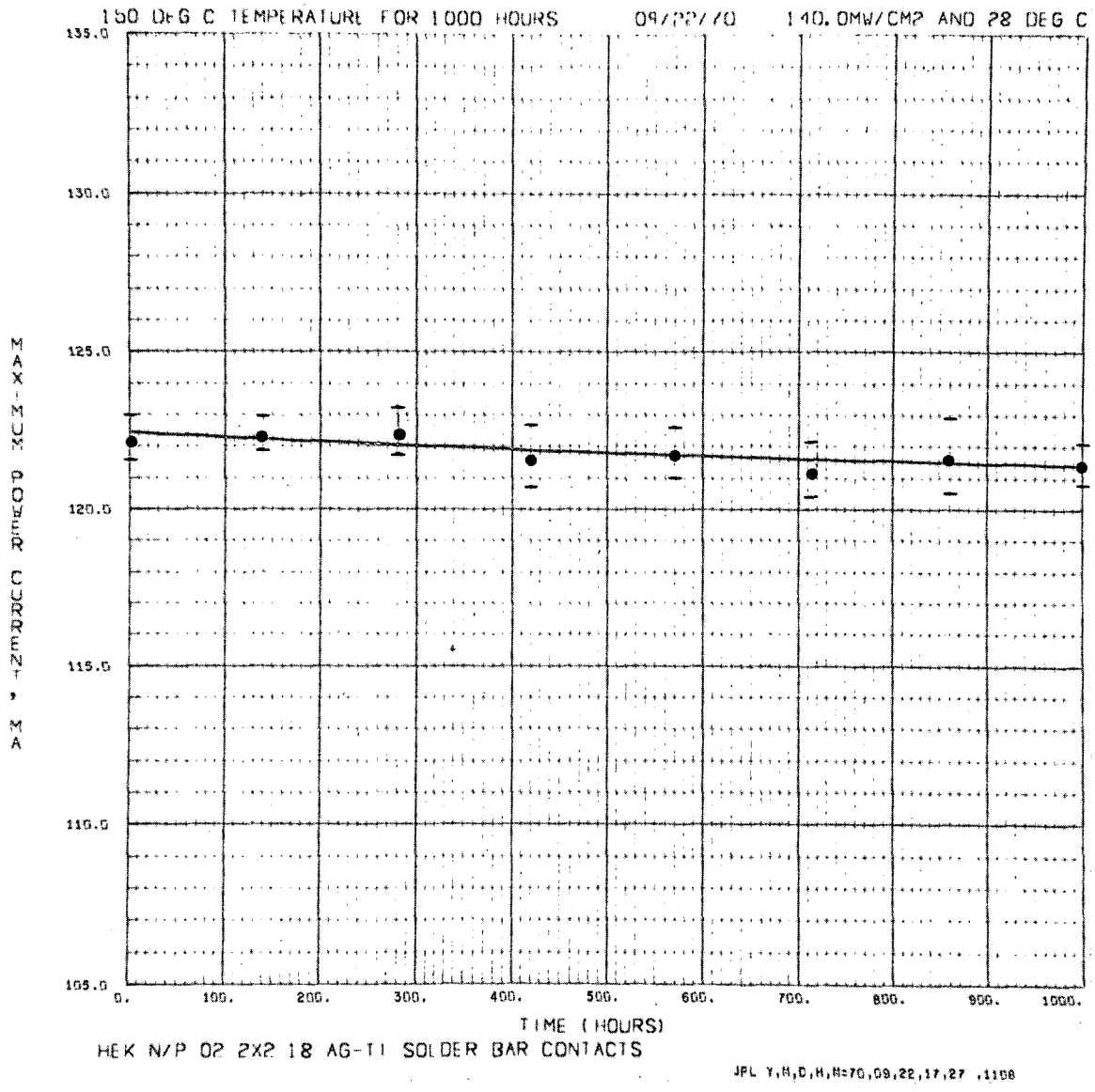


Fig. 64. Maximum-power current, cell type M, as a function of time, 150 °C storage

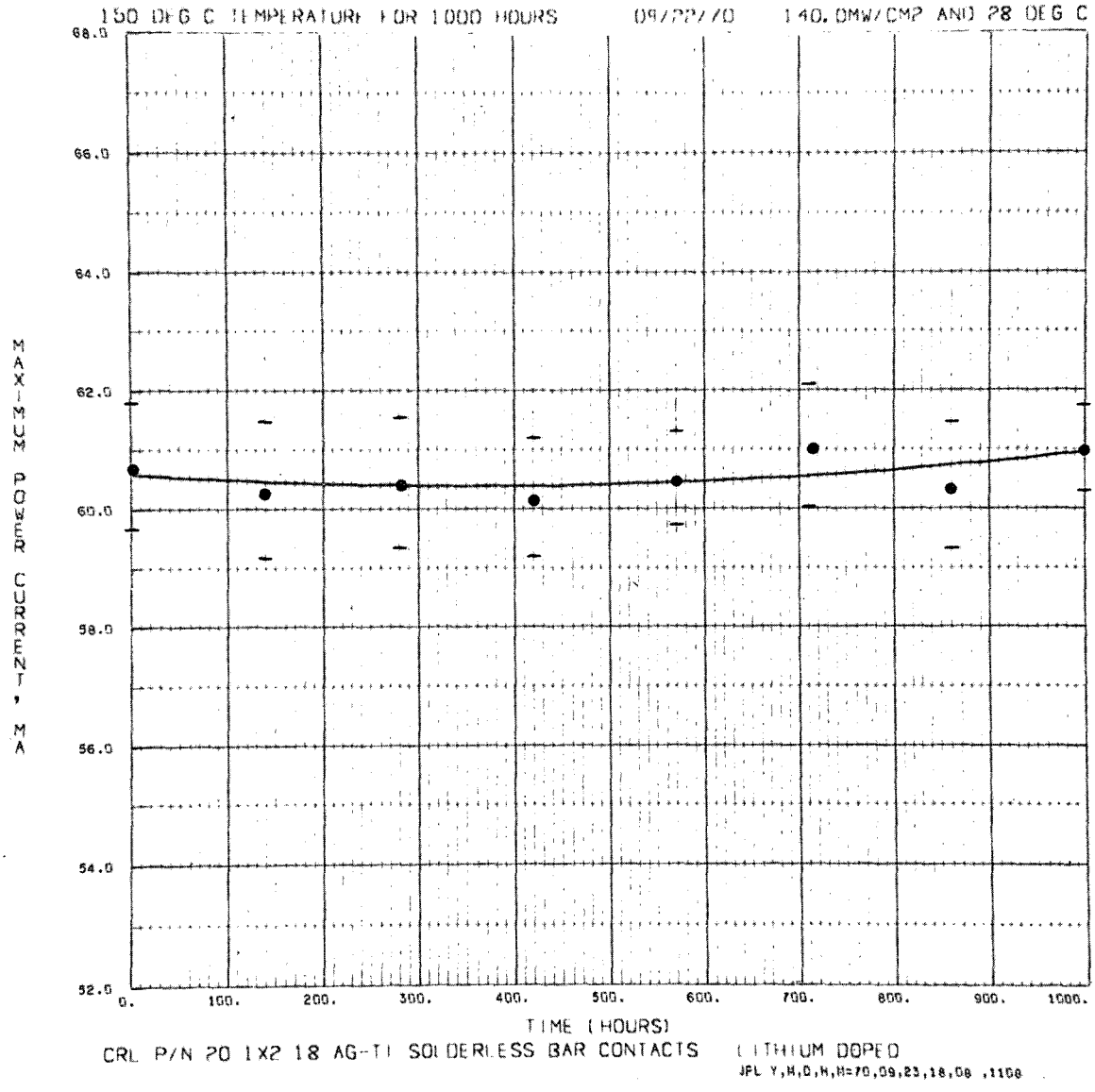


Fig. 65. Maximum-power current, cell type CL, as a function of time, 150 °C storage

Page intentionally left blank

125°C STORAGE

Page intentionally left blank

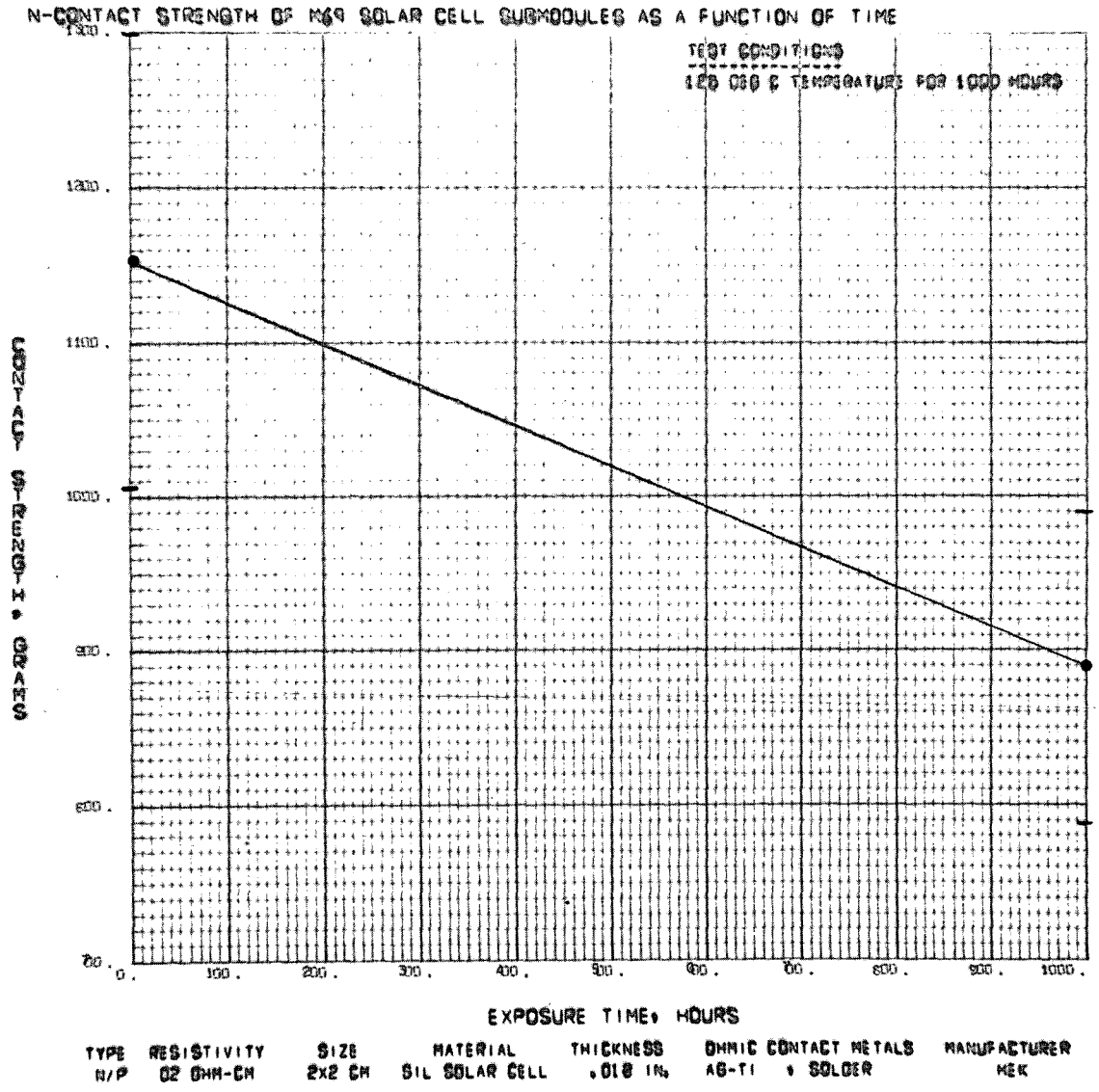


Fig. 66. Top-contact strength, cell type M69 module, as a function of time, 125°C storage

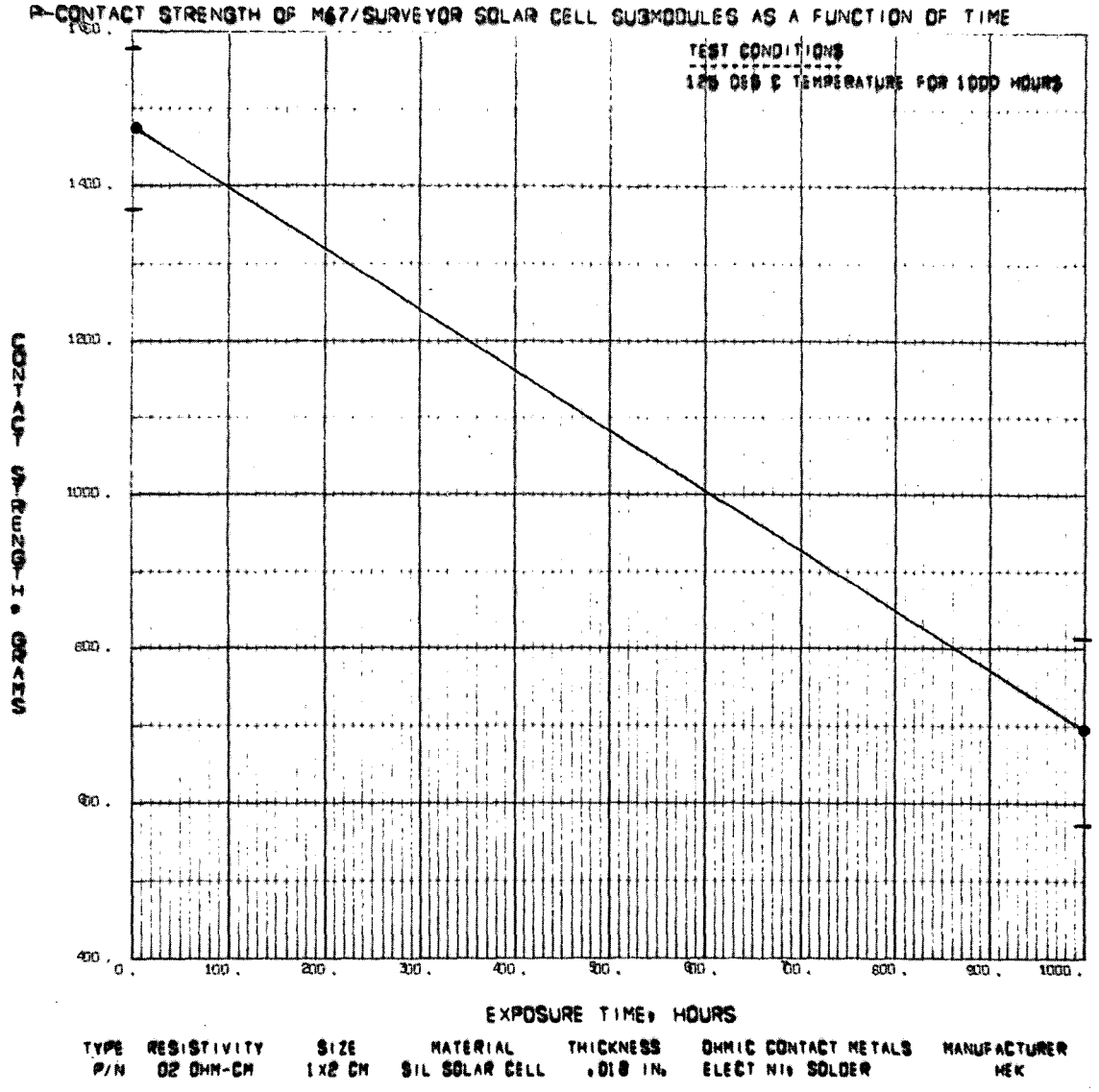


Fig. 67. Top-contact strength, cell type M67 module, as a function of time, 125°C storage

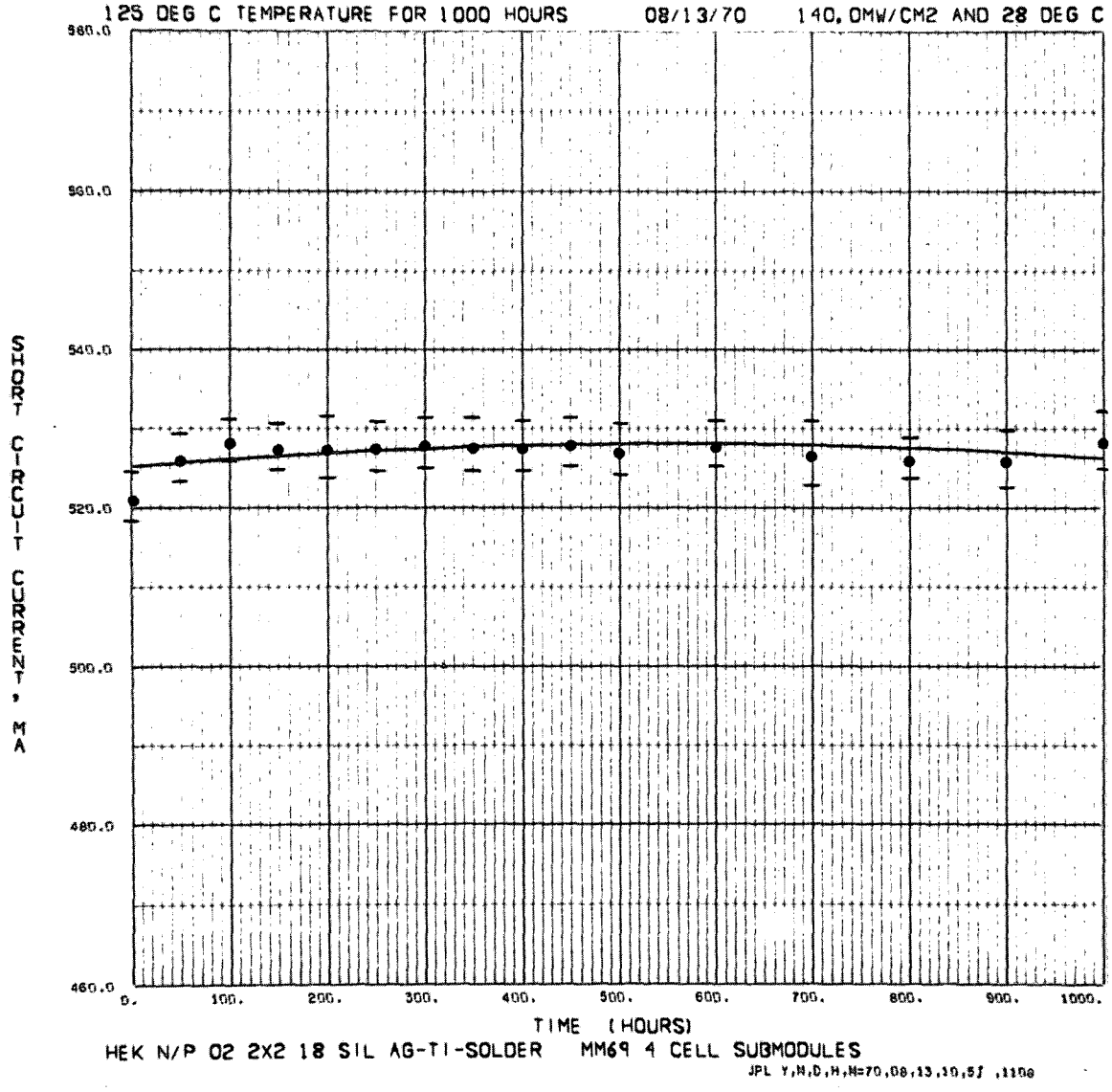


Fig. 68. Short-circuit current, cell type M69 module, as a function of time, 125°C storage

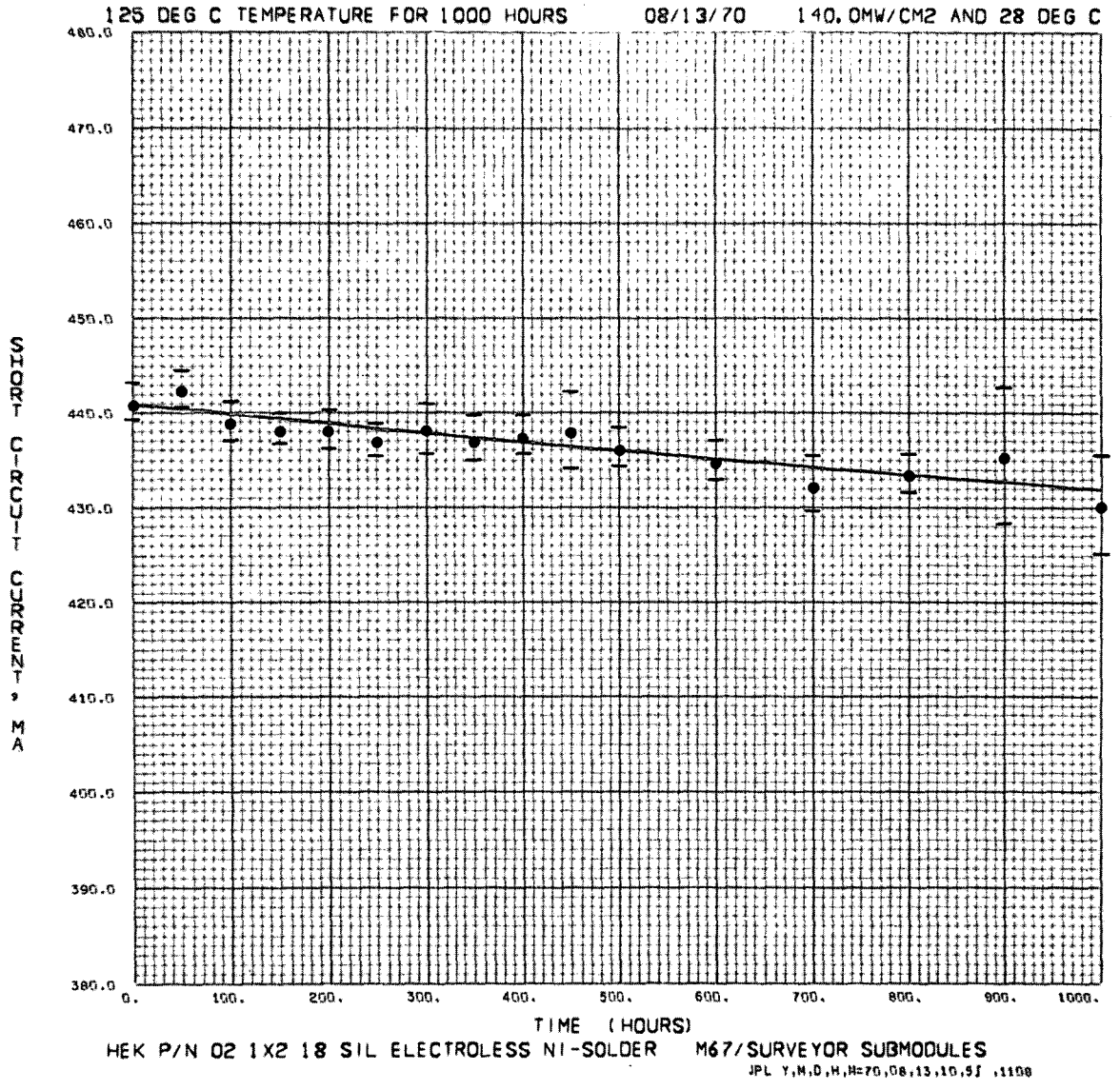


Fig. 69. Short-circuit current, cell type M67 module, as a function of time, 125°C storage

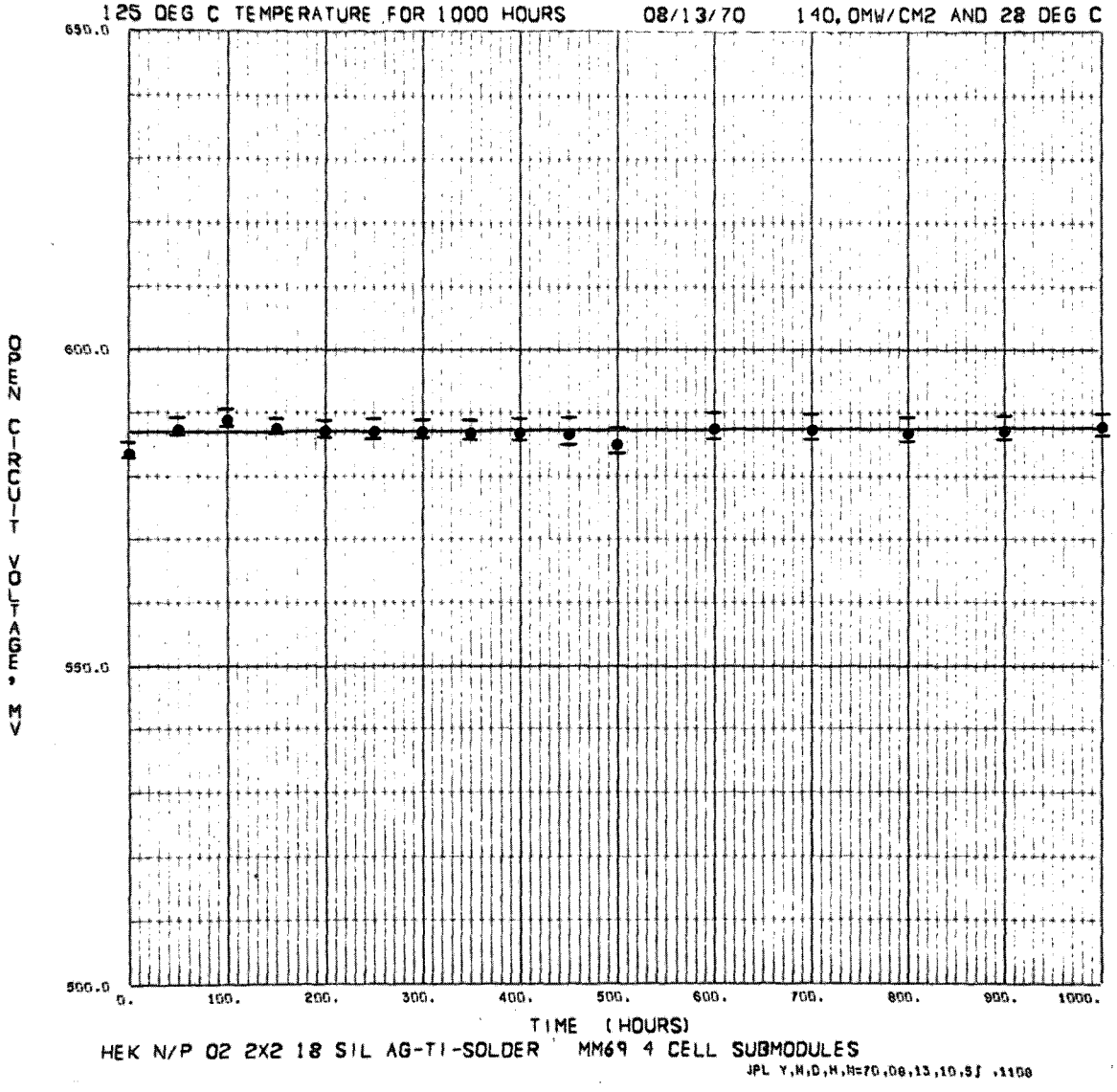


Fig. 70. Open-circuit voltage, cell type M69 module, as a function of time, 125°C storage

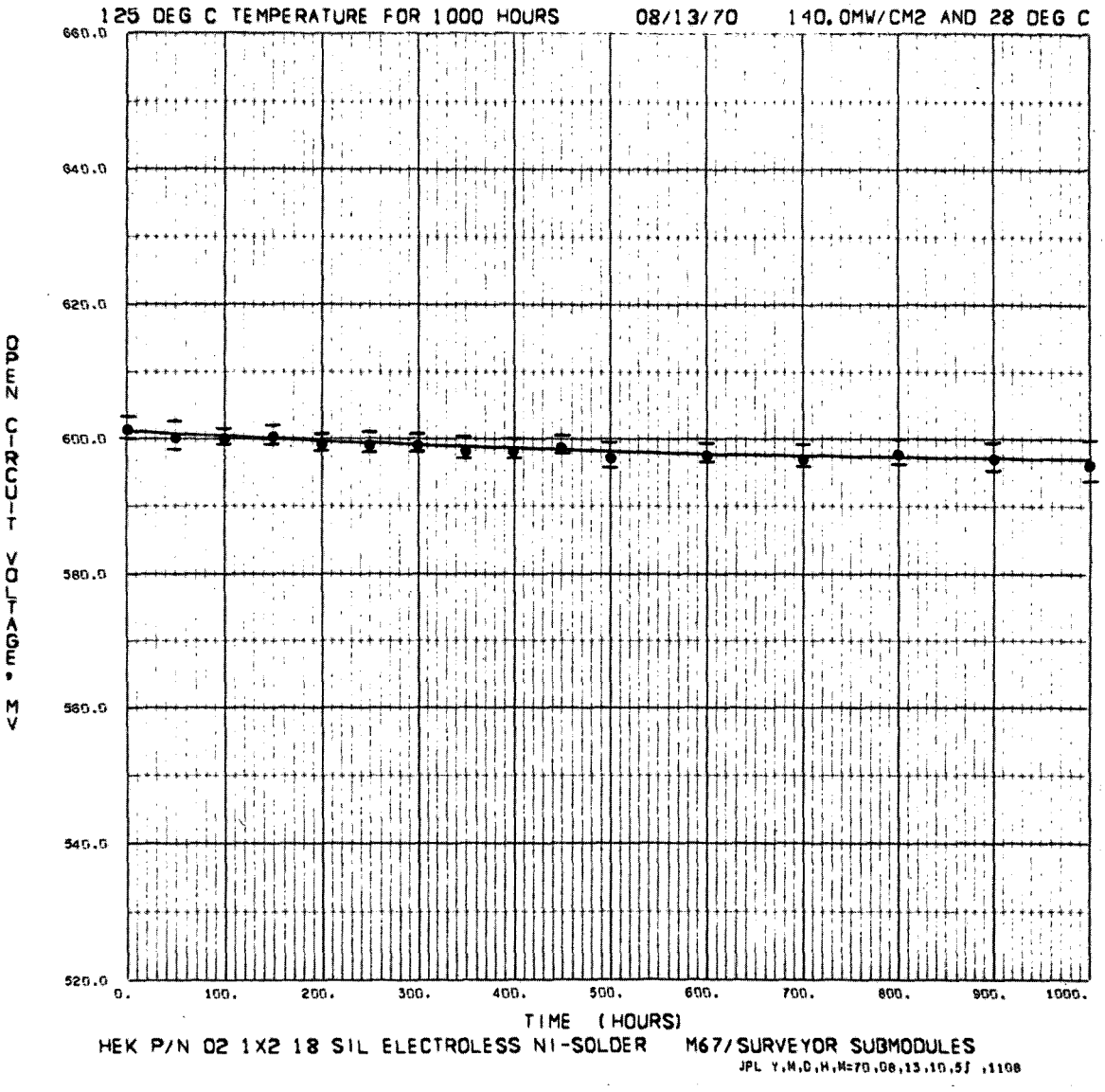


Fig. 71. Open-circuit voltage, cell type M67 module, as a function of time, 125°C storage

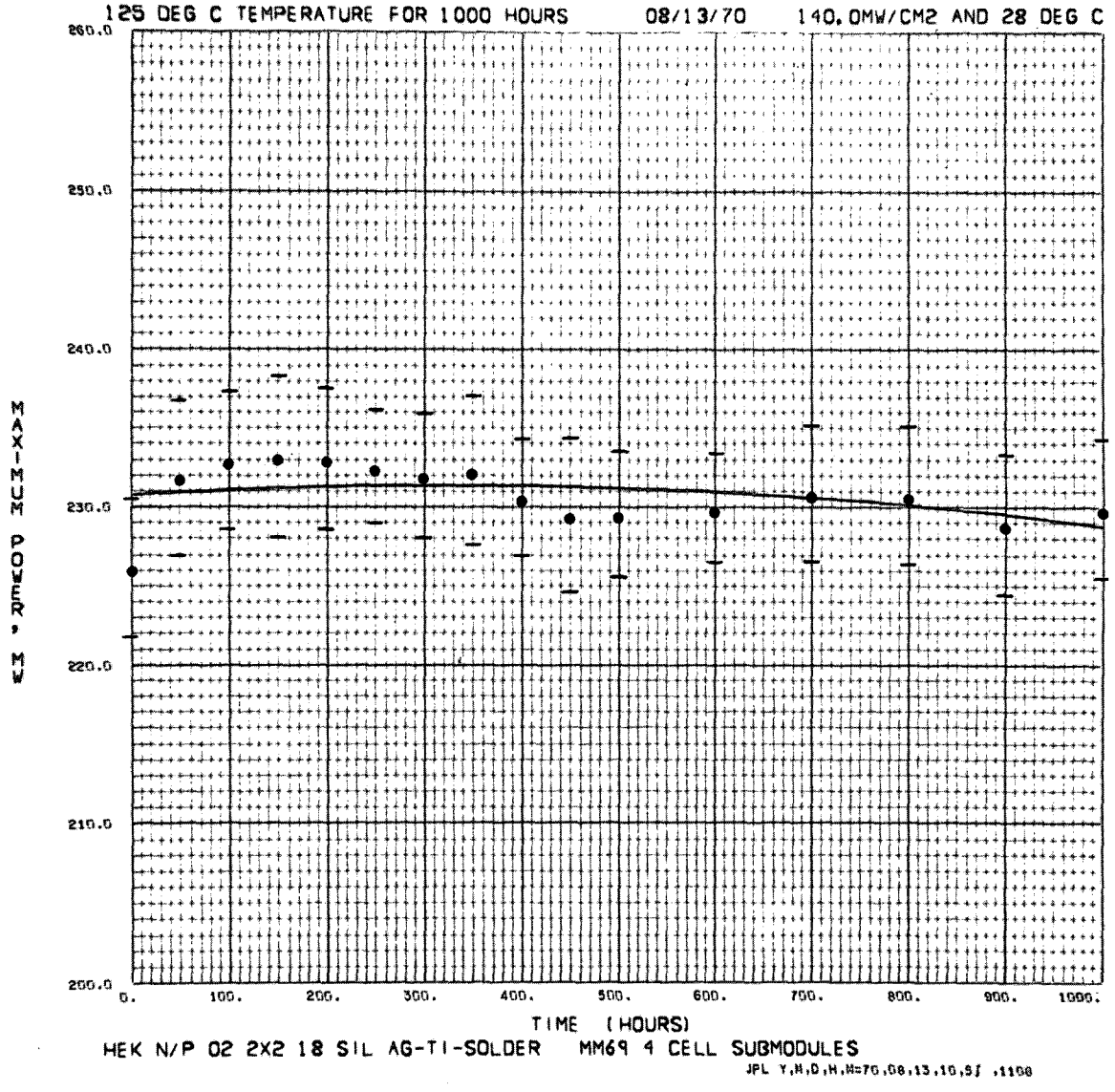


Fig. 72. Maximum-power voltage, cell type M69 module, as a function of time, 125°C storage

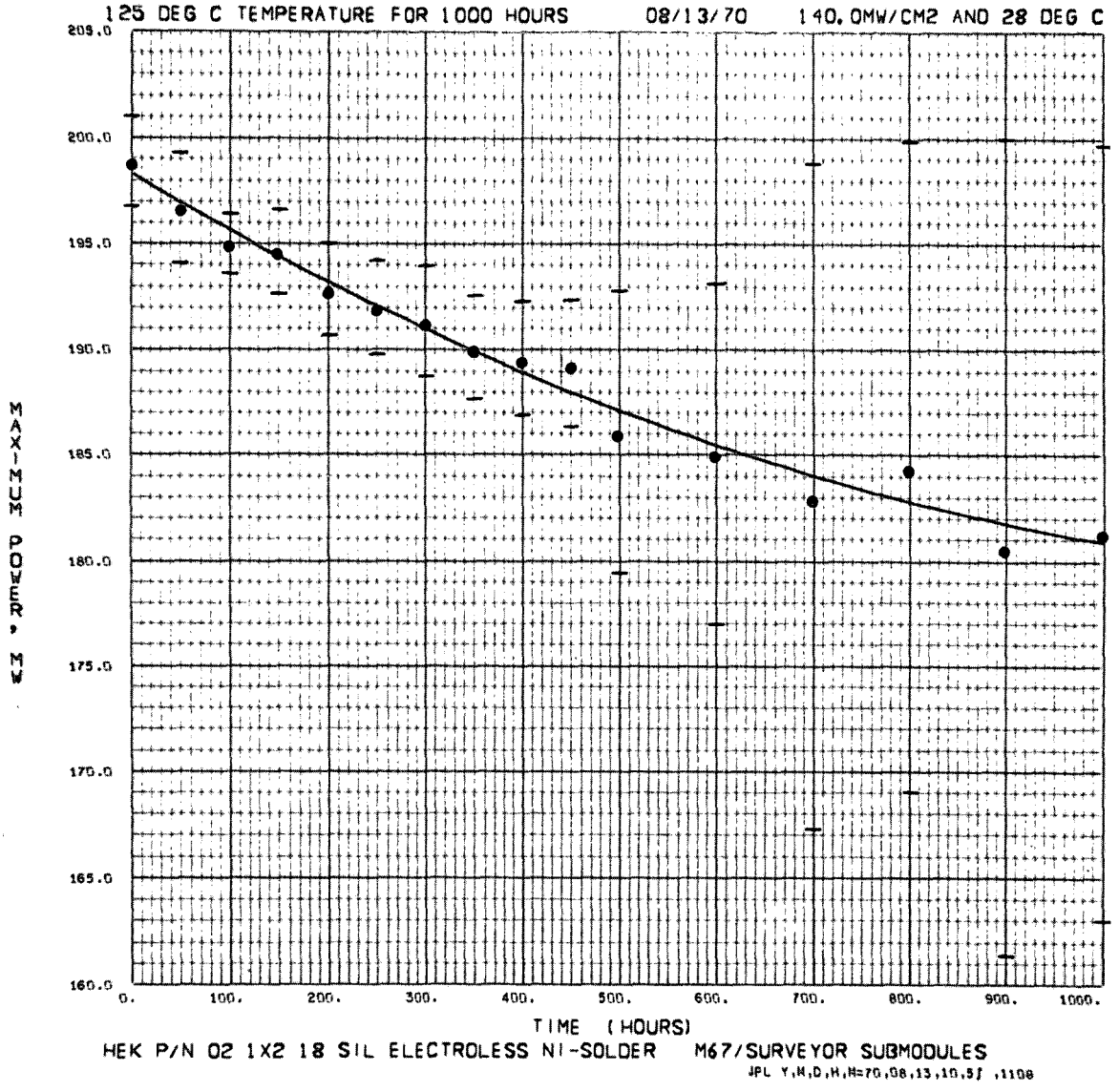


Fig. 73. Maximum-power voltage, cell type M67 module, as a function of time, 125°C storage

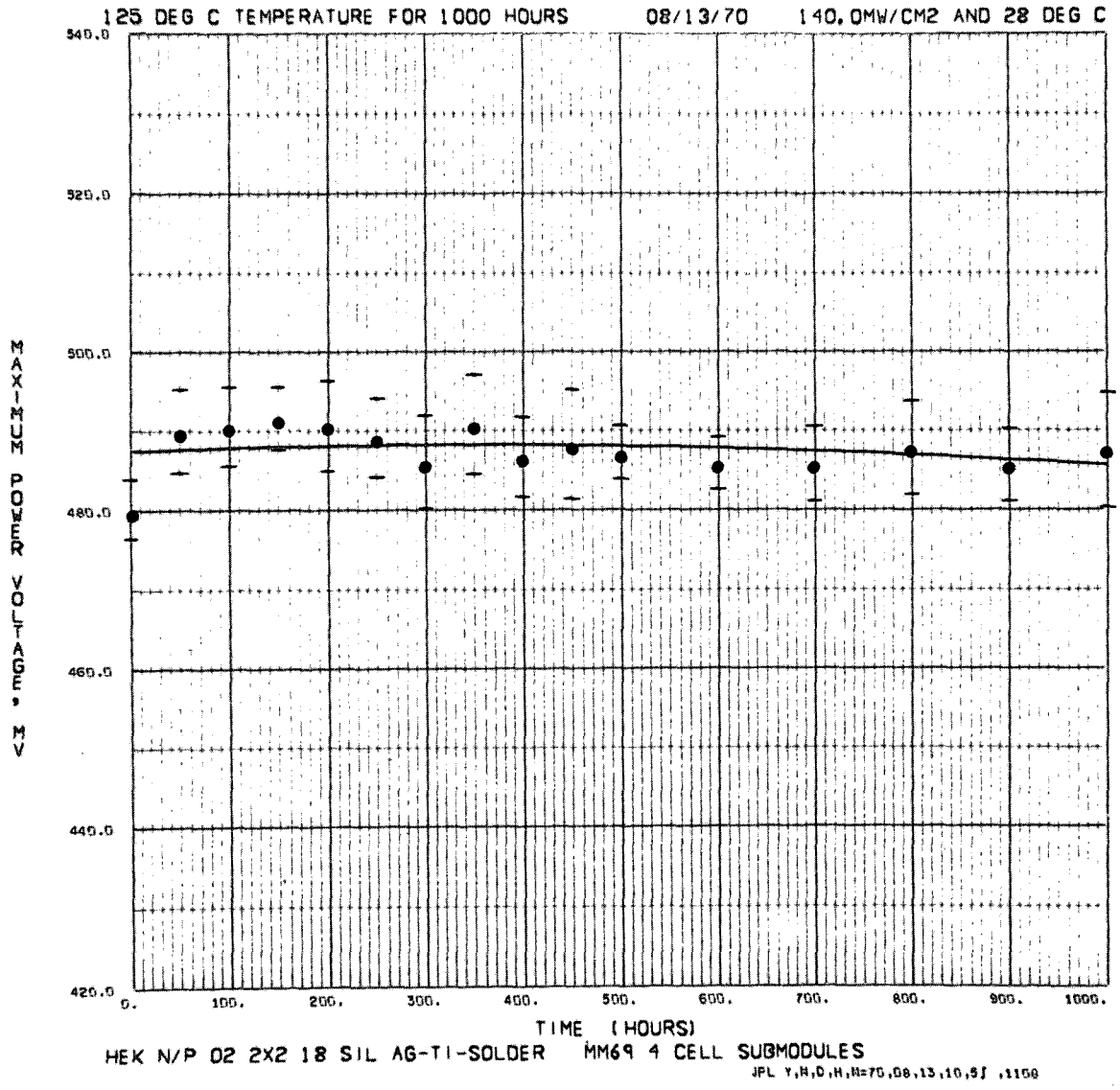


Fig. 74. Maximum-power voltage, cell type M69 module, as a function of time, 125°C storage

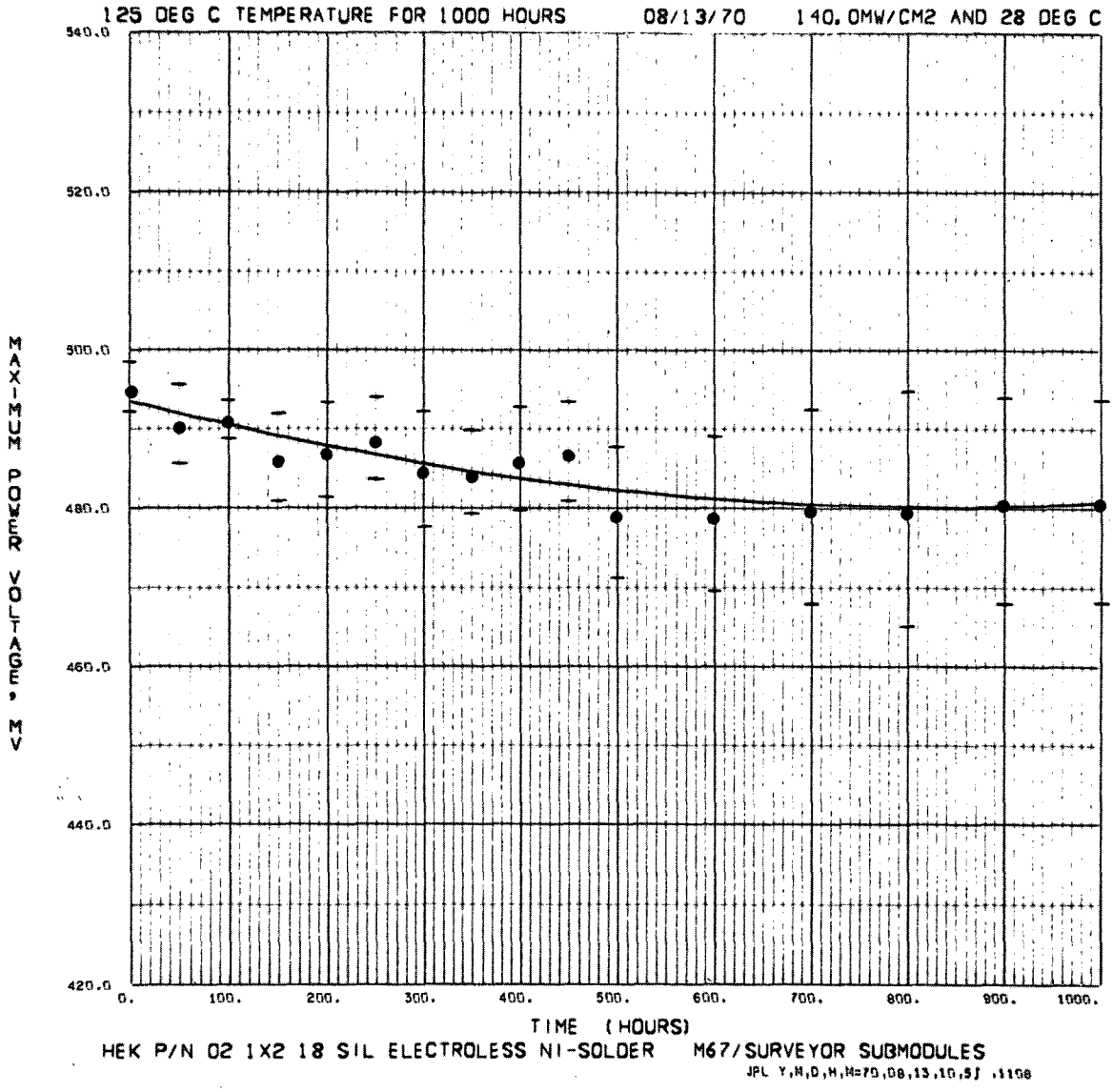


Fig. 75. Maximum-power voltage, cell type M67 module, as a function of time, 125°C storage

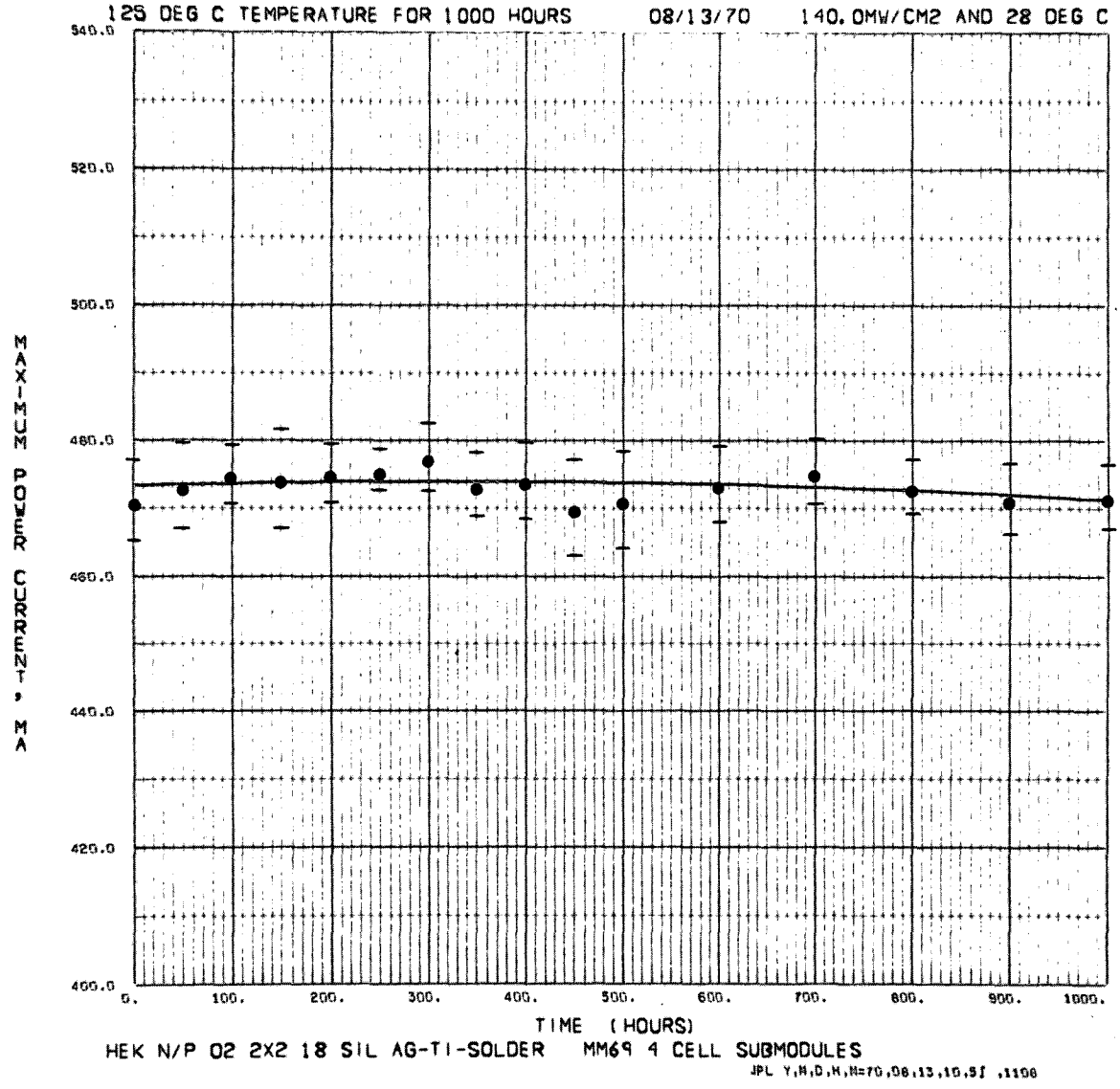


Fig. 76. Maximum-power current, cell type M69 module, as a function of time, 125°C storage

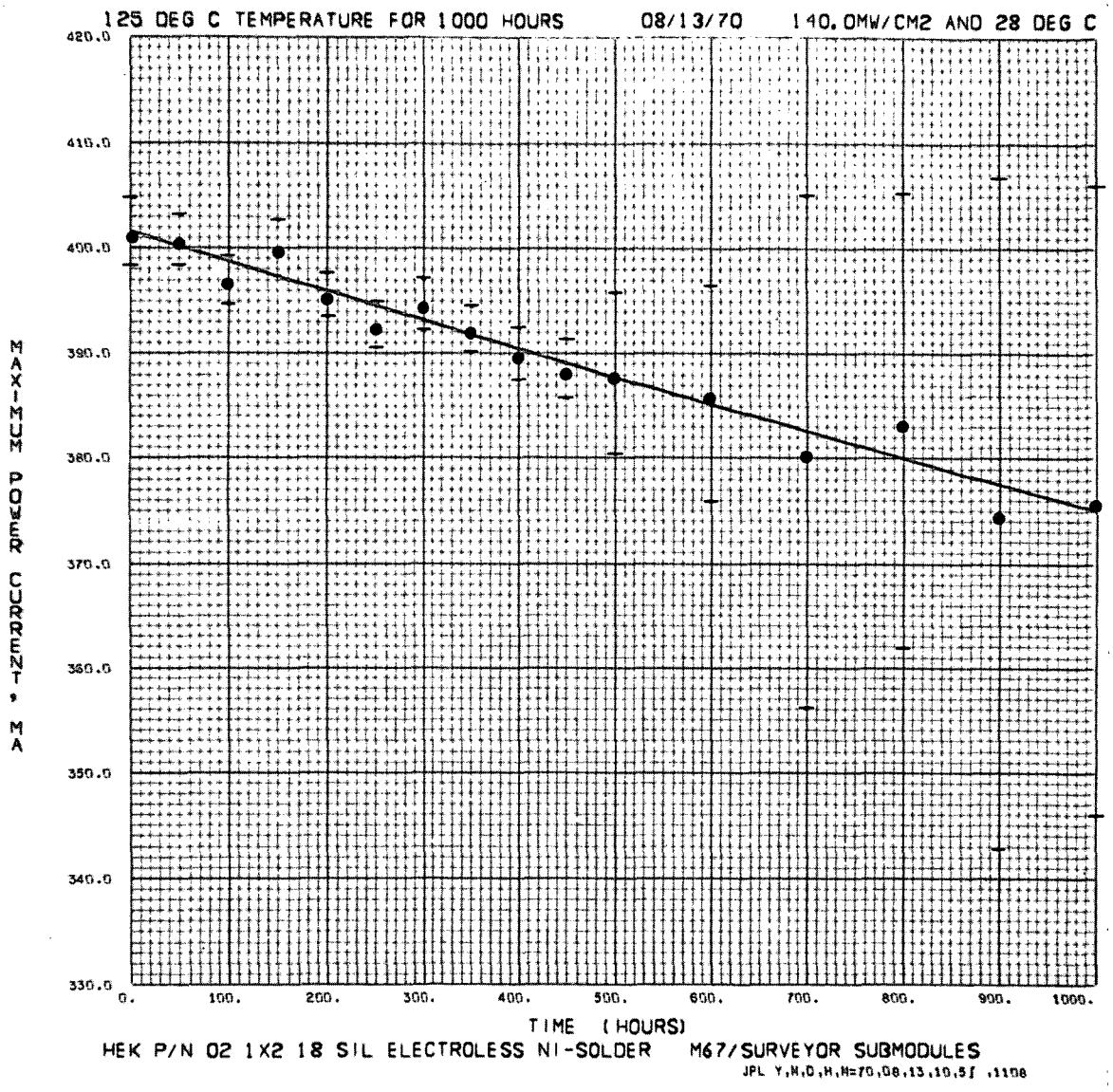


Fig. 77. Maximum-power current, cell type M67 module, as a function of time, 125°C storage

80°C STORAGE

Page intentionally left blank

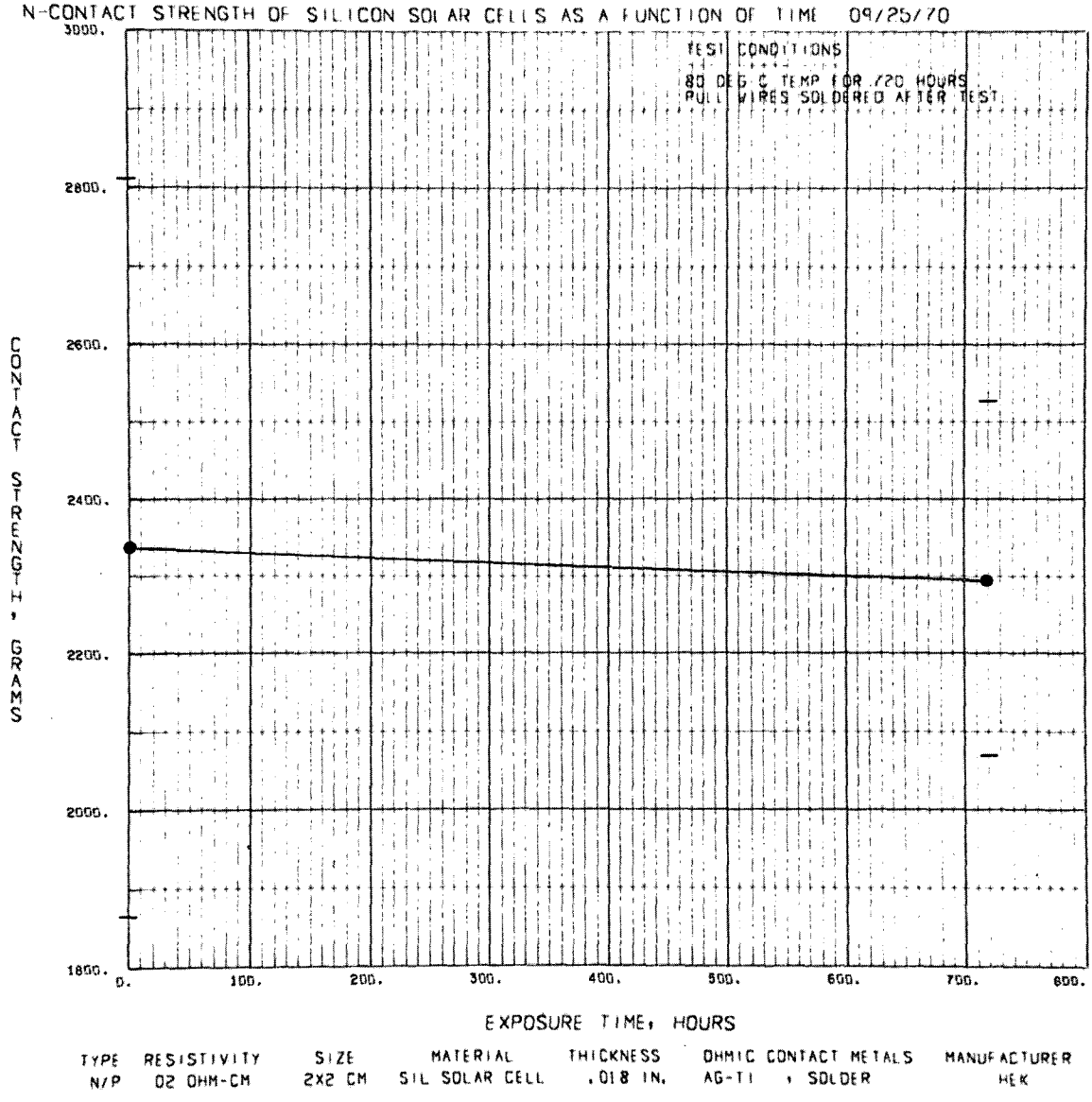


Fig. 78. Top-contact strength, cell type M, as a function of time, 80 °C storage

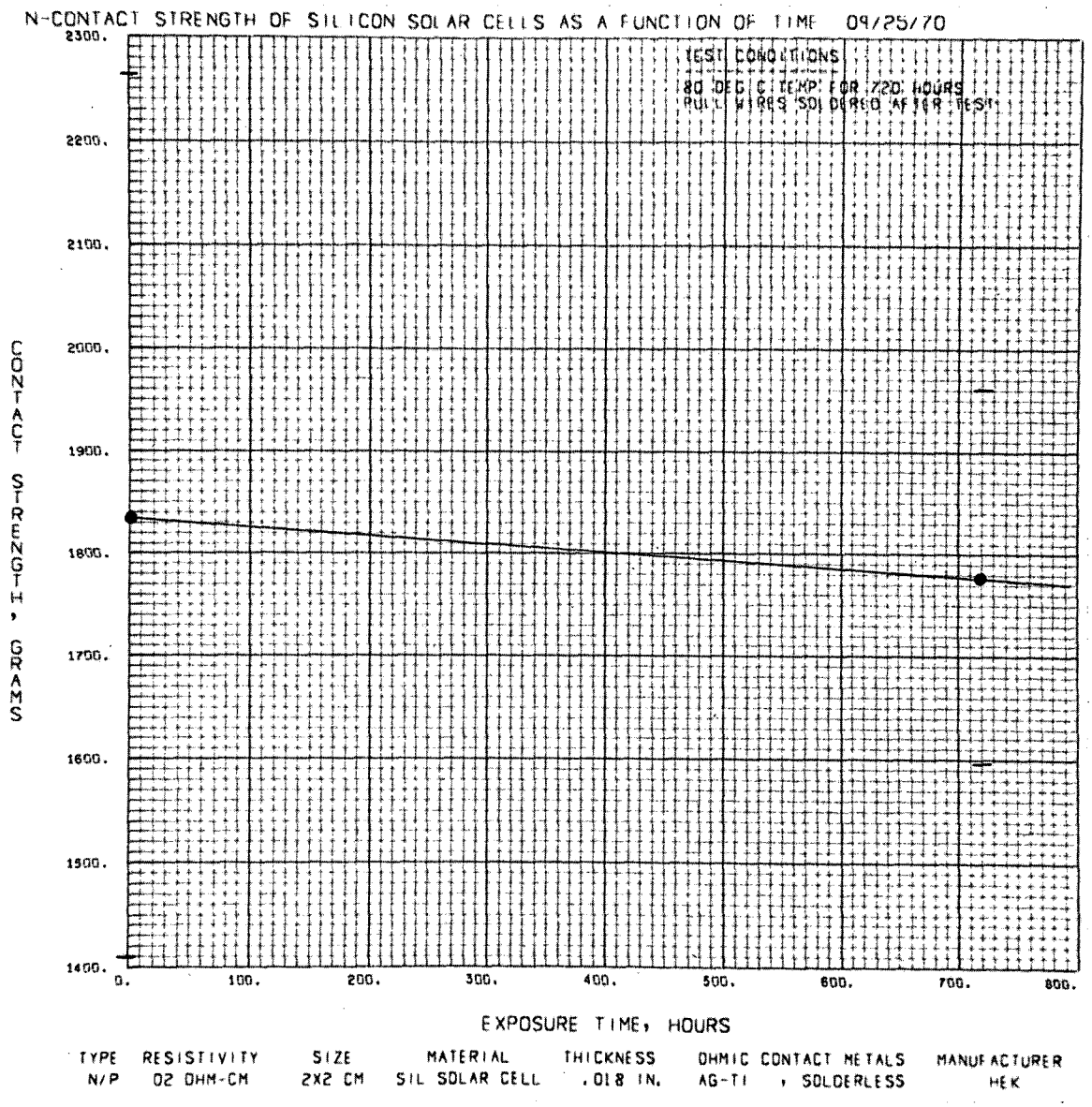


Fig. 79. Top-contact strength, cell type H, as a function of time, 80 °C storage

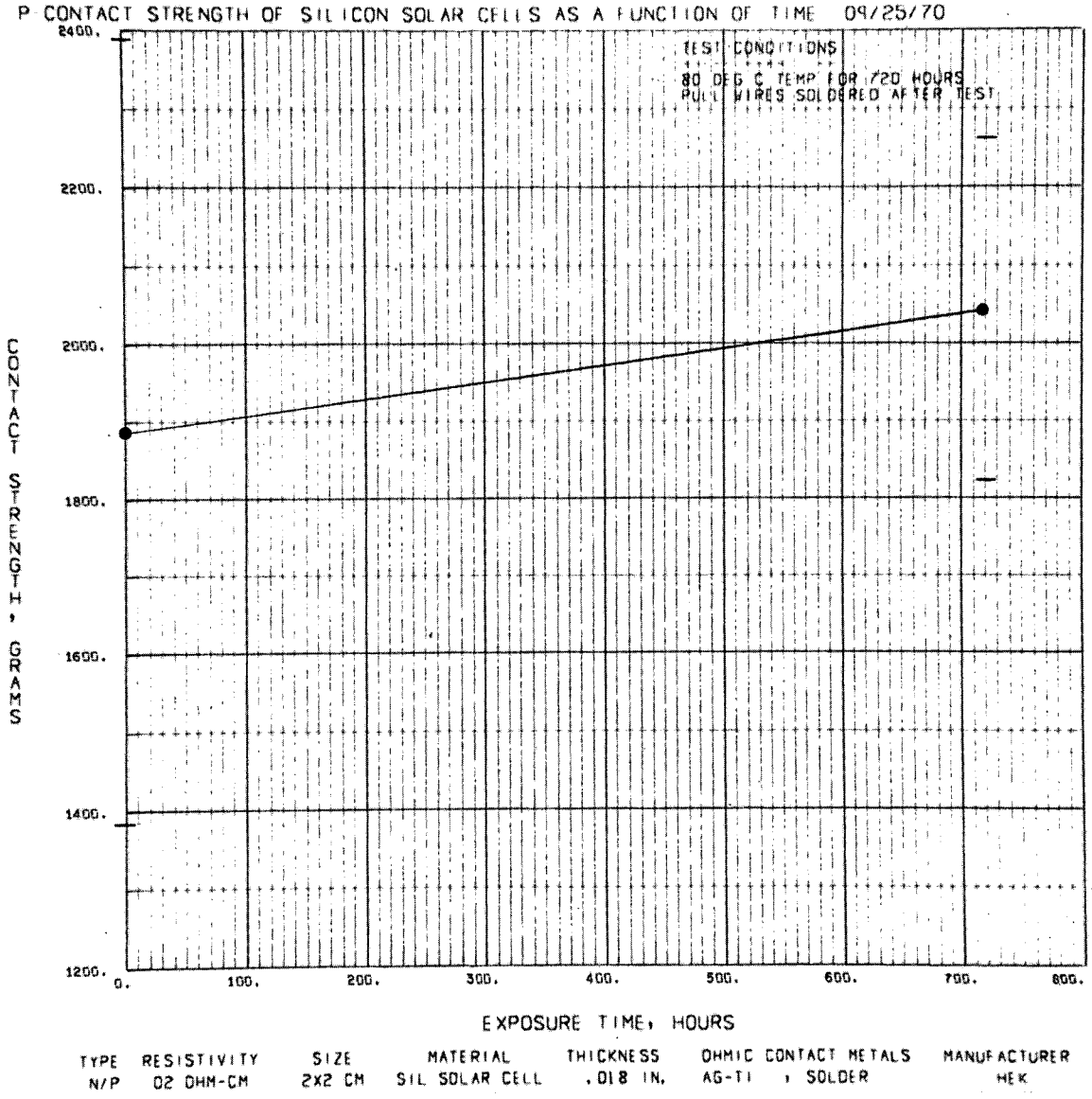


Fig. 80. Bottom-contact strength, cell type M, as a function of time, 80 °C storage

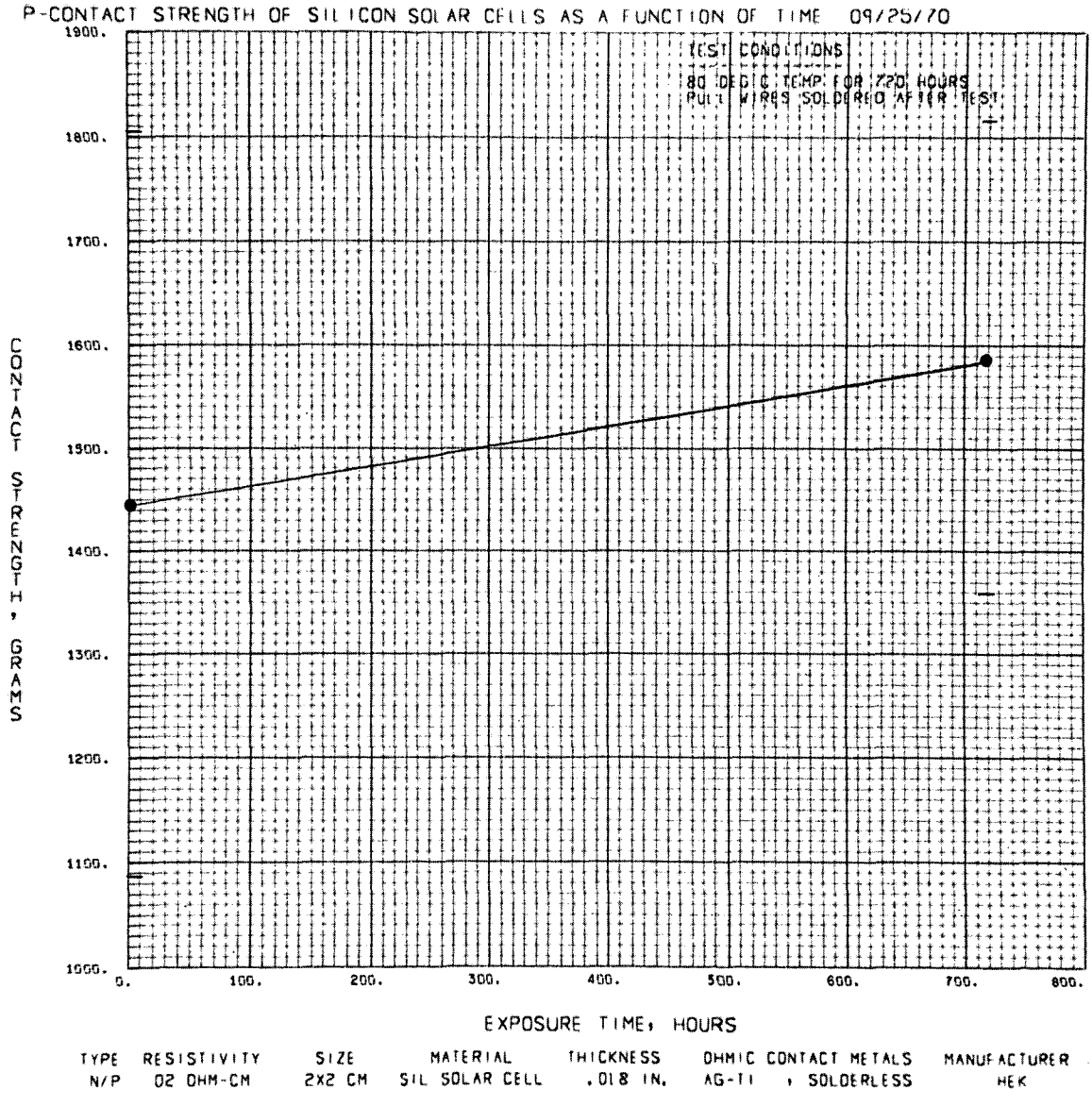


Fig. 81. Bottom-contact strength, cell type H, as a function of time, 80 °C storage

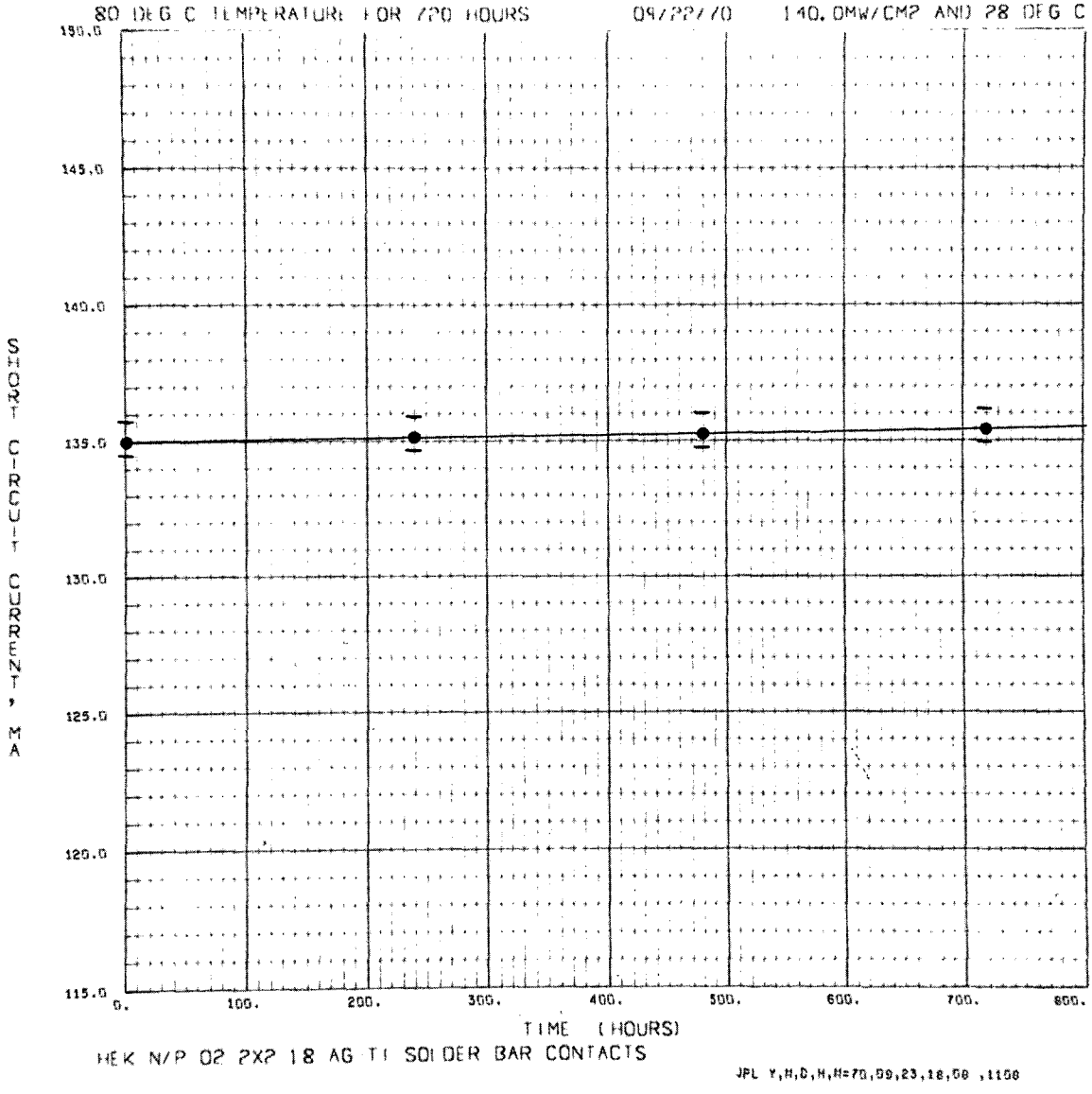


Fig. 82. Short-circuit current, cell type M, as a function of time, 80 °C storage

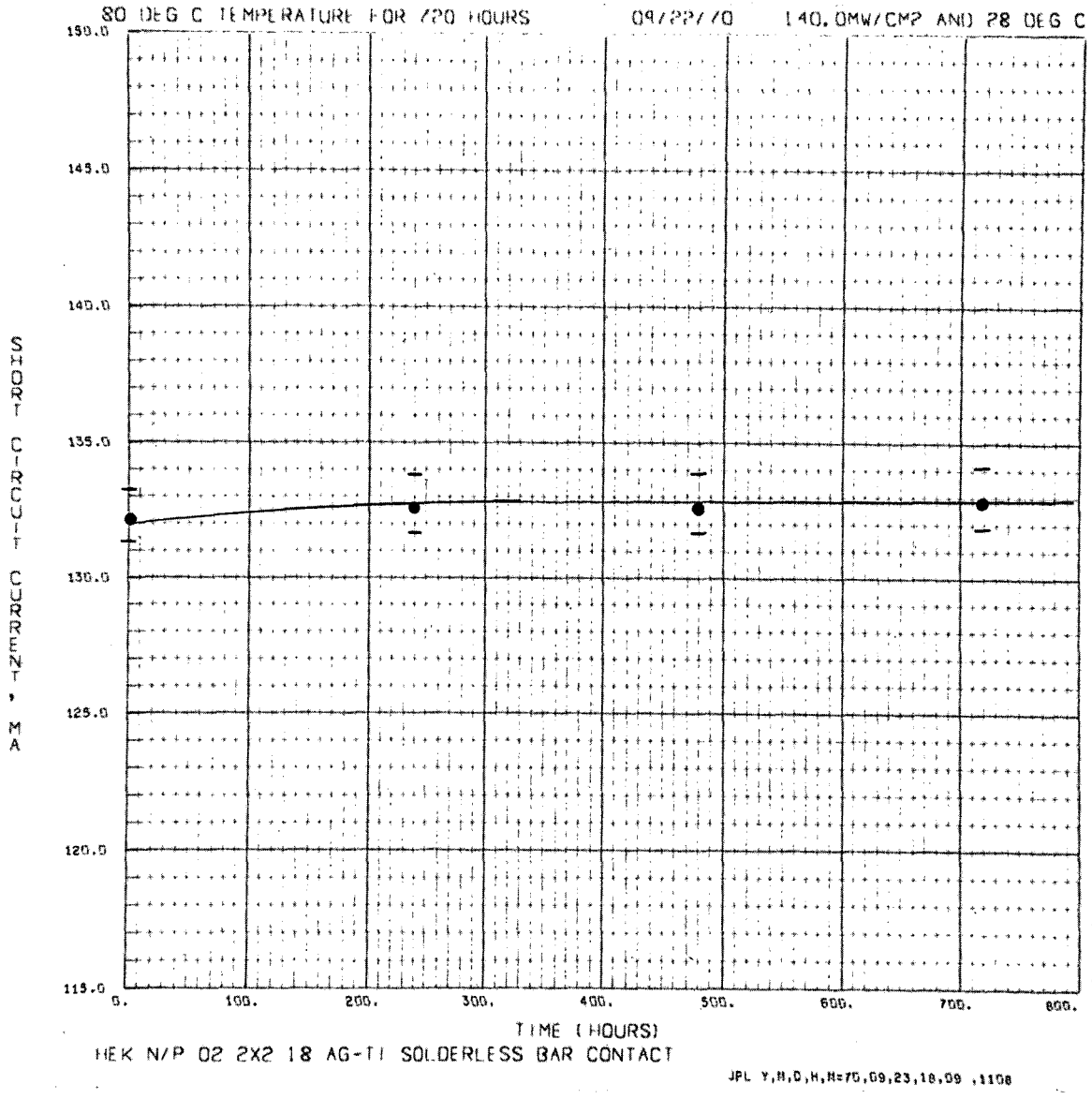


Fig. 83. Short-circuit current, cell type H, as a function of time, 80 °C storage

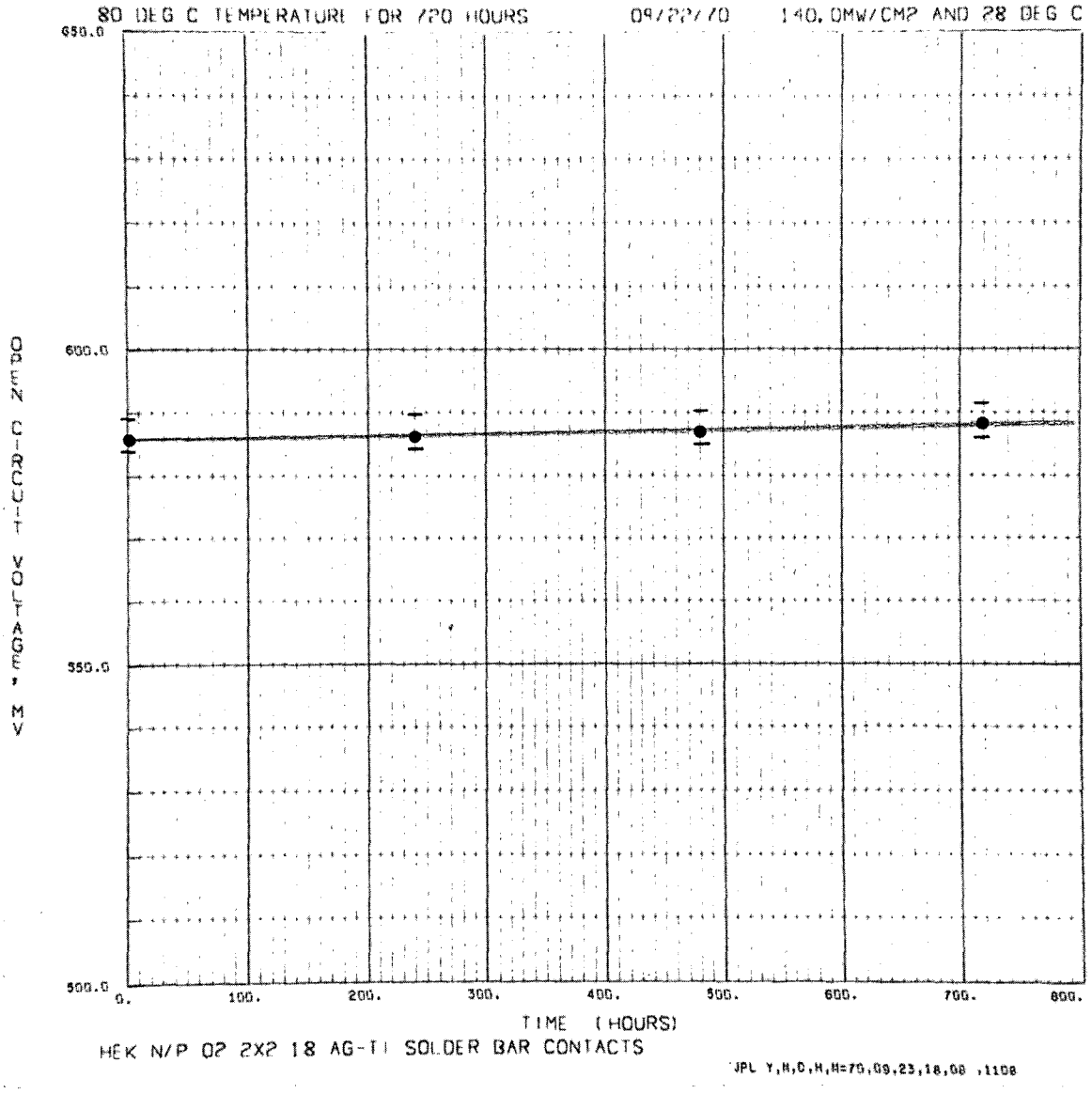


Fig. 84. Open-circuit voltage, cell type M, as a function of time, 80 °C storage

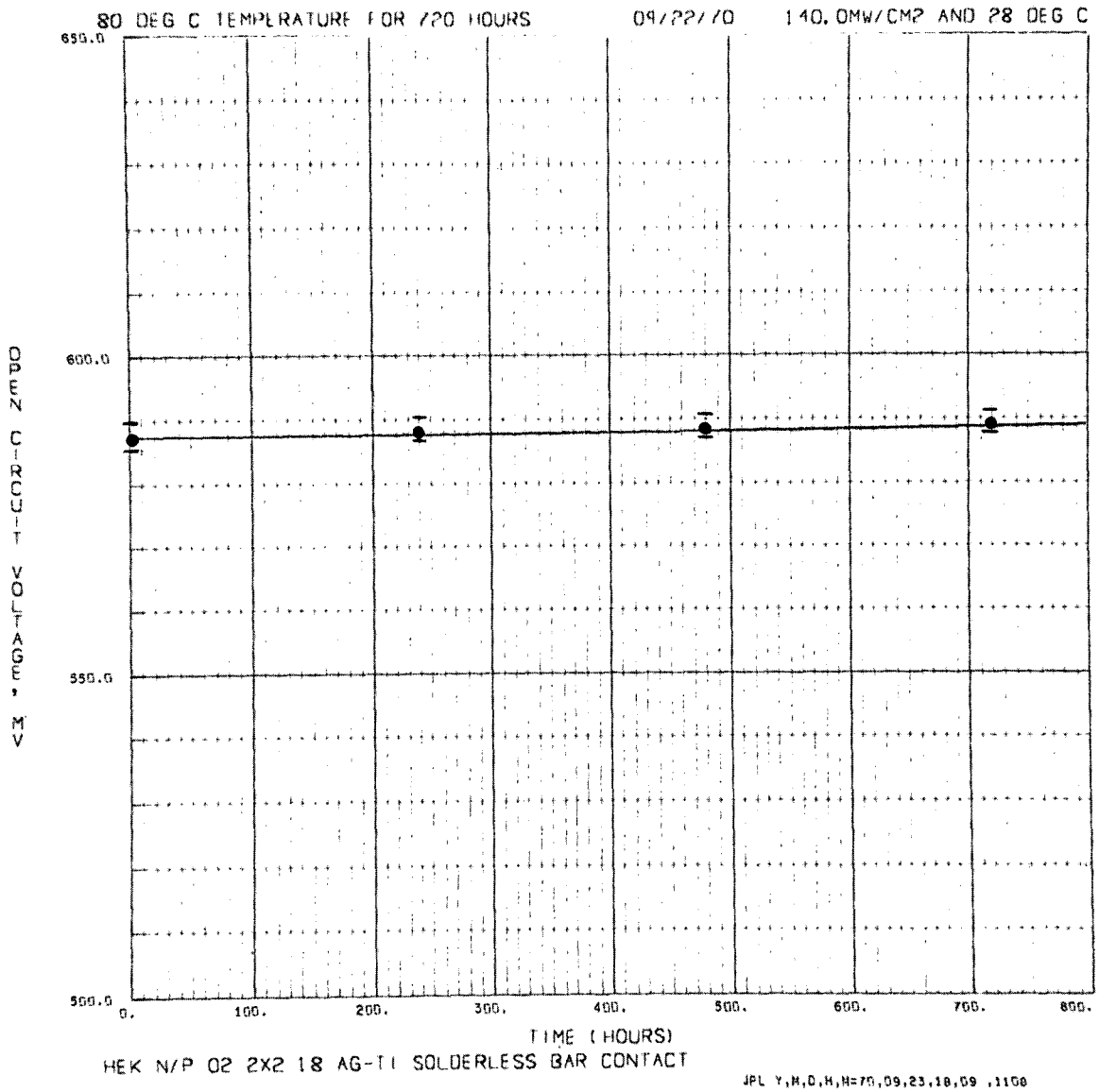


Fig. 85. Open-circuit voltage, cell type H, as a function of time, 80 °C storage

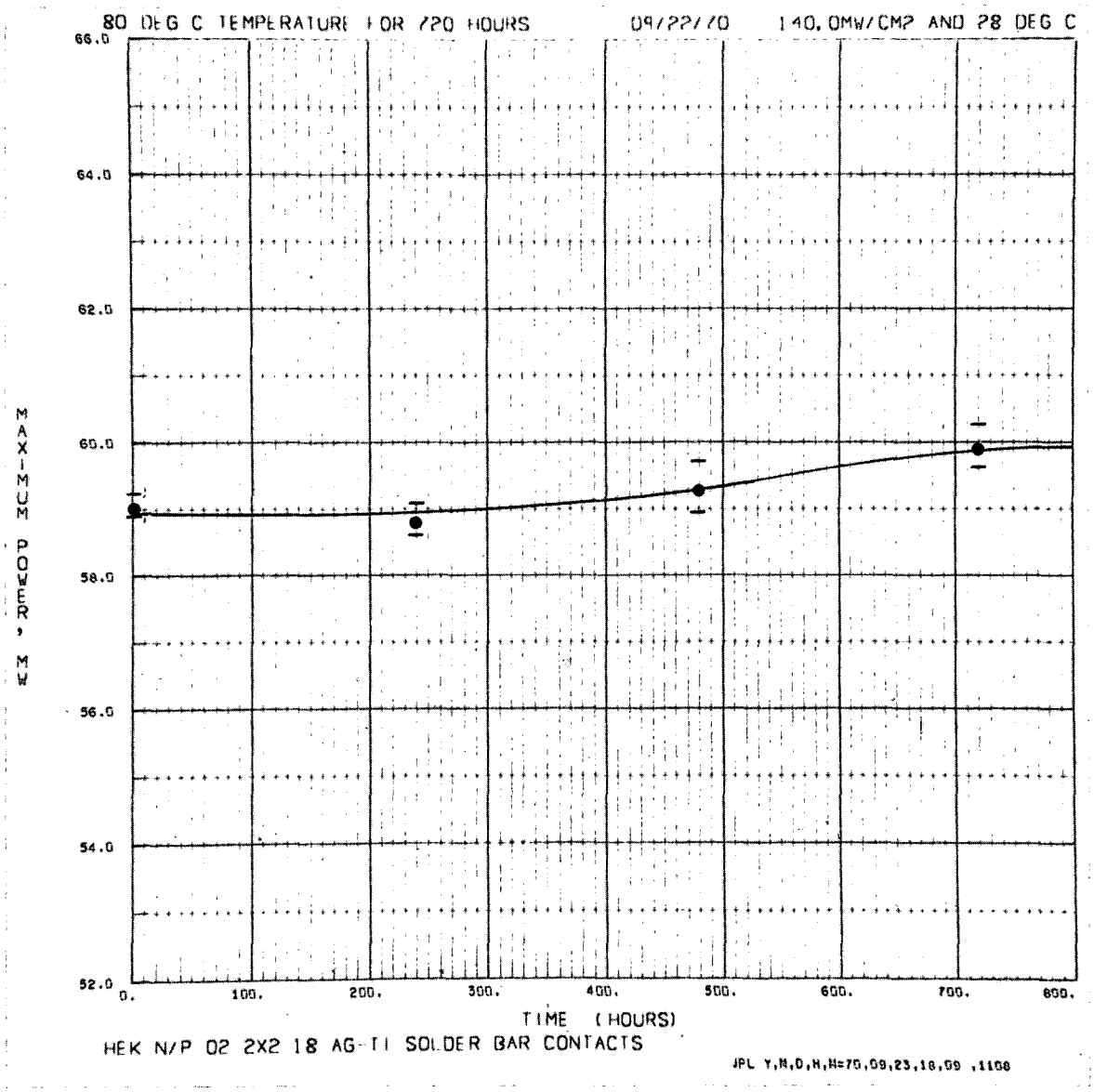


Fig. 86. Maximum-power voltage, cell type M, as a function of time, 80 °C storage

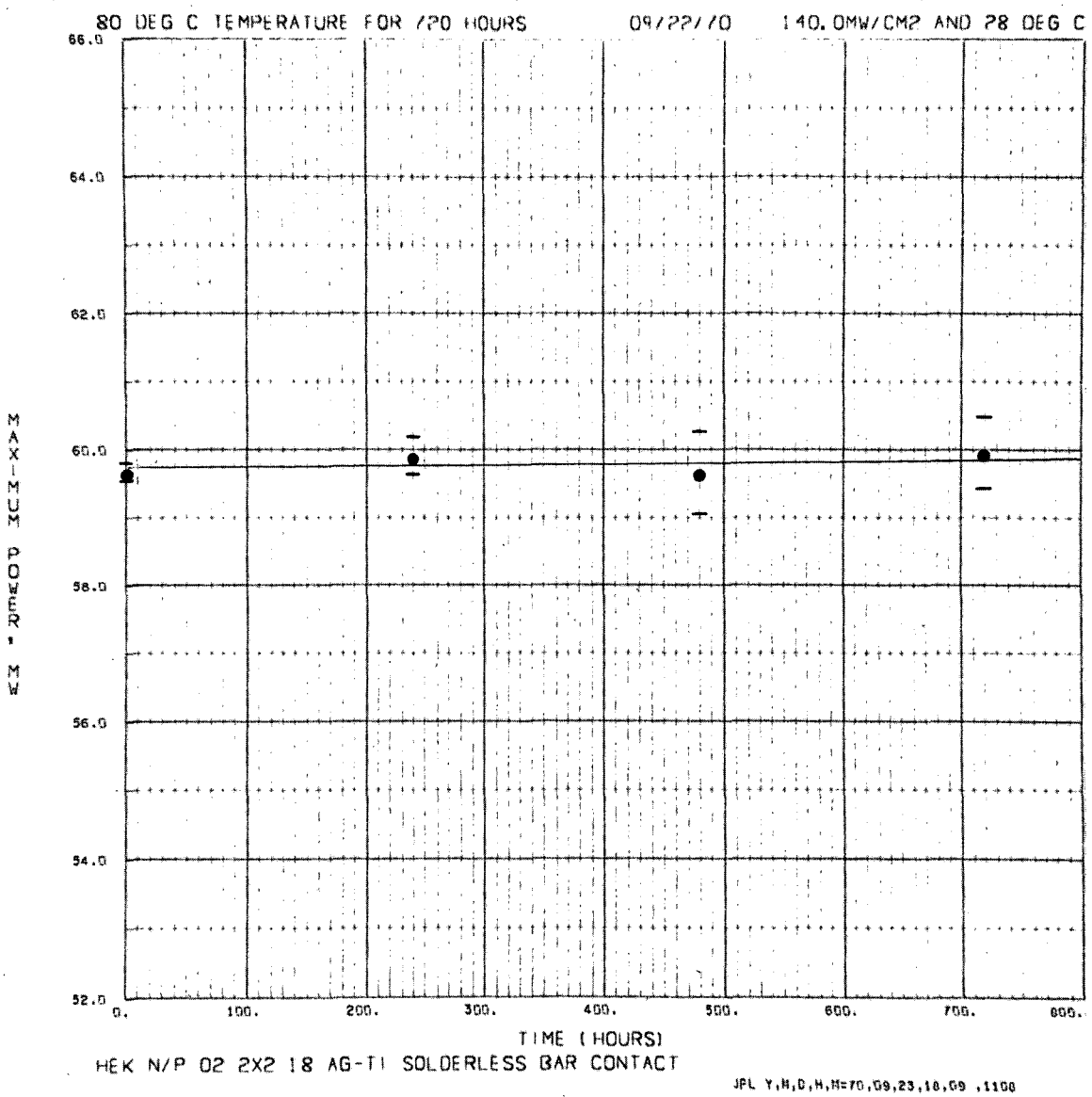


Fig. 87. Maximum-power voltage, cell type H, as a function of time, 80 °C storage

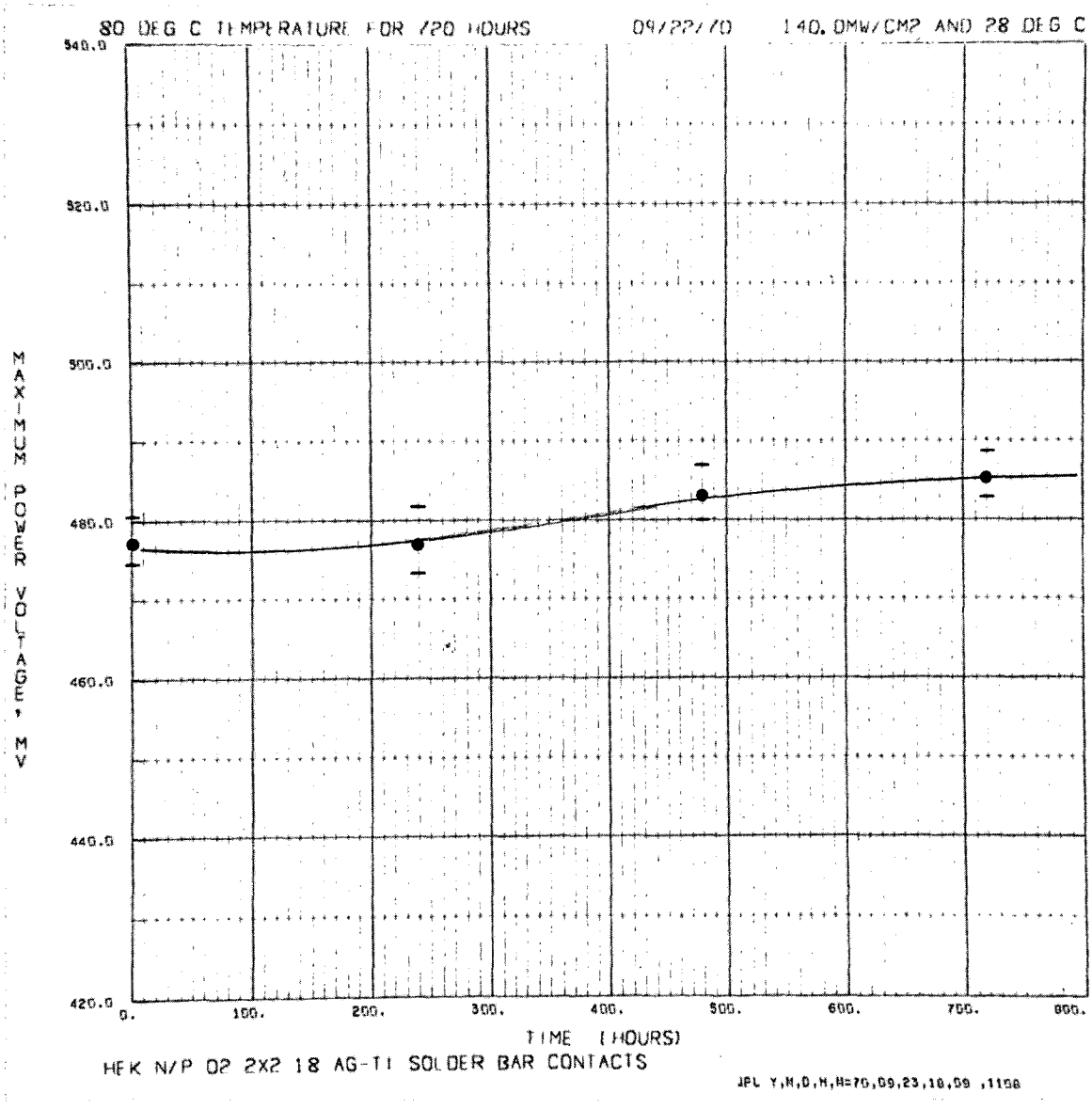


Fig. 88. Maximum-power voltage, cell type M, as a function of time, 80 °C storage

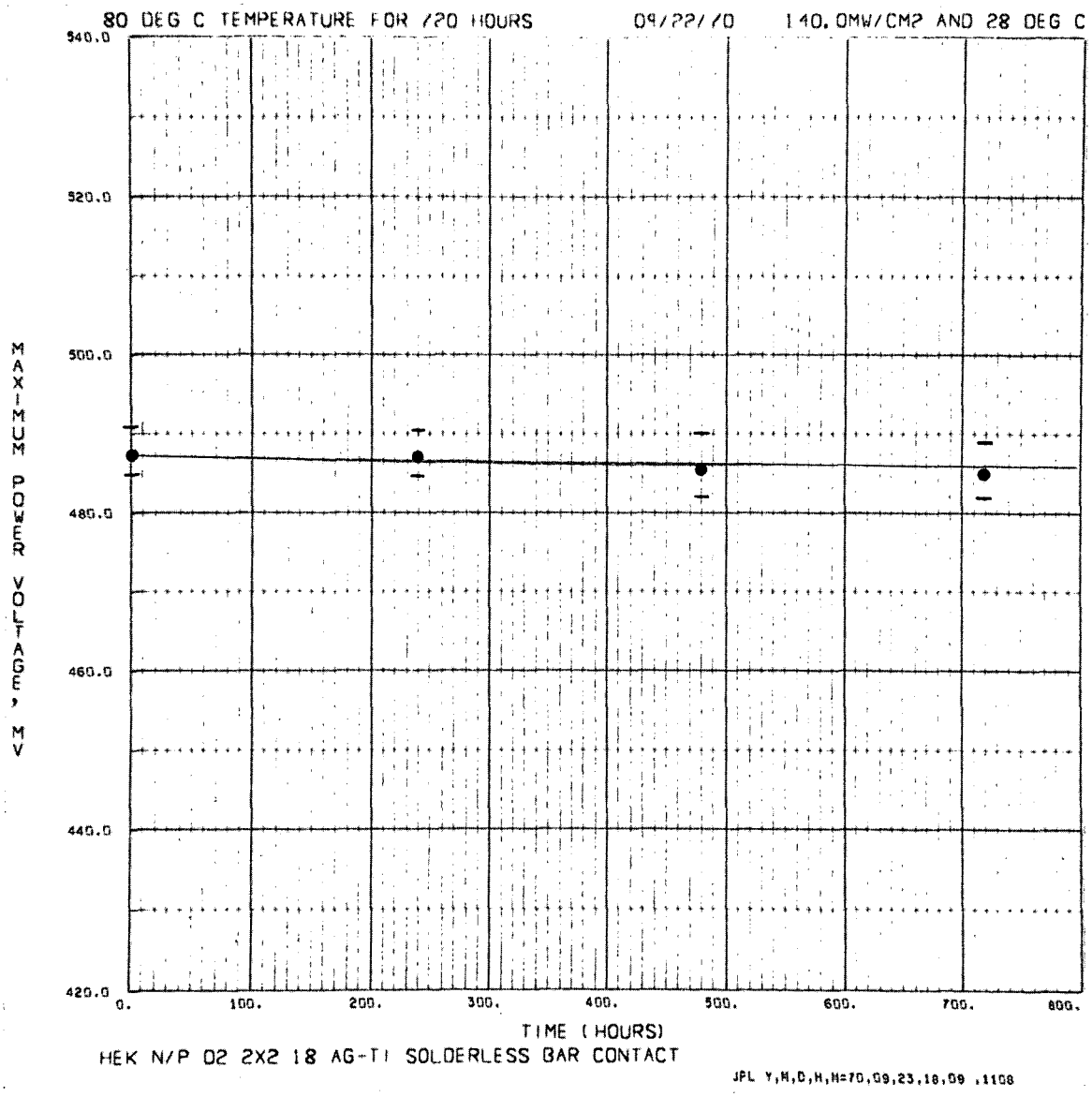


Fig. 89. Maximum-power voltage, cell type H, as a function of time, 80 °C storage

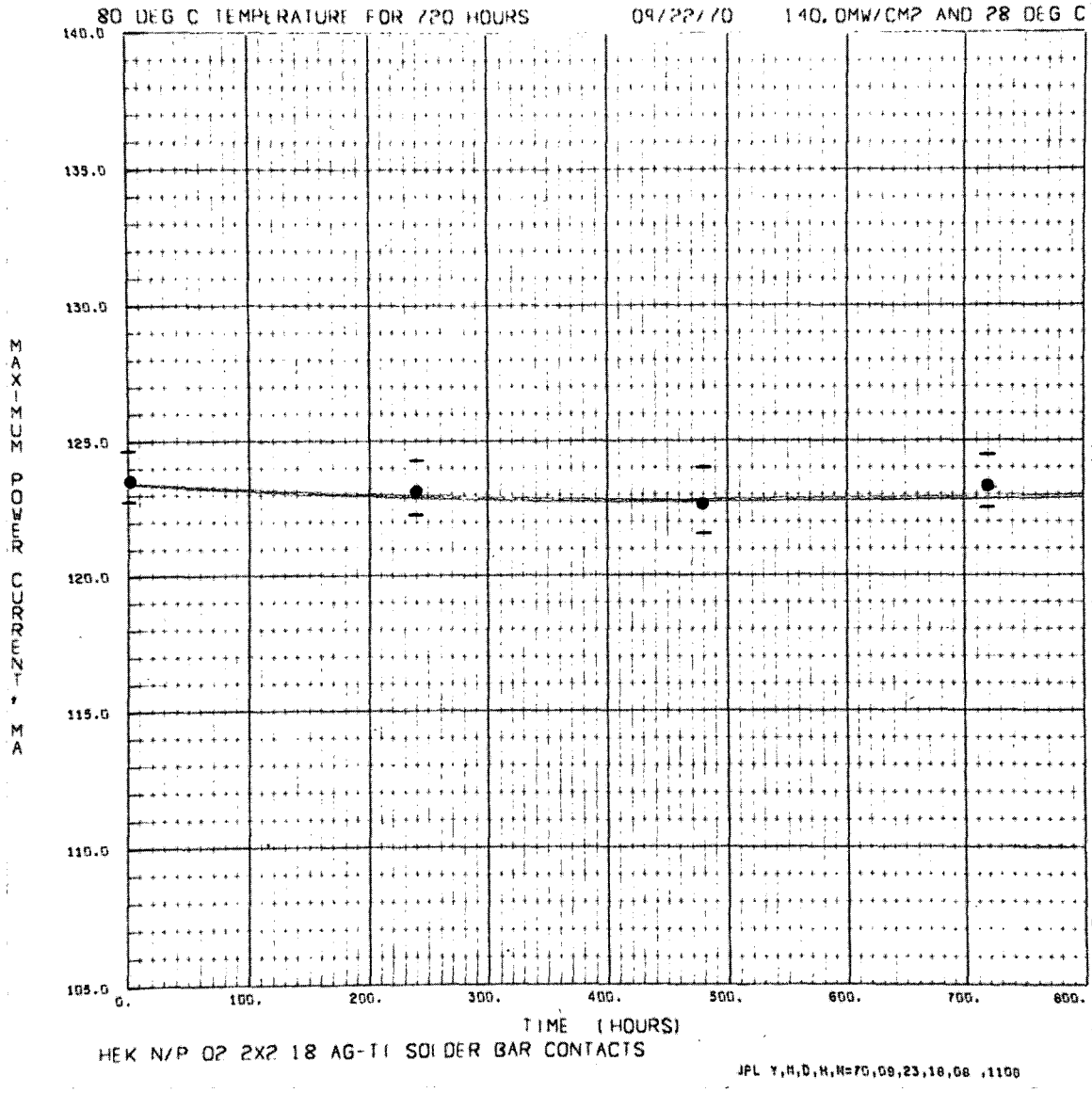


Fig. 90. Maximum-power current, cell type M, as a function of time, 80 °C storage

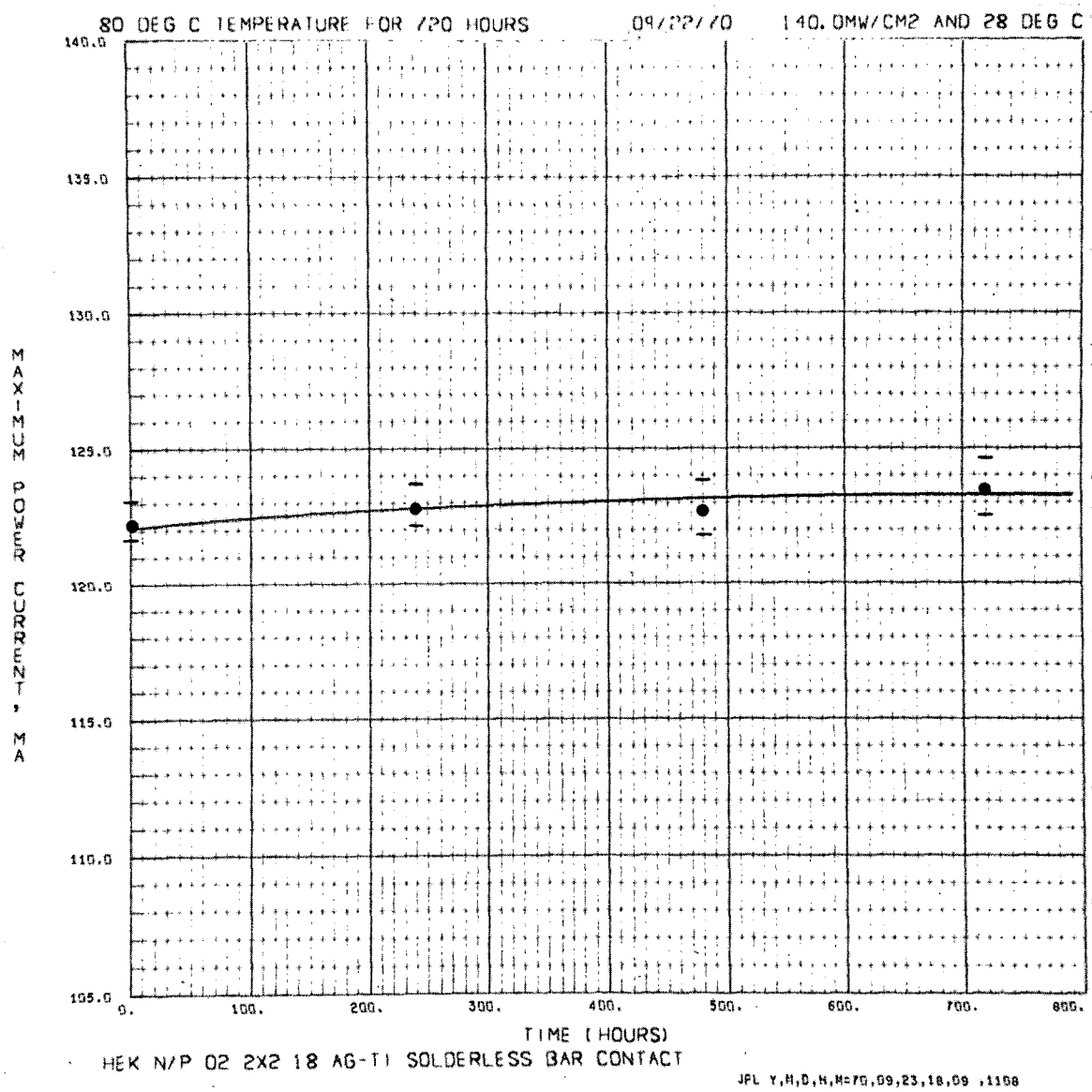


Fig. 91. Maximum-power current, cell type H, as a function of time, 80 °C storage

-196 °C (LIQUID NITROGEN) STORAGE

Page intentionally left blank

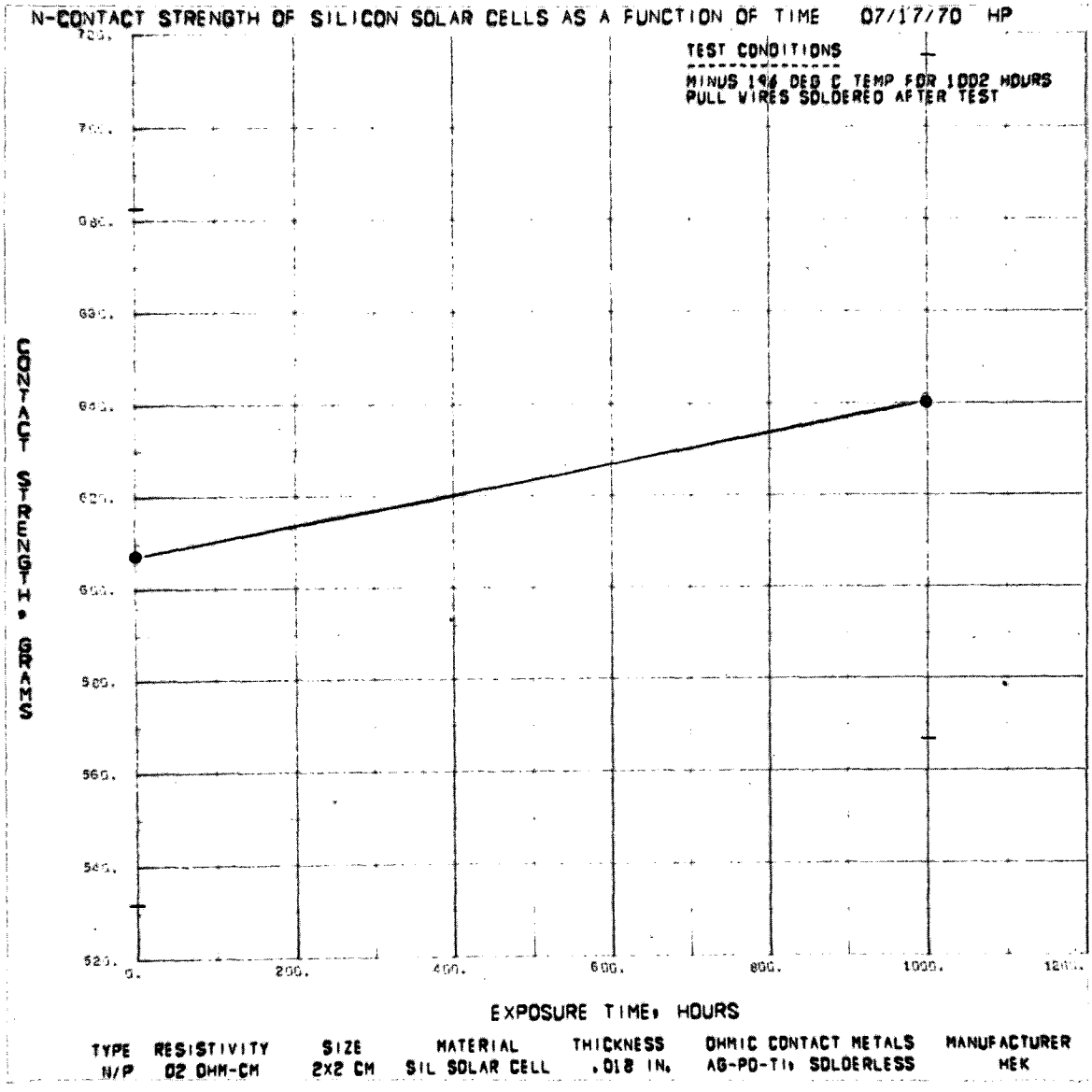


Fig. 92. Top-contact strength, cell type HP, as a function of time, -196°C storage

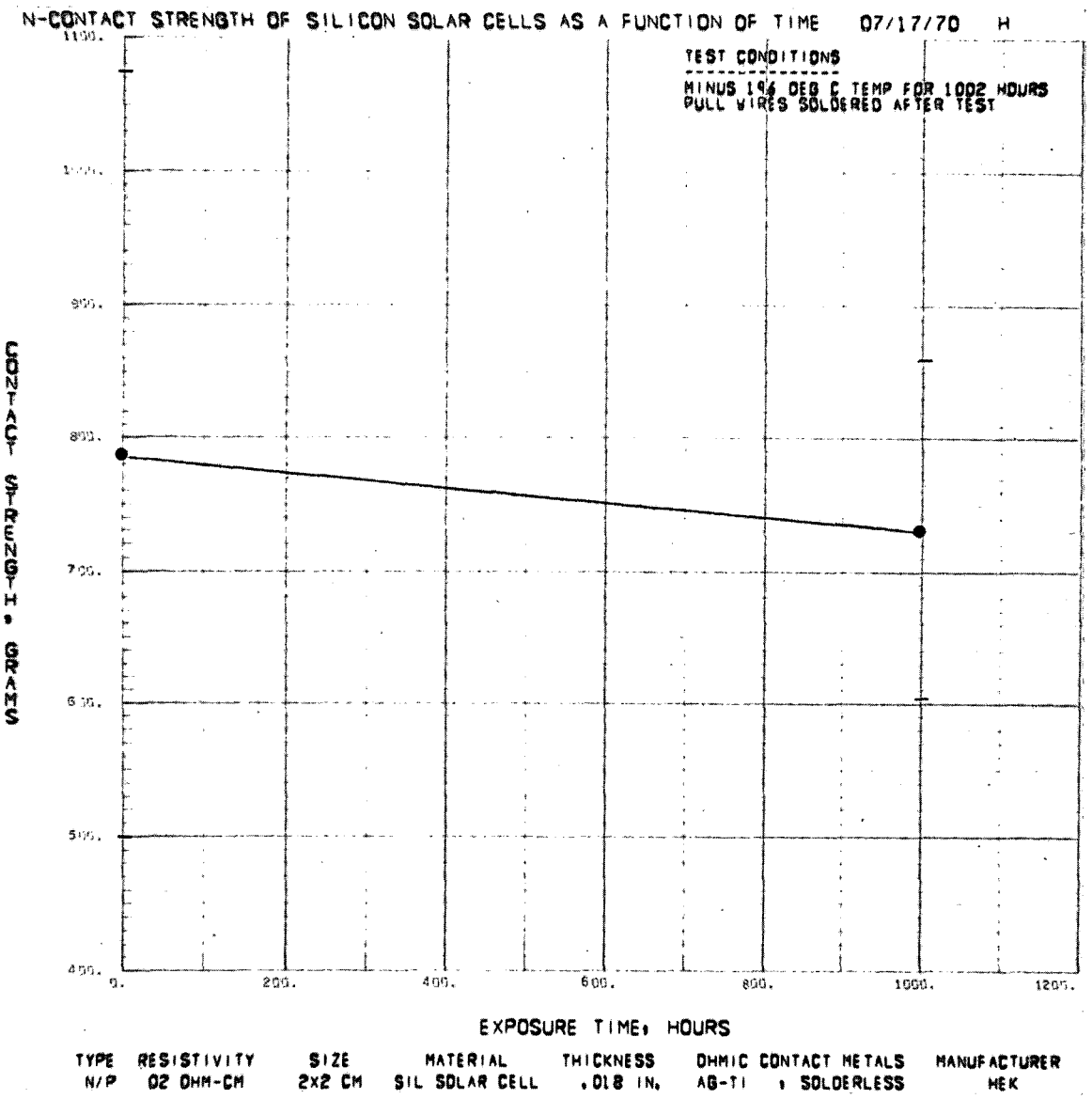


Fig. 93. Top-contact strength, cell type H, as a function of time, -196°C storage

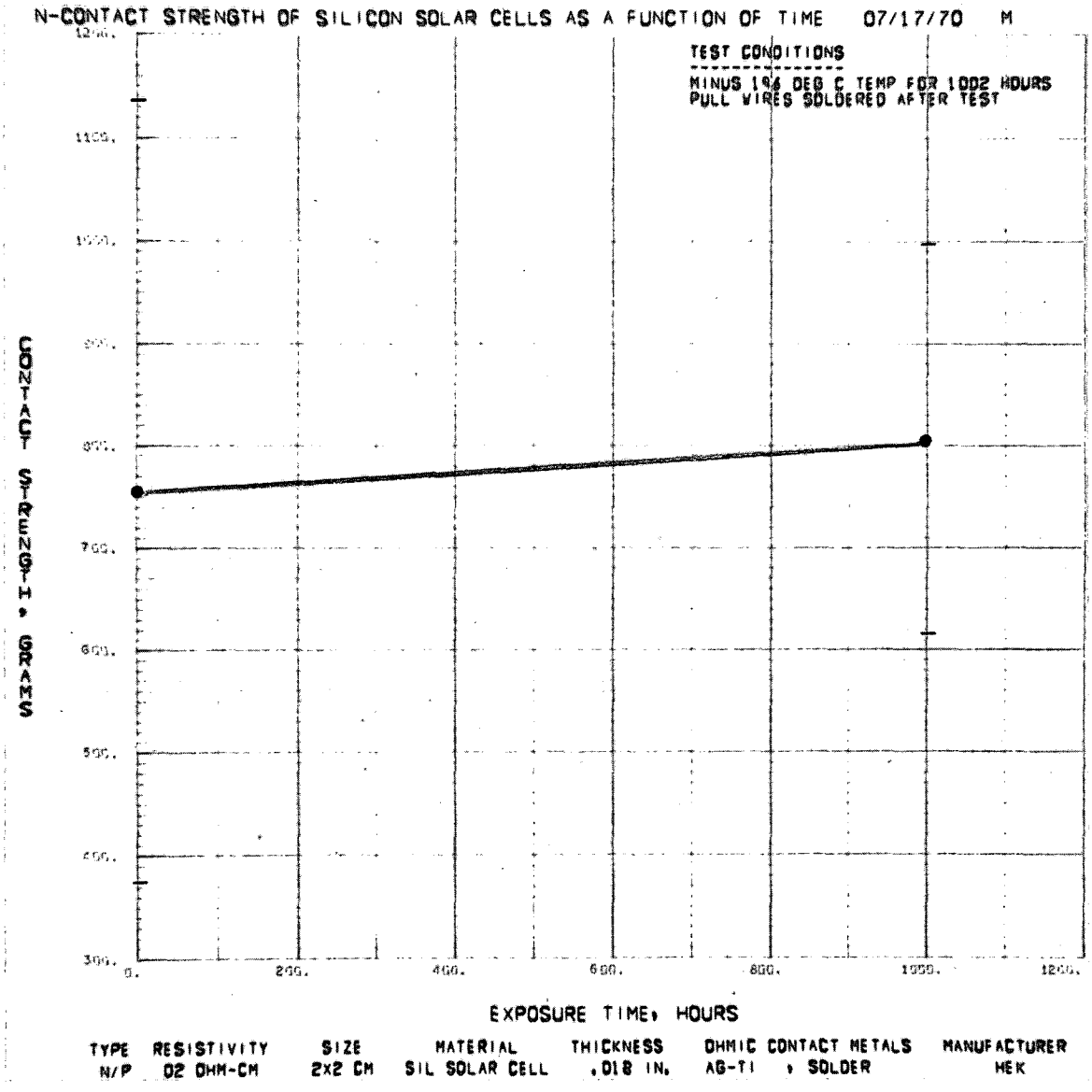


Fig. 94. Top-contact strength, cell type M, as a function of time, -196°C storage

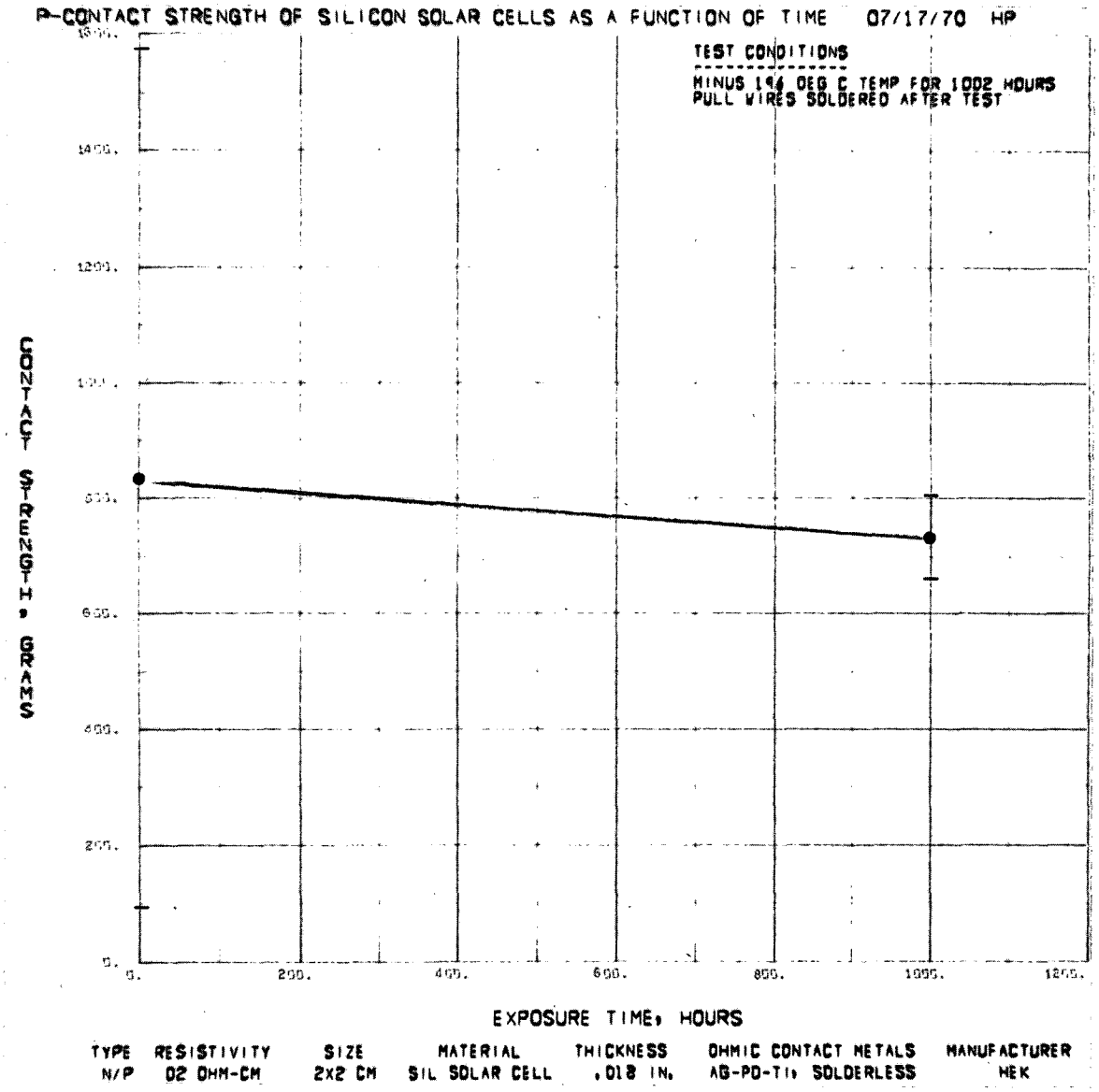


Fig. 95. Bottom-contact strength, cell type HP, as a function of time, -196°C storage

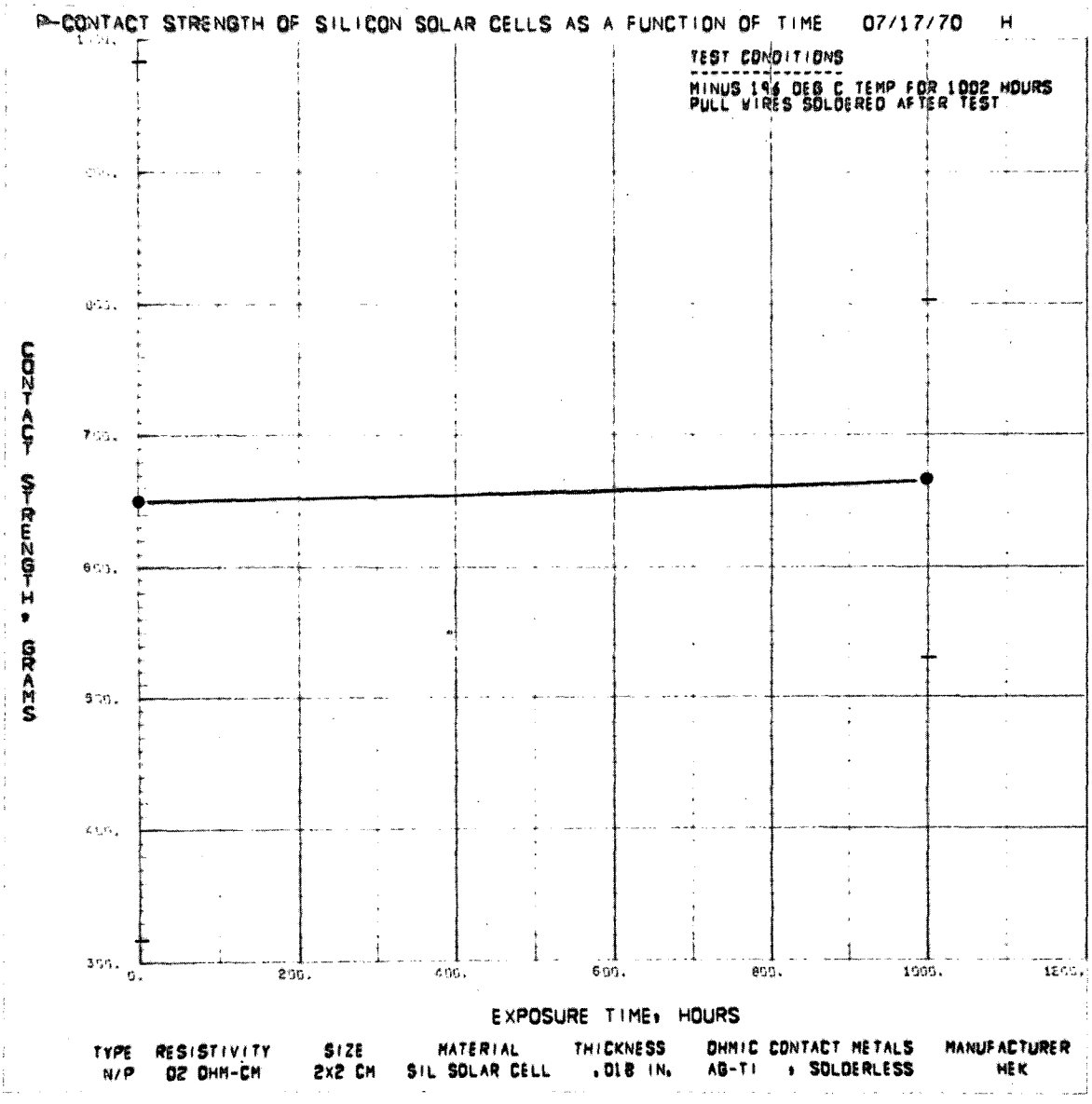


Fig. 96. Bottom-contact strength, cell type H, as a function of time, -196°C storage

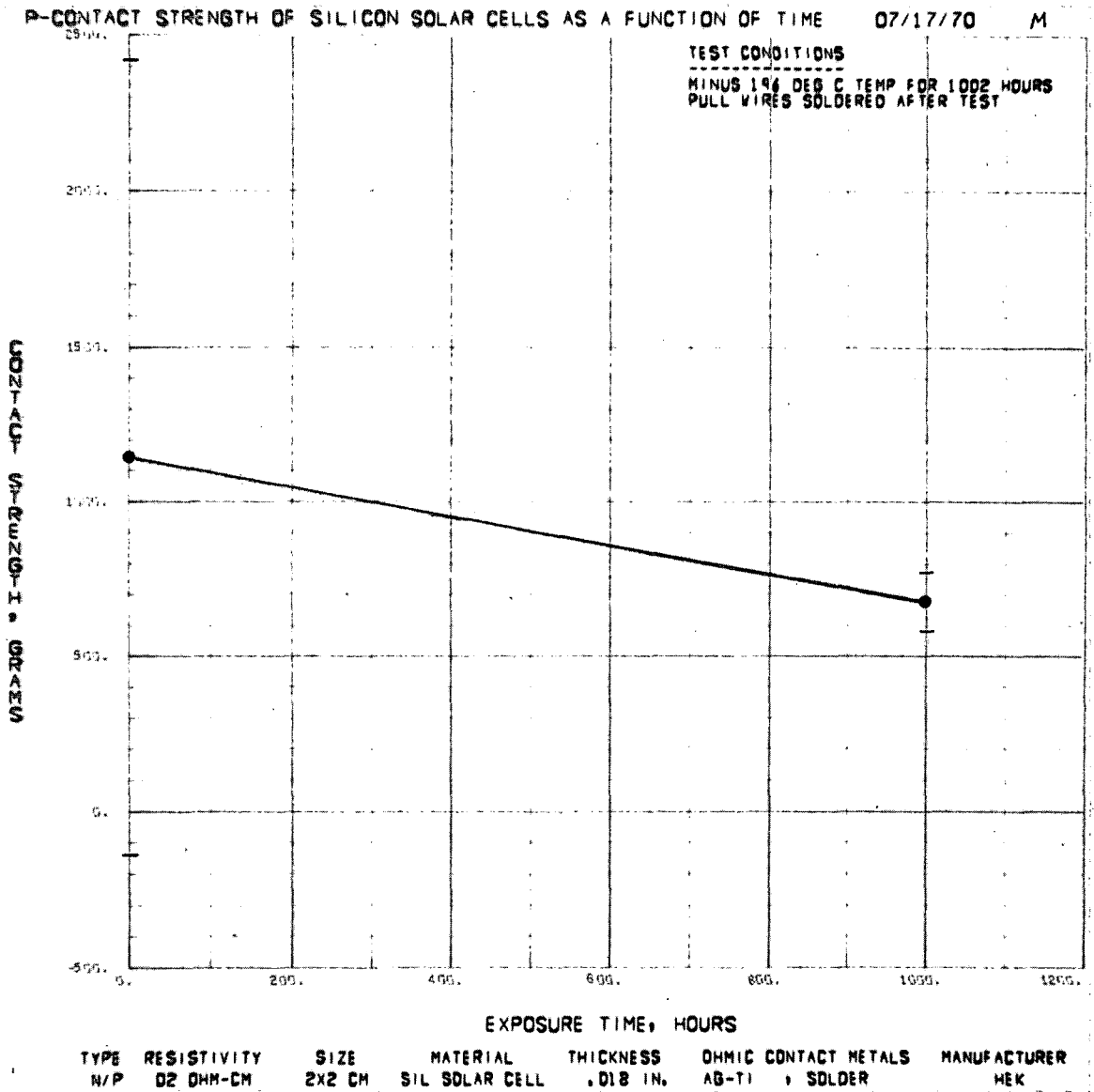


Fig. 97. Bottom-contact strength, cell type M, as a function of time, -196°C storage

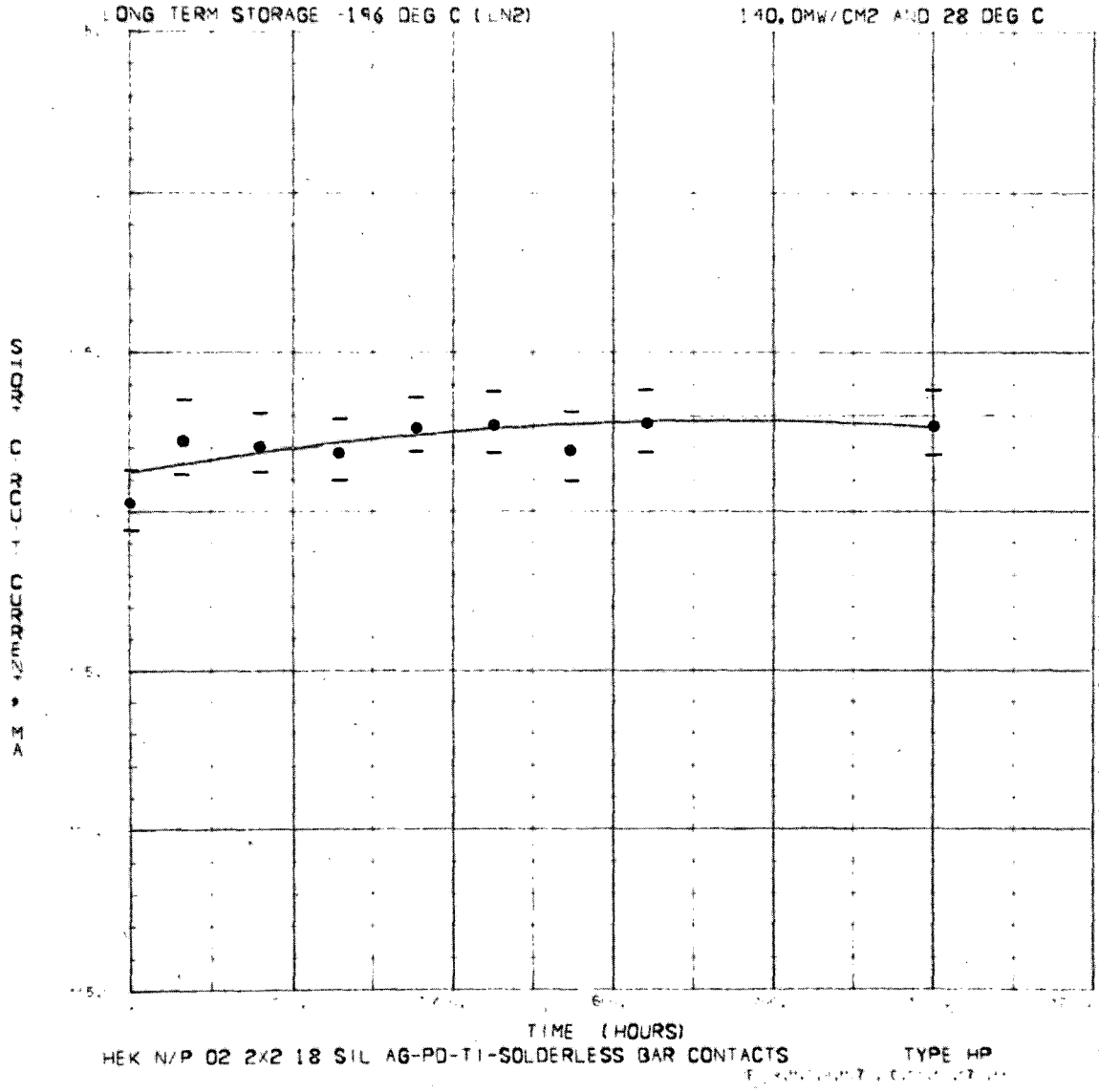


Fig. 98. Short-circuit current, cell type HP, as a function of time, -196°C storage

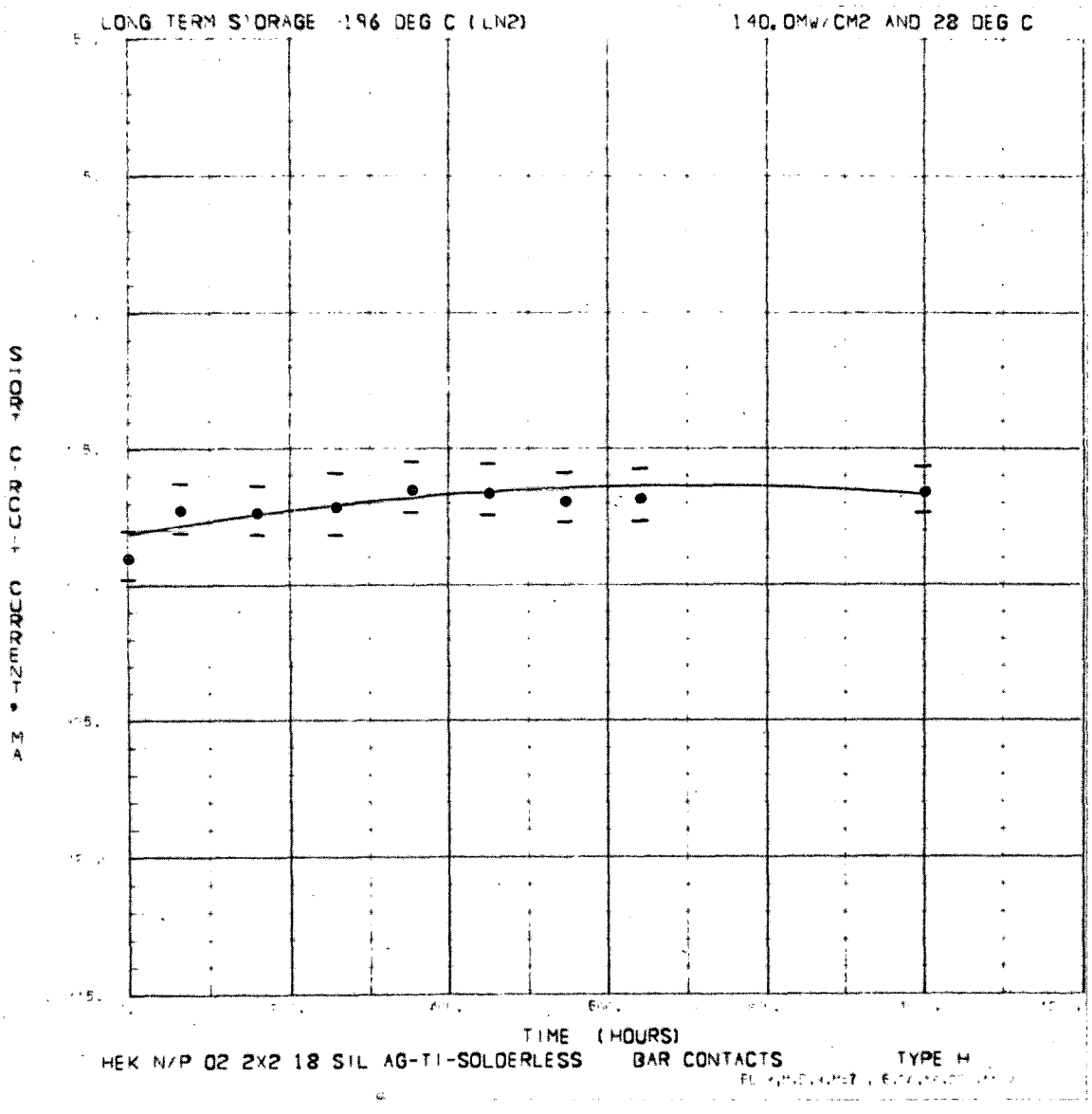


Fig. 99. Short-circuit current, cell type H, as a function of time, -196°C storage

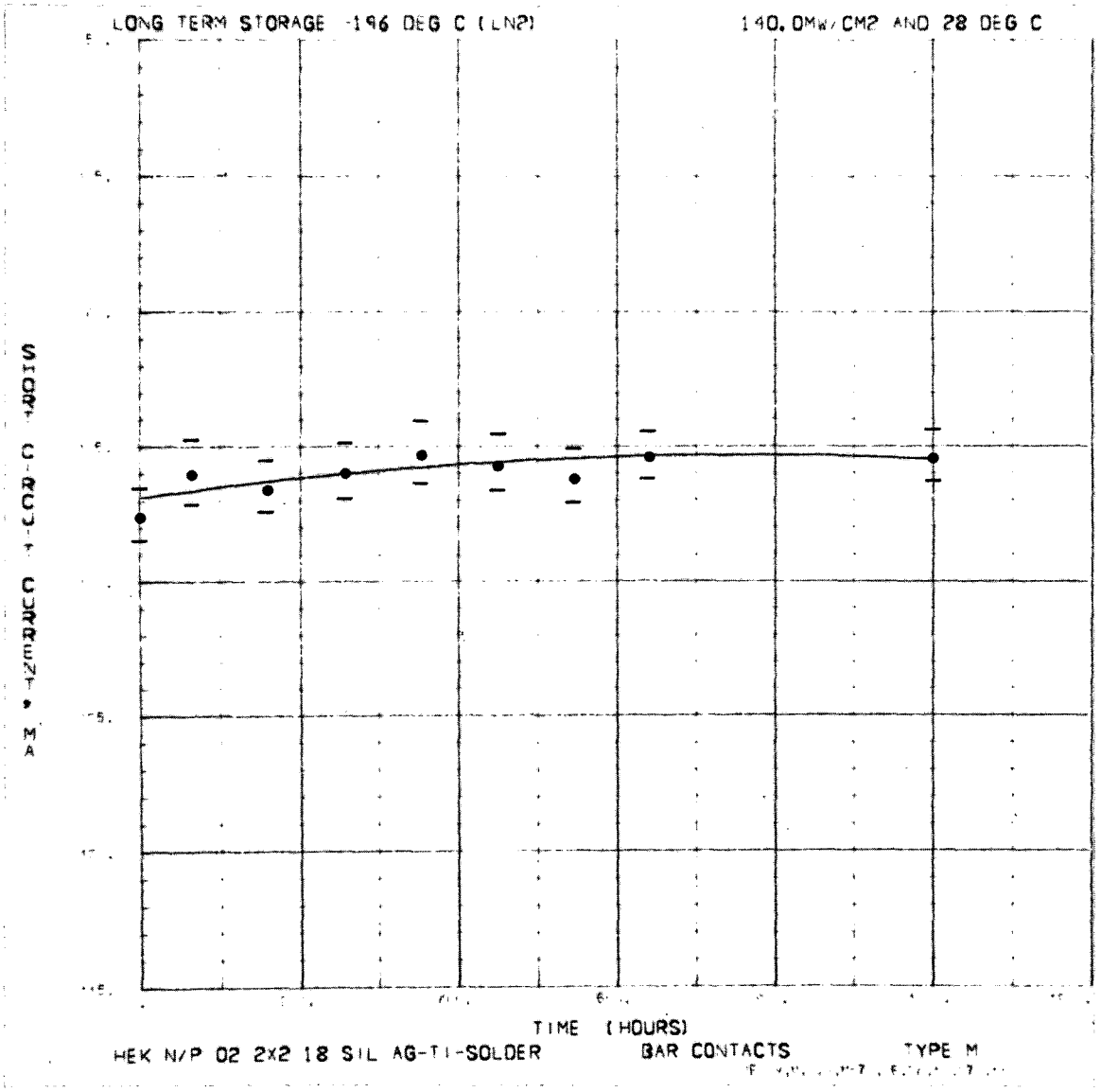


Fig. 100. Short-circuit current, cell type M, as a function of time, -196°C storage

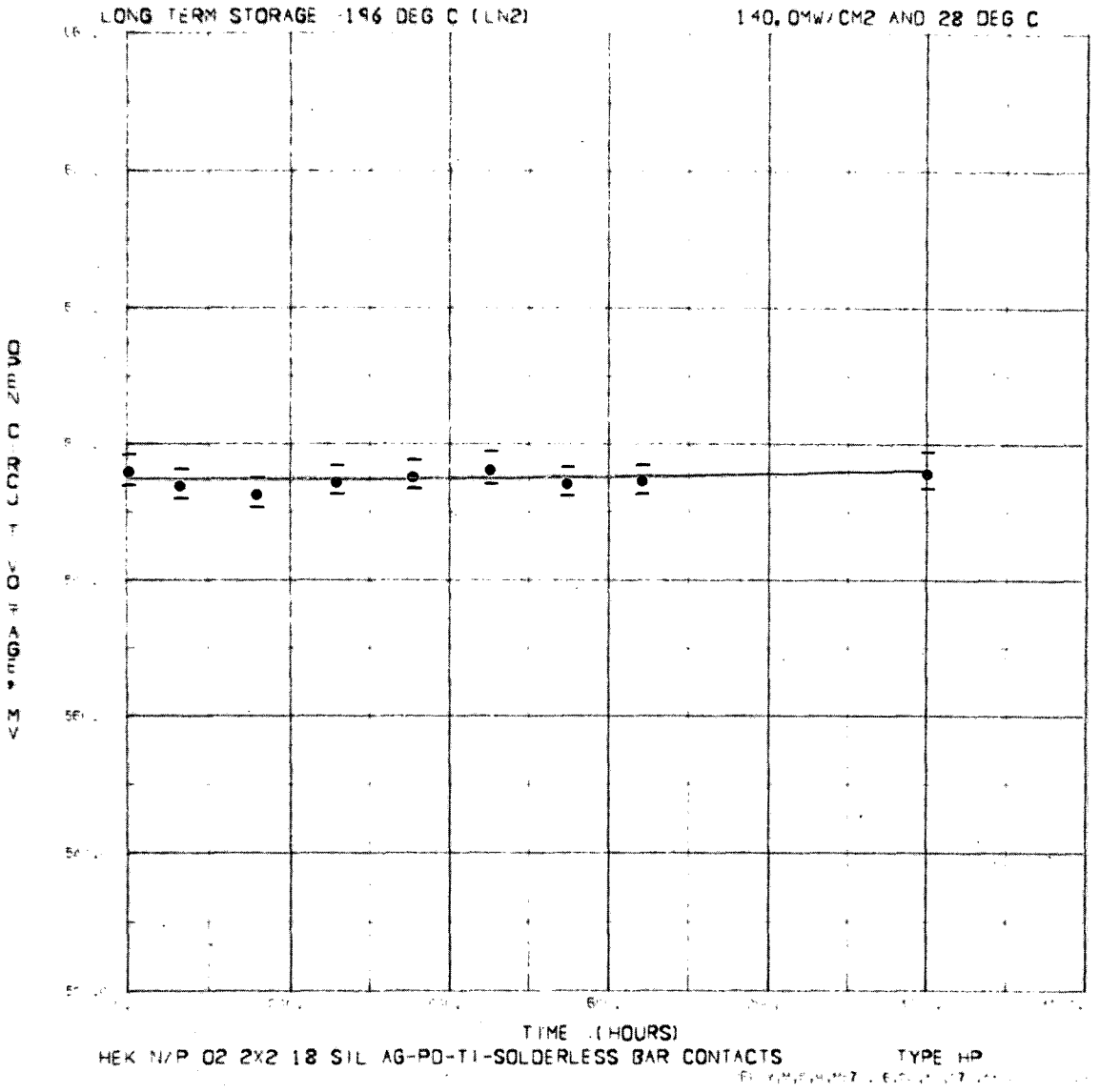


Fig. 101. Open-circuit voltage, cell type HP, as a function of time, -196°C storage

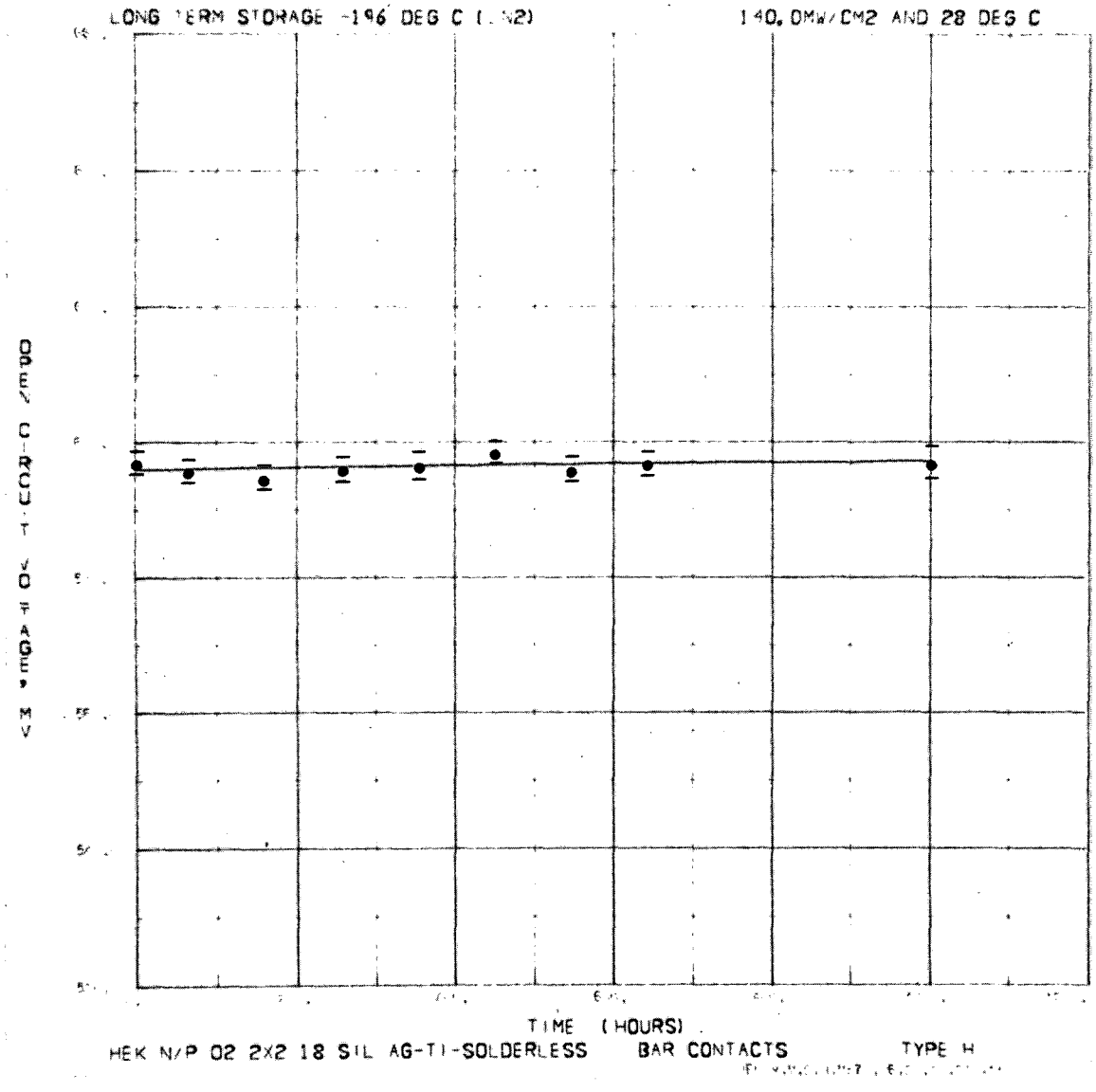


Fig. 102. Open-circuit voltage, cell type H, as a function of time, -196°C storage

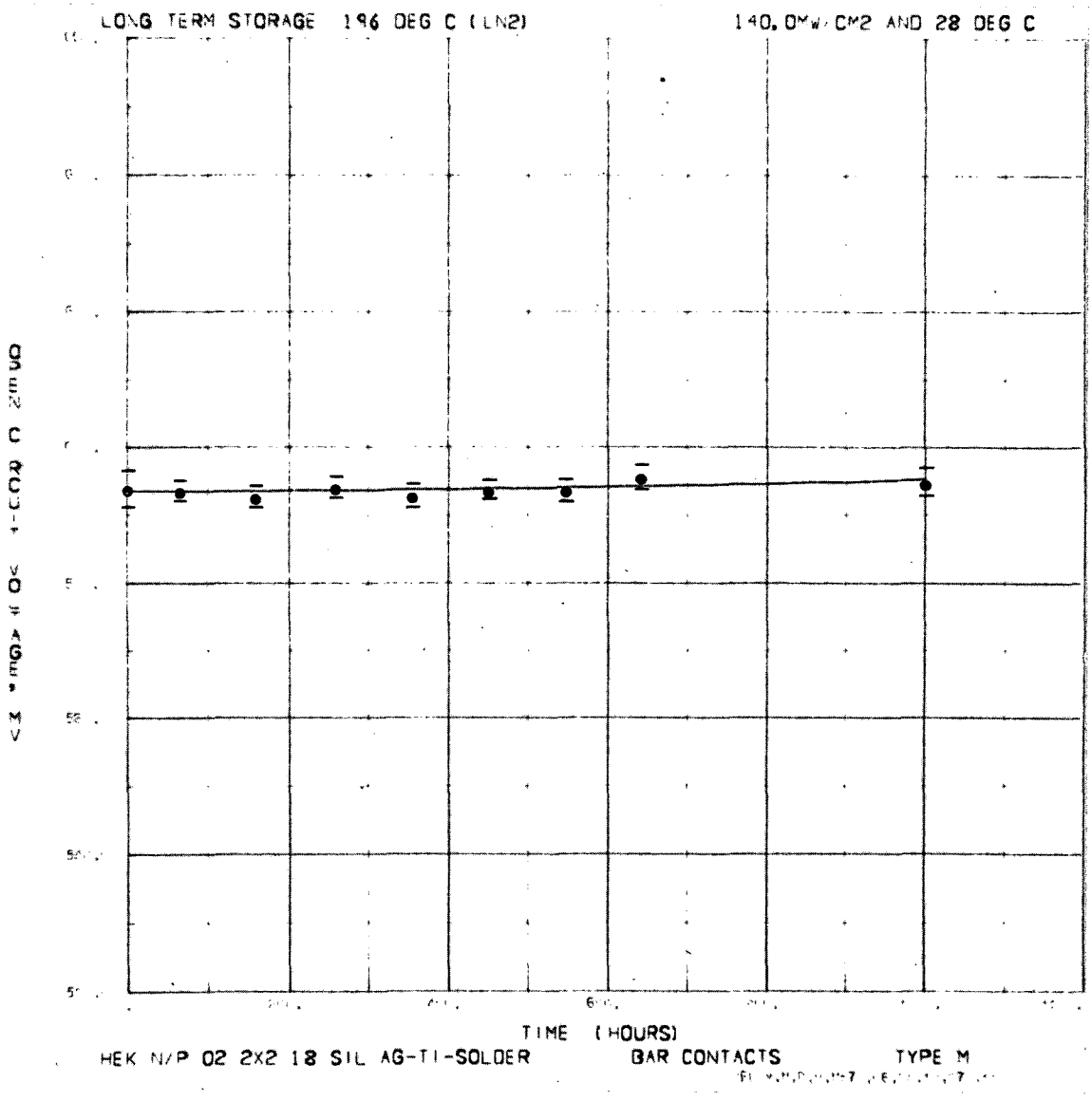


Fig. 103. Open-circuit voltage, cell type M, as a function of time, -196°C storage

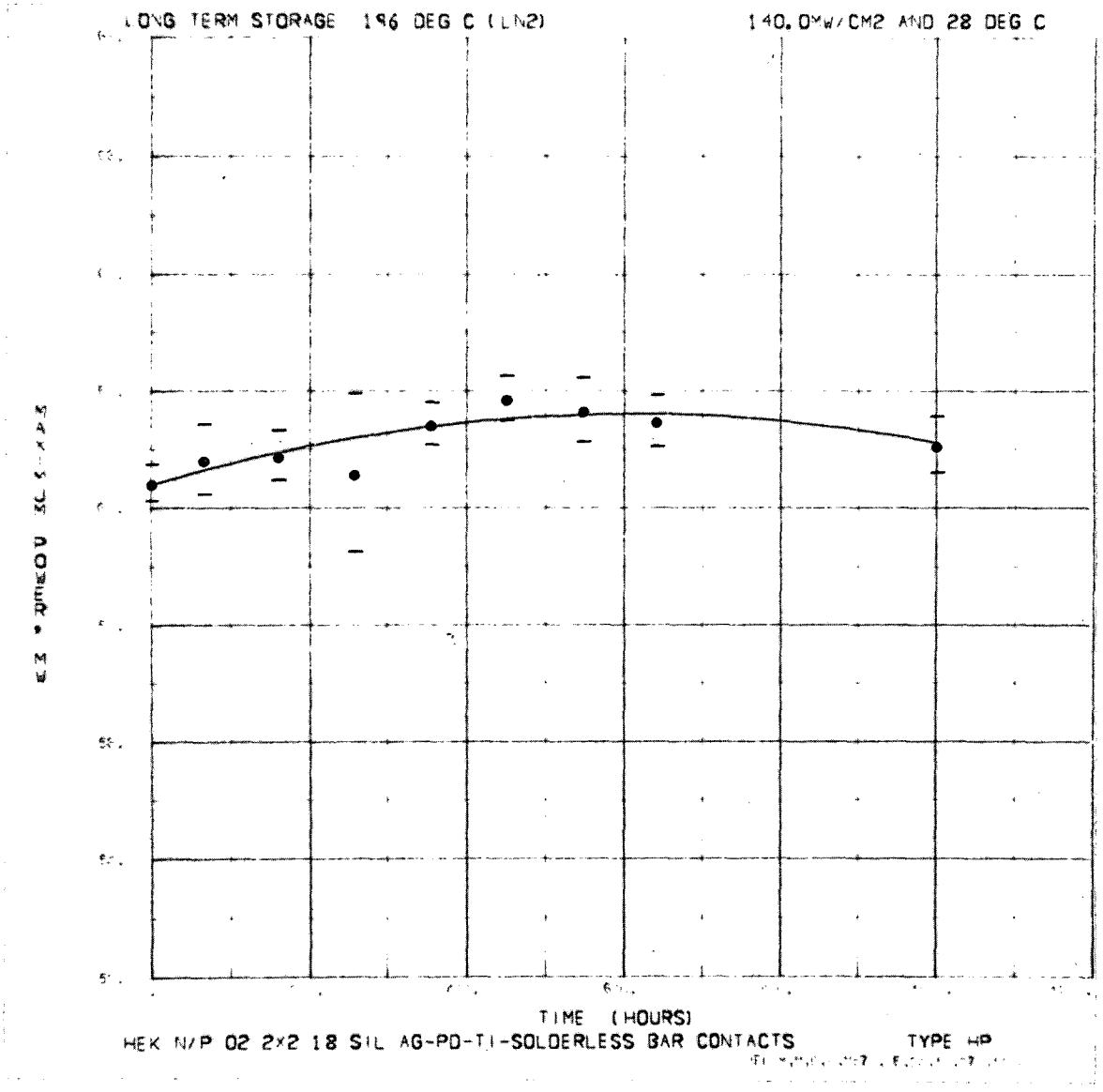


Fig. 104. Maximum-power voltage, cell type HP, as a function of time, -196°C storage

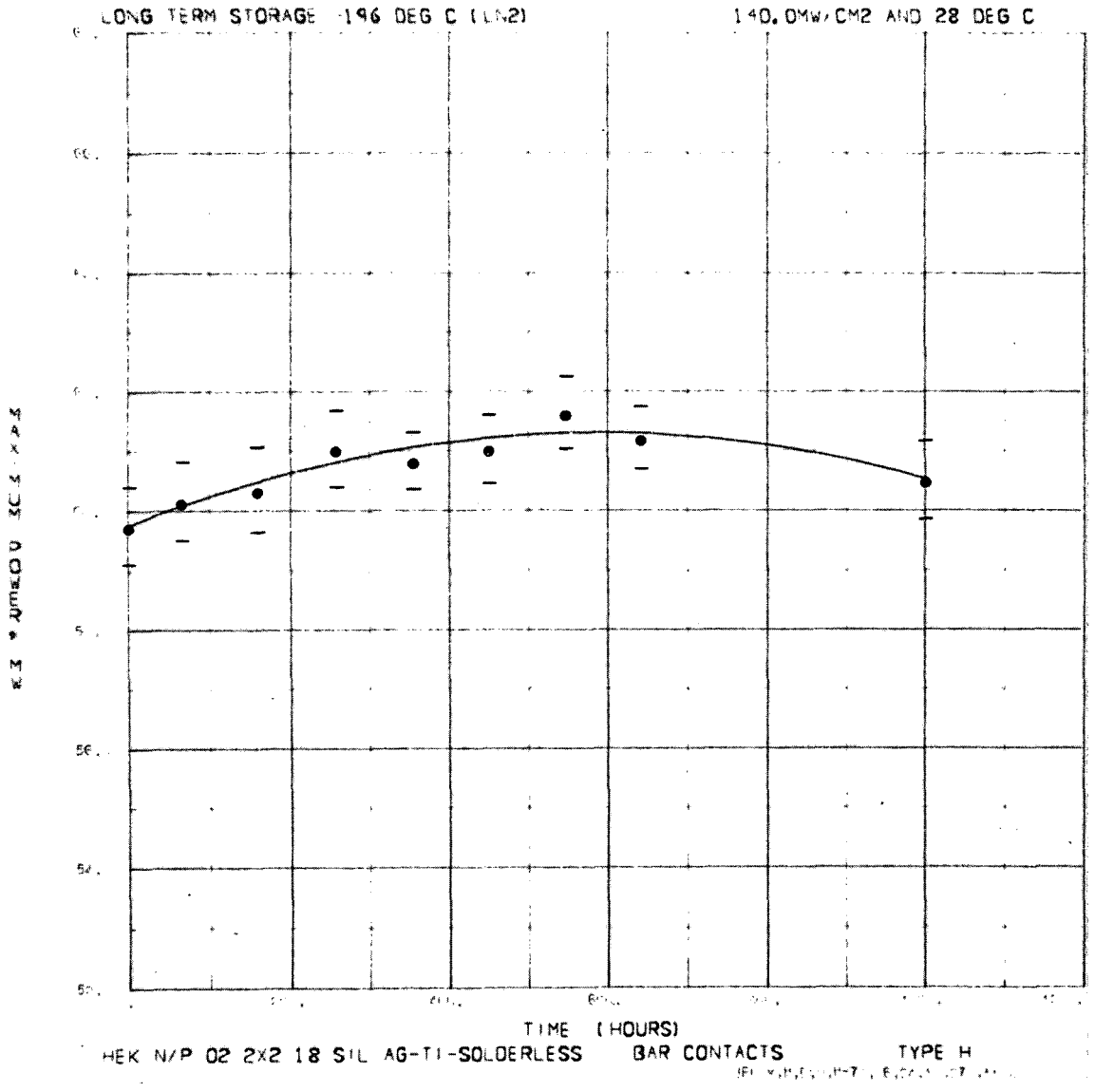


Fig. 105. Maximum-power voltage, cell type H, as a function of time, -196°C storage

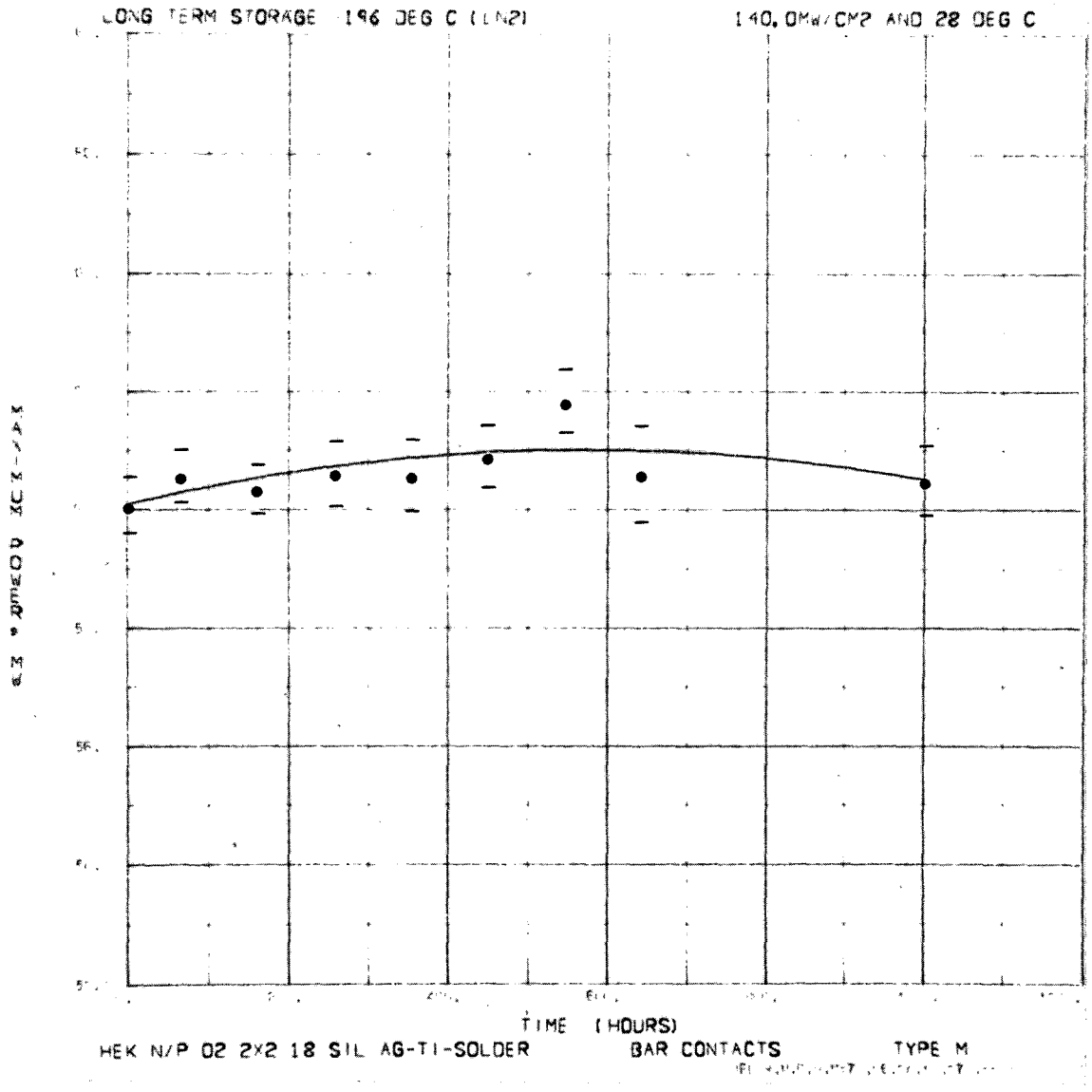


Fig. 106. Maximum-power voltage, cell type M, as a function of time, -196°C storage

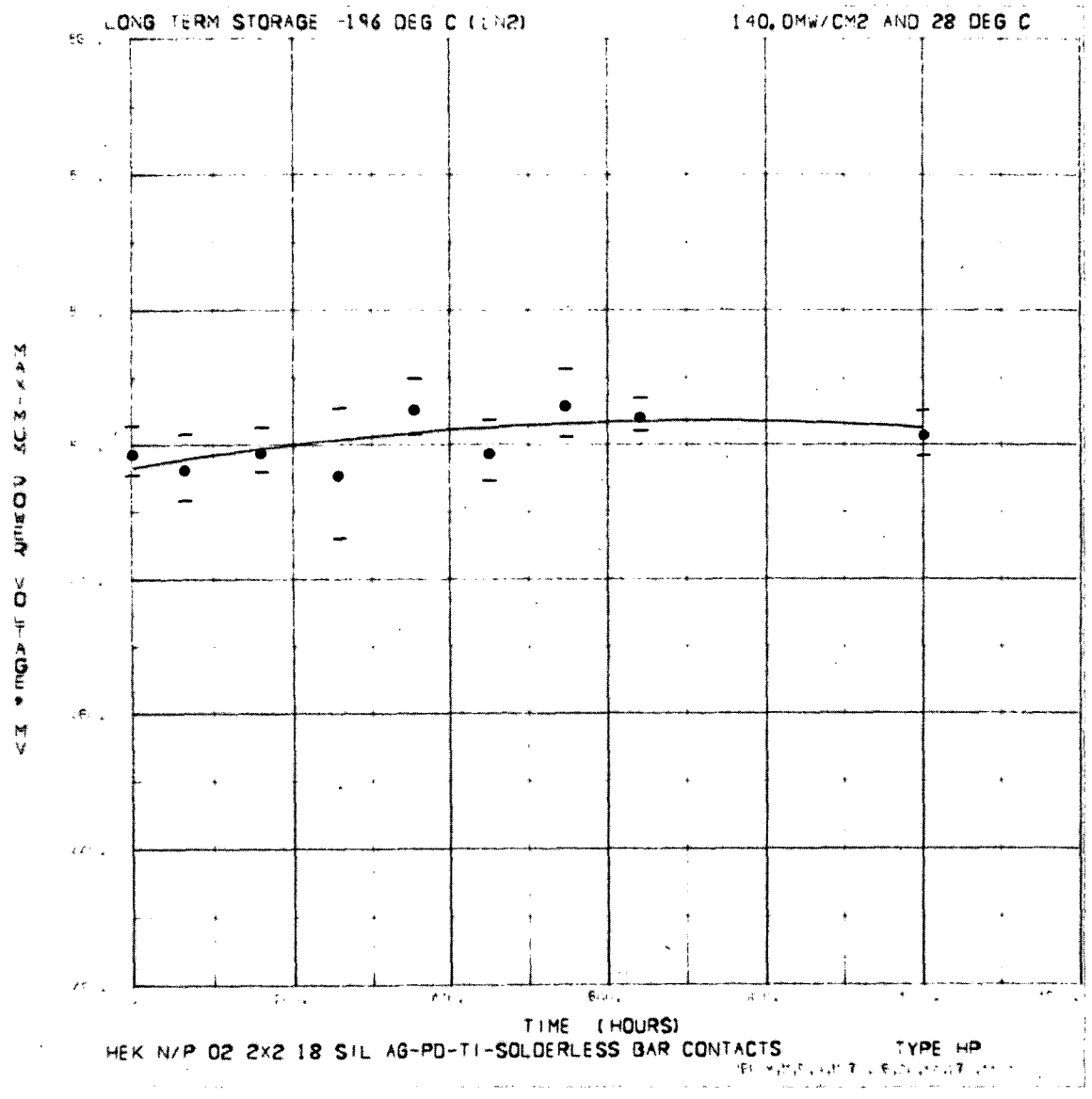


Fig. 107. Maximum-power voltage, cell type HP, as a function of time, -196°C storage

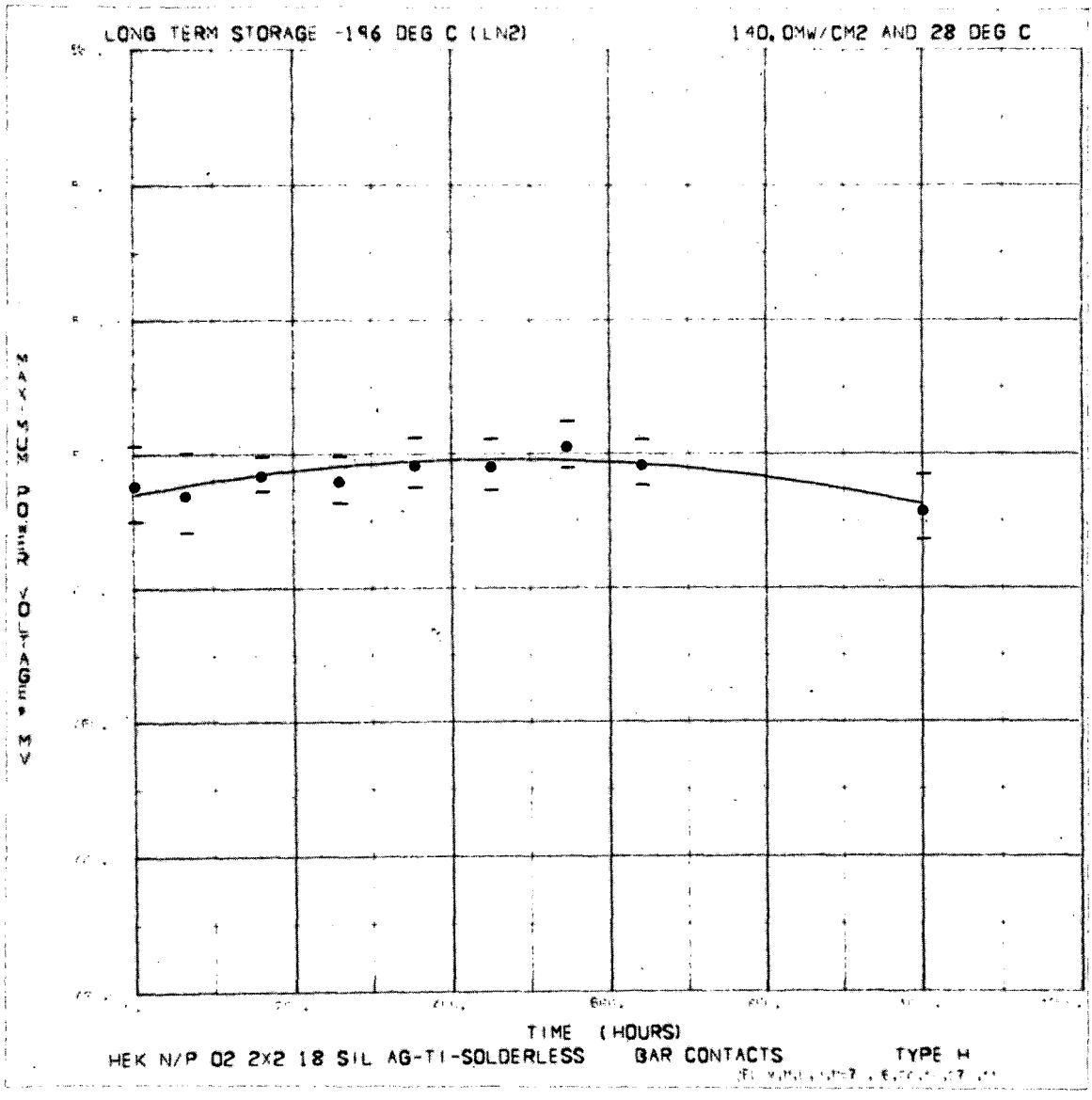


Fig. 108. Maximum-power voltage, cell type H, as a function of time, -196°C storage

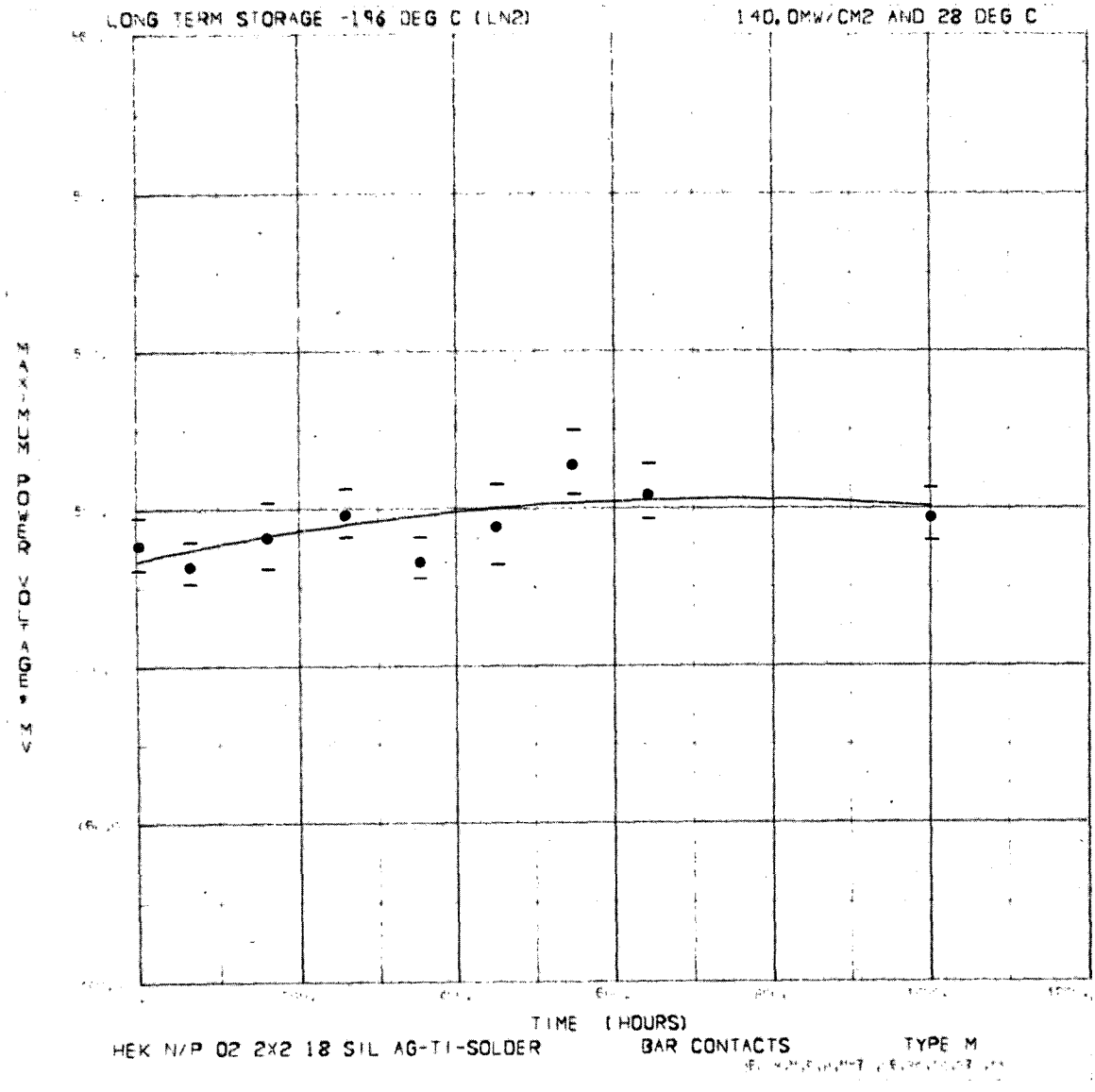


Fig. 109. Maximum-power voltage, cell type M, as a function of time, -196°C storage

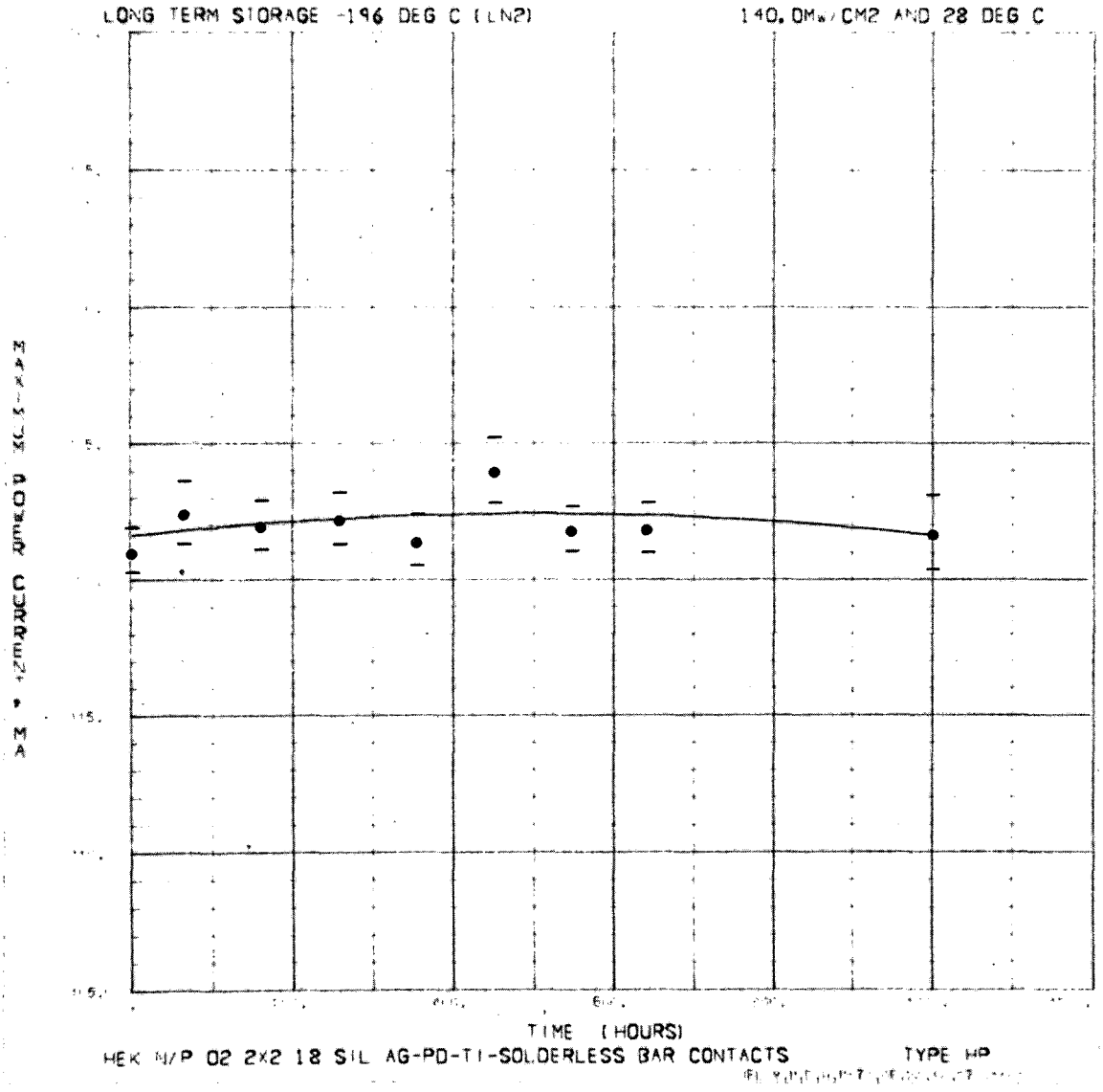


Fig. 110. Maximum-power current, cell type HP, as a function of time, -196°C storage

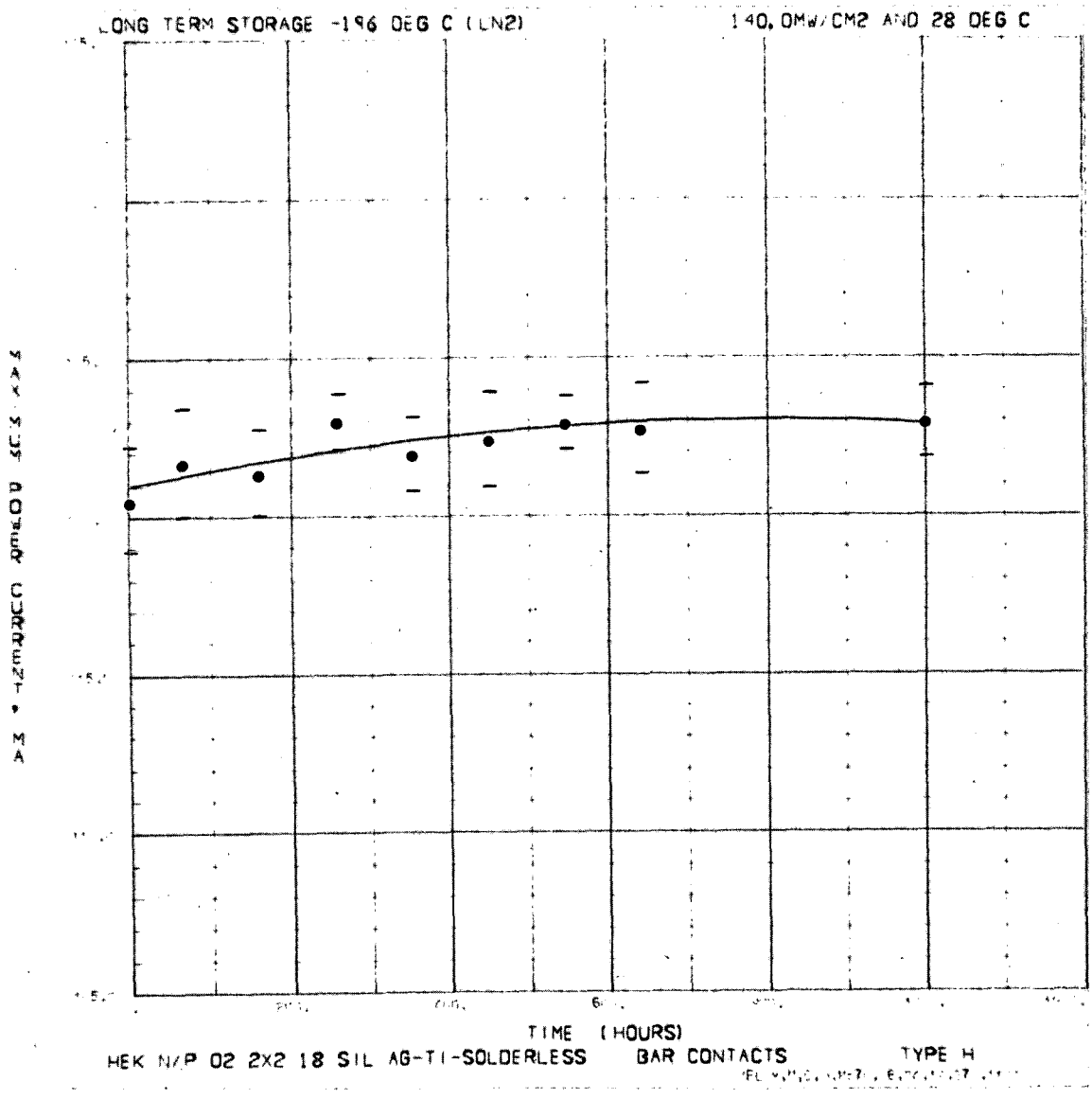


Fig. 111. Maximum-power current, cell type H, as a function of time, -196°C storage

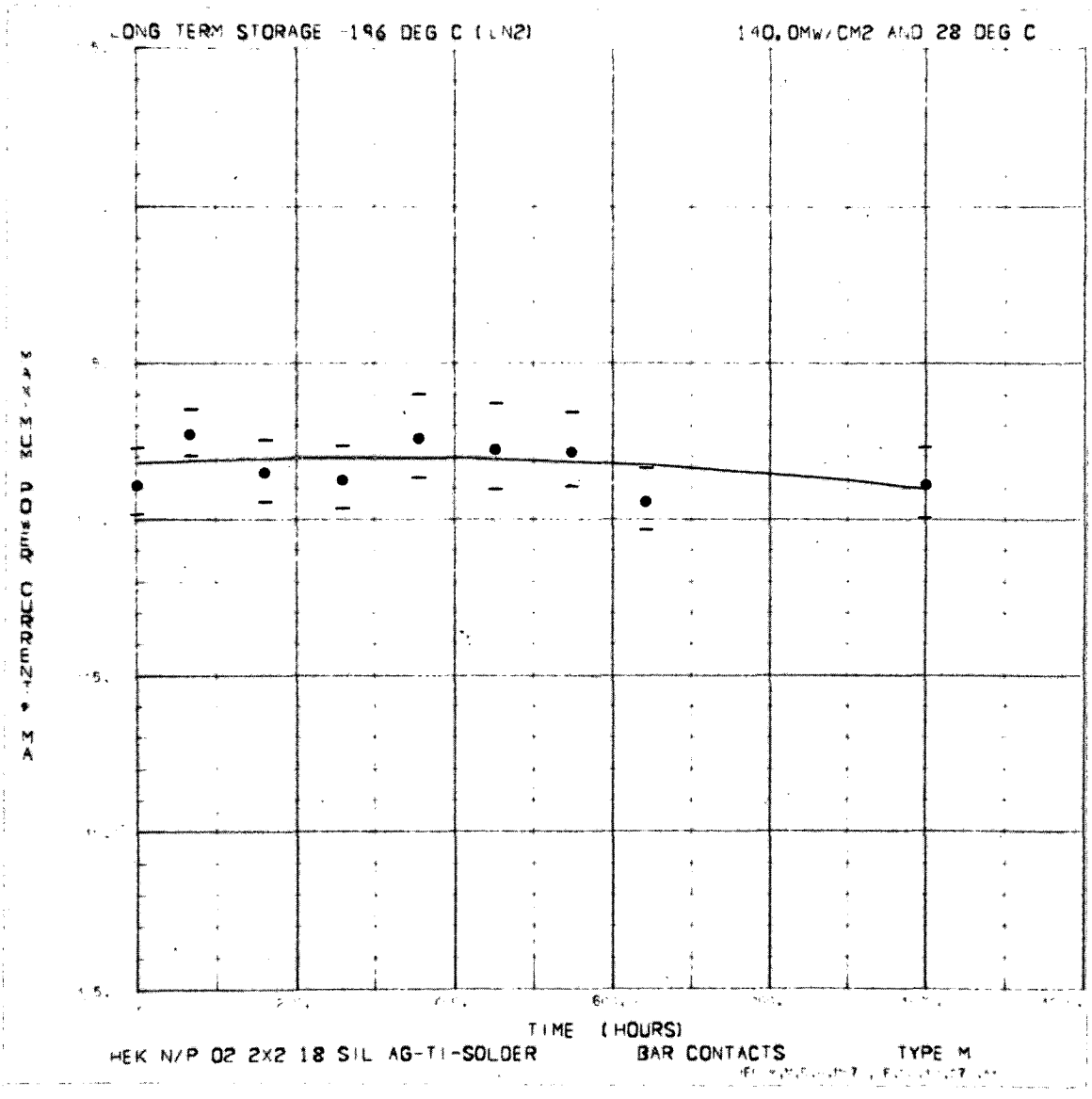


Fig. 112. Maximum-power current, cell type M, as a function of time, -196°C storage